9 Geologic interpretation of the seismic profiles of the Eastern Traverse (lines E1–E3, E7–E9): eastern Swiss Alps

O. A. Pfiffner & L. Hitz

Contents

9.1 Introduction

O. A. Pfiffner

The eastern traverse was originally conceived as a continuous seismic line crosscutting the Alps in a N-S direction. The main line shot was E1 (formerly also called NRP 20-EAST) and included also the registration of wide angle fan shots. The good results obtained from line E1 encouraged subsequent registration of two additional lines, a strike line (E2) and a N-S line through the Engadine window (E3). In this chapter the single lines are first discussed separately, followed by a 3D analysis combining these lines and the fan shots.

Lines E1, E2, E3 and the fan recordings E7 through E9 extend across the thin-skinned and thick-skinned compressional structures of the Helvetic zone in the northern part of the Alps and the Penninic and Austroalpine zones in the interior of the Alps (Figure 9-1). They transect deep portions of metamorphic zones exposed due to extensive uplift and erosion that started in the Tertiary and persists today. The lines cover major Alpine structures that are constrained by geologic surface data. These Alpine structures include shallow to moderately dipping thrust faults that juxtapose rocks of very different lithologies and physical characteristics; some rocks are highly anisotropic due to extensive deformation at elevated temperatures. The longest, north-south line E1 is more or less perpendicular to the regional trend of Alpine structures, but some of these structures possess a considerable plunge toward the east. By using downdip-downplunge projection there is a direct geometric tie between exposed and seismically imaged structures. Futhermore a joint interpretation of physically crossing lines (i. e. crossing reflectors at depth) attempted to gain insight into the 3D geometry of this part of Alpine crust.

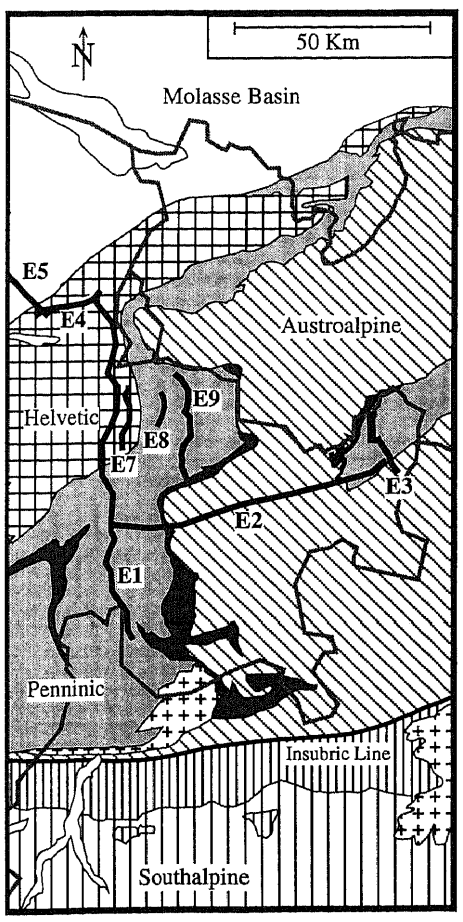

Figure 9-1
Tectonic map showing major units (nappe systems) and traces of seismic lines.

The Swiss Alps are divisible into five major geologic units defined by the pecularities of their Mesozoic-Cenozoic sedimentary sequences. From north to south they are the Molasse, the Helvetic zone (including the basement uplift of the Aar massif), the Penninic zone, the Austroalpine nappes, and the Southern Alps (Figure 9-1).

The **Molasse** comprises Oligocene to Miocene strata which were deposited on slightly tilted Mesozoic-Eocene strata that represent the autochthonous cover of the European crystalline basement; the latter outcrops in the Black Forest and Bohemian massif of southern Germany. Molasse sediments are considered to be late synorogenic. In the south they are deformed; they were tilted, detached from their substratum, and now form an imbricate fan (see Pfiffner et al., Chapter 8). In the **Helvetic zone**, Mesozoic-Oligocene sediments overlie Variscan basement. Within this basement three major units are recognized. The oldest unit consists of pre-Variscan polymetamorphic gneisses, metasediments, and schists with a steeply dipping foliation. These rocks were intruded by a series of late-Variscan, 330- to 270-Ma-old granitoids. Finally, a Permo-Carboniferous volcaniclastic sequence overlies (or is locally intruded by) the granitoids; these volcaniclastic rocks were in part tightly folded during the Variscan orogeny and now outcrop along narrow, steeply dipping zones. The cover sequence starts with thin epicontinental sediments including dolomites of Triassic age, followed by Jurassic to Eocene platform carbonates and locally Eocene-Oligocene flysch. In Eocene to Miocene times, these cover sediments were in part detached from their basement, compressed, thrust northward and now form the Helvetic cover nappes. Beneath the Helvetic nappes compression led to a thick-skinned fold-and-thrust belt, cored by the Aar massif basement uplift (see Pfiffner et al., Chapter 13.1). Alpine metamorphism is anchizonal in the north and epizonal in the south.

In the **Penninic zone**, Mesozoic-Eocene sediments overlie a Variscan basement similar to that of the Helvetic zone. Unlike in the latter, however, extensive Alpine deformation resulted in a gently dipping foliation. The cover sequence was in many instances completely detached from the crystalline basement. As a result the Penninic nappe pile consists of basement nappes on one hand, and cover nappes on the other hand. Both nappe types suffered an extensive imbrication during the early deformational history, followed by intensive post-nappe folding leading to very complex 3D geometries for many of the thrust sheets (see also schmid et al., Chapter 14).

The Mesozoic sediments of the **Austroalpine nappes** and the **Southern Alps** were deposited on the stretched passive margin of the Periadriatic promontory in the south Tethys Ocean. The cover overlies Variscan basement affected by Alpine deformation. Most of the lines of this transect pass "beneath" the Austroalpine nappes, which were eroded from the Penninic and Helvetic zones in Oligocene and Miocene times. However the strike line E2 passes through an axial depression where Austroalpine nappes are preserved between the Toce-Lepontine area and the Engadine window. Given the large recording offsets and the poor resolution of the explosion seismic experiment at shallow depth, hardly any information was gathered for the Austroalpine nappes and the former plate boundary underneath it.

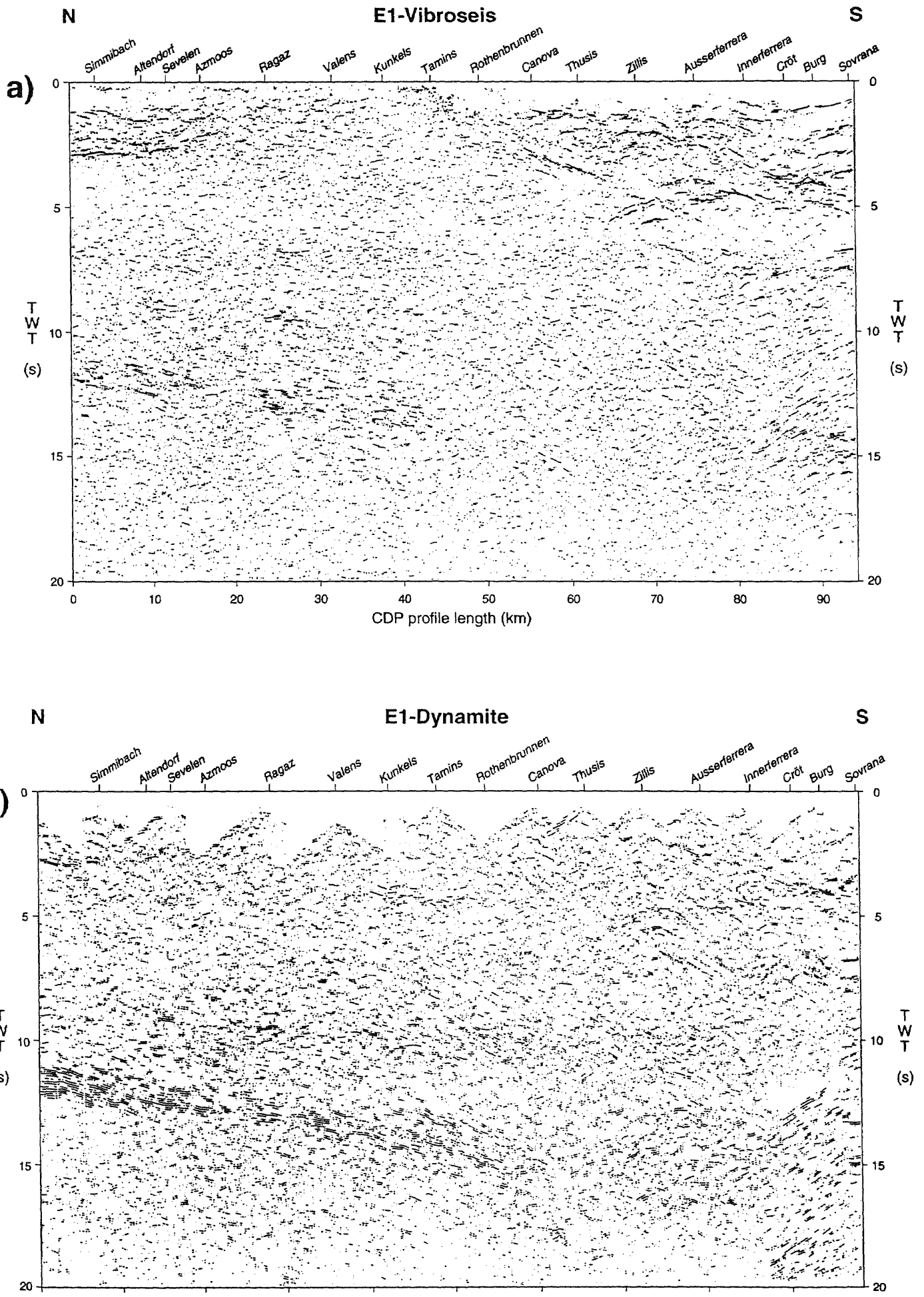

Figure 9-2
a) Unmigrated coherency enhanced Vibroseis data of line E1 (GOLD section from Valasek 1992).
b) Unmigrated coherency enhanced explosion seismic data of line E1 (GOLD section from Valasek 1992).
Names are shot points of explosion data which serve as geographic reference system throughout this Chapter.

9.2 Seismic line E1: Crustal shortening in the transect through the Helvetic and Penninic nappes and the Adriatic wedge

O. A. Pfiffner

Line E1 runs north-south across the Helvetic and Penninic nappes and intersects strike line E4 which is linked to the eastern Molasse transect (lines E5 and E6 discussed in Pfiffner et al., Chapter 8) and strike line E2 discussed below in section 9.3. In addition to the E1 vibroseis profile, which was designed to yield high resolution information on the upper crust, a deeper-penetrating explosion data set (near vertical reflection) was collected along the same line.

9.2.1 The data

The seismic data are presented in Plates 9-1 (explosion data set) and 9-2 (vibroseis data set). In Figure 9-2 coherency enhanced sections of the Vibroseis and the explosion seismic stacks are displayed. A comparison of the two stacks reveals a great similarity. The higher resolution of the Vibroseis data in the shallow part is readily explained by the low-fold coverage of the explosion seismic line. On the other hand the explosion seismic data yielded better results in the deeper part (for which they were conceived to begin with). Unmigrated line drawings for both data sets are given in Figures 9-3 and 9-4a. The computer-generated line drawings in Figure 9-3 emphasize the similarities and differences in the two seismic data sets. Comparing these computer-generated line drawings to the hand-produced line drawings shown in Figure 9-4a reveals only slight differences between the two techniques. The hand-produced line drawing appears somewhat cleaner, which is due to "filtering" of low amplitude and discontinuous signals. Although this

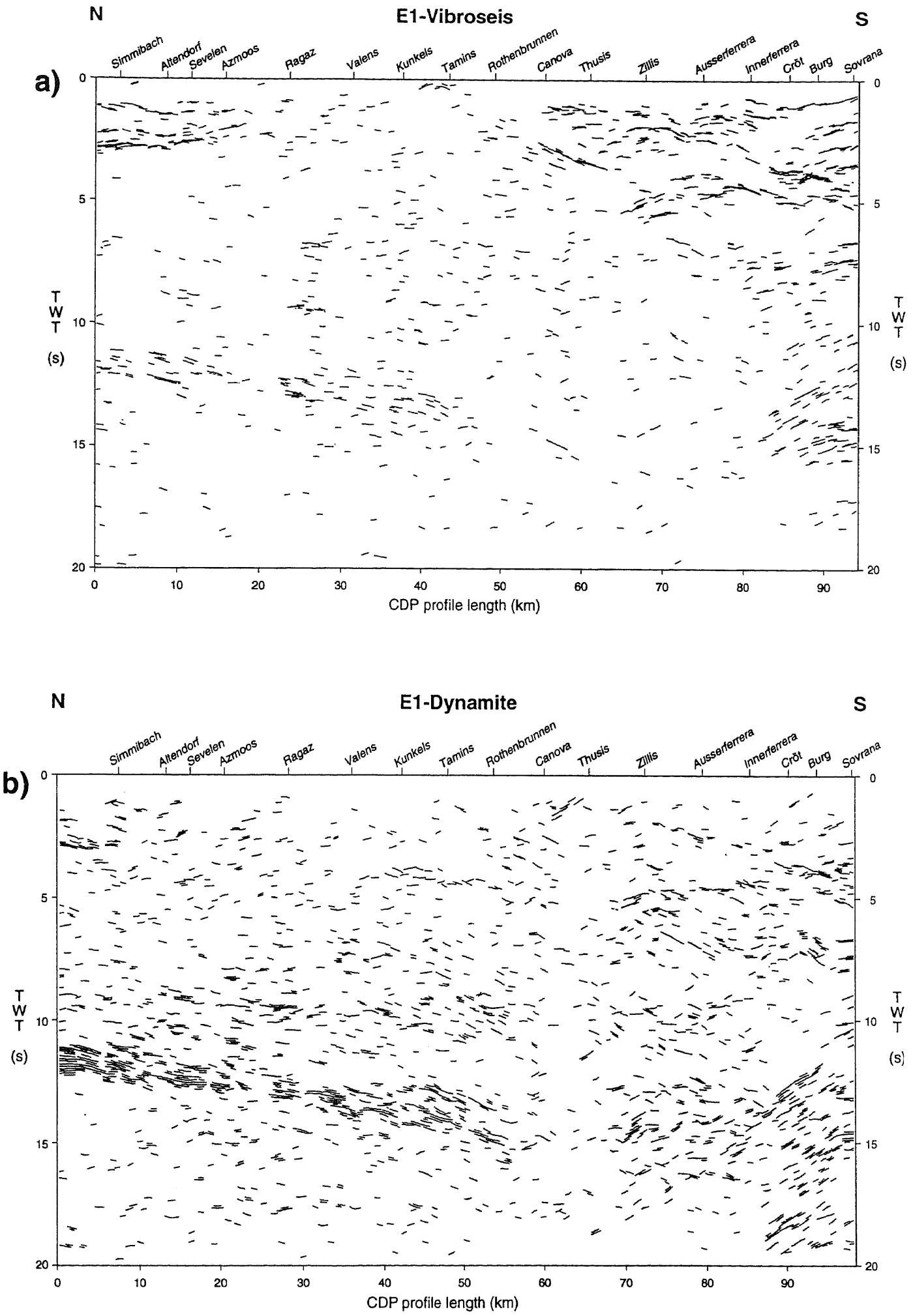

Figure 9-3
a) Computer generated line drawing of unmigrated Vibroseis data (from Valasek 1992).
b) Computer generated line drawing of explosion seismic data data (from Valasek 1992).

subjective filtering may suppress real short reflections, it also emphasizes the more obvious reflections, on which the process of geologic interpretation concentrated to begin with. The difference is most obvious beneath shot points Tamins and Kunkels and at around 5 s TWT beneath Valens-Simmibach. The numerous short reflections recognizable in this area in the computer-generated line drawings of Figure 9-3 could not be interpreted subsequently. Migration of the seismic data cleared up some of the complex patterns, but created new problems in other instances. Figure 9-4b is a migrated version of the computer-generated Vibroseis stack. Upon comparison with the non-migrated data in Figure 9-4a or 9-3 one notes that the depth-migrated reflections at 30 – 40 km depth form a rather continuous band in the northern half and are cleaned up in the southern half of line E1. On the other hand the depth-migrated shallow reflections are in places less coherent. In an area of considerable dips and cross-dips a conventional 2D migration is bound to mis-place reflections from a complex 3D structure and should thus be applied with care (Stäuble et al. 1993, Litak et al. 1993). Due to these difficulties the identification of individual reflection events will be discussed on the coherency-enhanced, unmigrated Vibroseis stack (Figures 9-5a). The geologic profile constructed on the basis of the interpreted seismic data is a vertical section through the final version obtained from 3D modeling.

Considering the entire line E1 shown in Figure 9-2 and 9-5a, crustal reflections in the shallow part (down to around 5 s TWT) are prominent in the north (Helvetic nappes) and in the south (Penninic nappes), with the Aar massif in the central part being largely transparent. At mid-crustal level (5–10 s TWT) weak, discontinuous reflections can be recognized. A prominent band of reflections finally, is distinguished at lowermost crustal level (11–15 s TWT) and can be traced across the northern half of the profile. At the southern end deep reflections are predominantly north dipping.

The **shallow reflections** in the **northern half** of the Vibroseis section, down to 3 s two-way-travel time (TWT), extend over the Helvetic zone. Coherent reflections can be seen mainly in the north; they degrade in strength toward the south. A detailed interpretation of these reflections is given by Pfiffner et al. in Chapter 13.1. The most noticeable reflection, marked *B1* in Figure 9-5a, is situated at 2.8 s at the northernmost end. It is characterized by its high amplitude, double cyclic nature. south of sevelen this strong reflection begins to dip upward and then continues as discrete panels of progressively

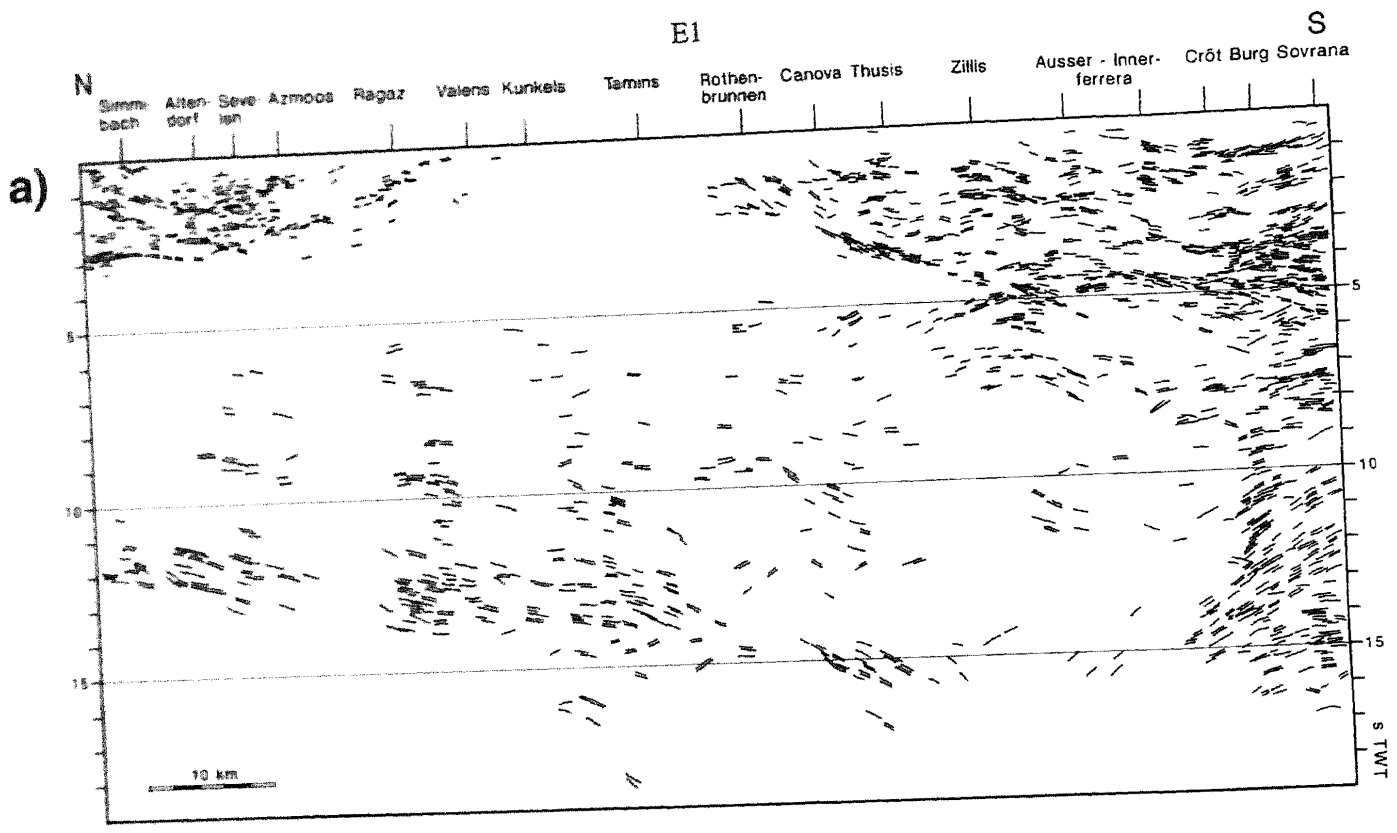

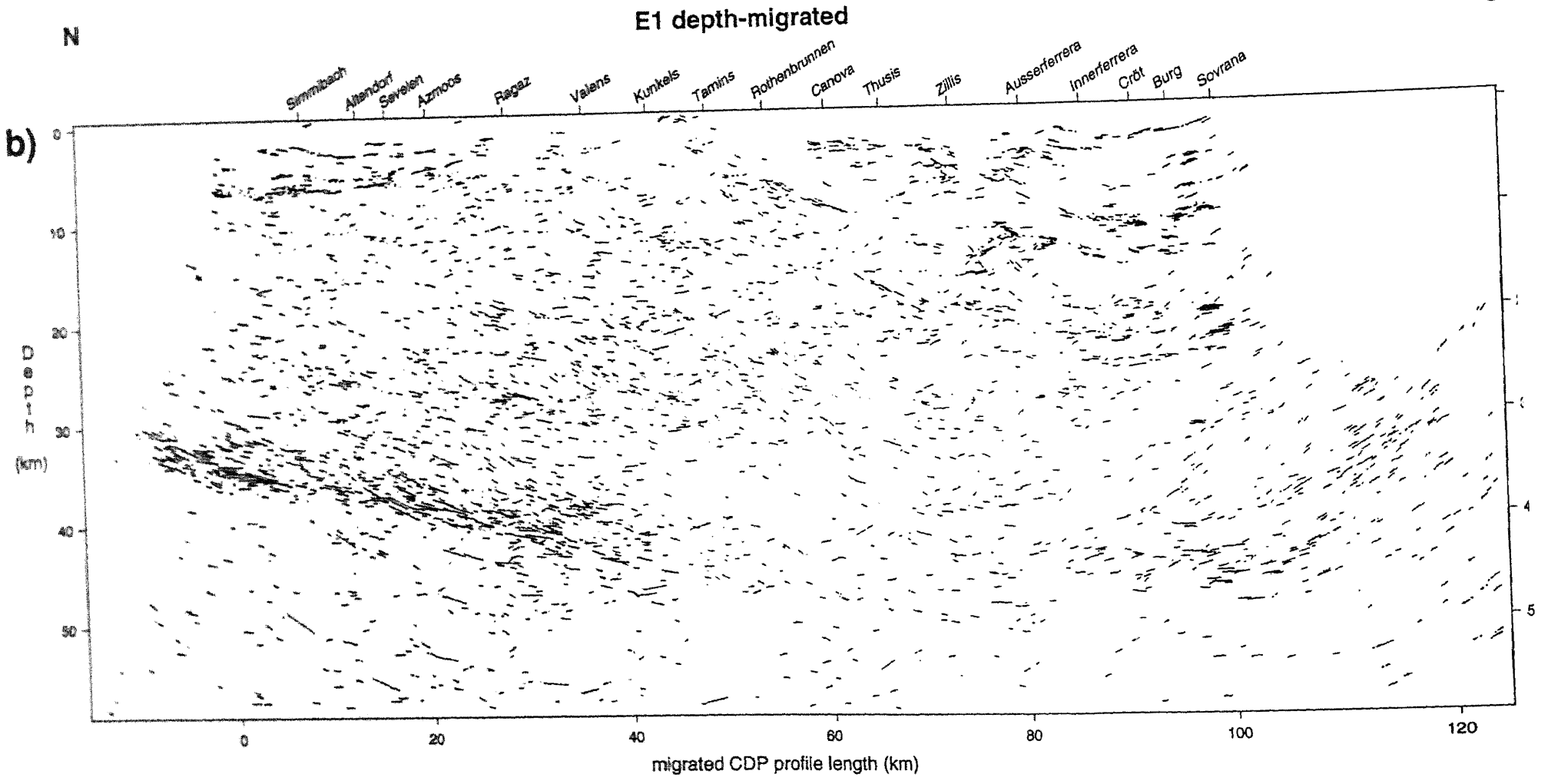

Figure 9-4
a) Hand-produced line drawing of unmigrated Vibroseis data, combining partial stacks of variable offsets (from Pfiffner et al. 1991).
b) Depth-migrated stack of the computer-generated line drawing (from Valasek 1992).

weaker reflections (*B2* in Figure 9-5a) rising stepwise toward the south. Between 1 and 1.6 s TWT north of Simmibach a pattern of several south dipping reflections is notable. These events, marked *J* in Figure 9-5a, also show a double cyclic swing and high amplitudes.

The **shallow reflections** in the **southern half** of the section, shown in Figures 9-2 and 9-5a, extend over the Penninic zone. strong reflections occur between 0 and 7 s TWT are mainly south dipping in the north (*B3* in Figure 9-5a) and north dipping in the southern portion (*sp, Ch, Ad*) with several reflections crossing each other *(B4)*.

Three **deep reflection packages** are observed on the vibroseis section of Figures 9-2 and 9-5a. These deep reflections can also be recognized in the explosion data set (Pfiffner et al., 1988). The first package, marked *C* in Figure 9-5a, comprises sparse, discontinuous, short reflections within an ill-defined zone extending from about 9 s beneath Sevelen to 10 s TWT beneath Tamins. steeply north dipping reflections at 8 to 14 s TWT *(CA)* at the southern end of the section form a second package of reflections.

The third package, m in Figure 9-5a, is a highly reflective band with a duration of 1-1.5 s. It is located at a depth of around 11 s TWT at the northern end of line E1 and extends southward with a shallow southerly dip to a depth of 15 s TWT at its deepest point beneath Canova. Near the southern end of the section it reappears at 13–15 s TWT.

In several areas the reflection quality of deep reflections degrades. Examples are seen beneath the segment between shot points sevelen and Ragaz, and in the area beneath Tamins, both of which coincide also with dense population and industrialization. We feel, therefore, that this particular seismic character is not necessarily due to a change in the geologic structure, but rather be related to difficult recording environments.

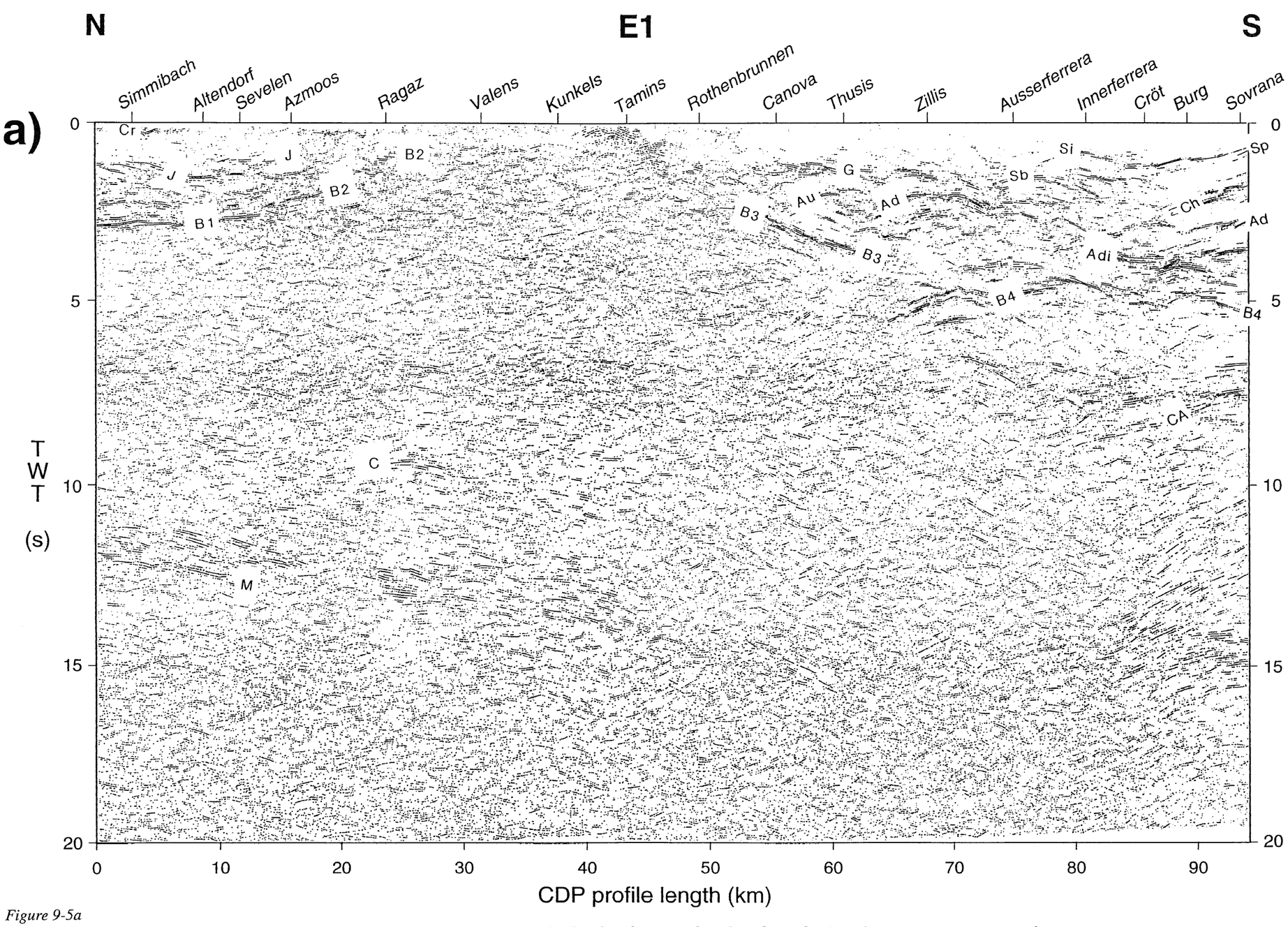

Figure 9-5a
Identification of reflection groups on unmigrated coherency enhanced Vibroseis stack. The identification is based on the evaluation of structure contour maps of potential reflectors.
Cr: top Cretaceous, J: top Jurassic, B1, B2, B3, B4: top crystalline basement of European crust (Autochthonous foreland, Aar, Gotthard, Simano), G: top Grava, Au: top Aul, Ad: top Adula, Adi: Adula internal, Ch: top Chiavenna, Sp: top Splügen, Sb: base Suretta, Si: Suretta internal, C: European Conrad, CA: Adriatic Conrad, M: Moho.

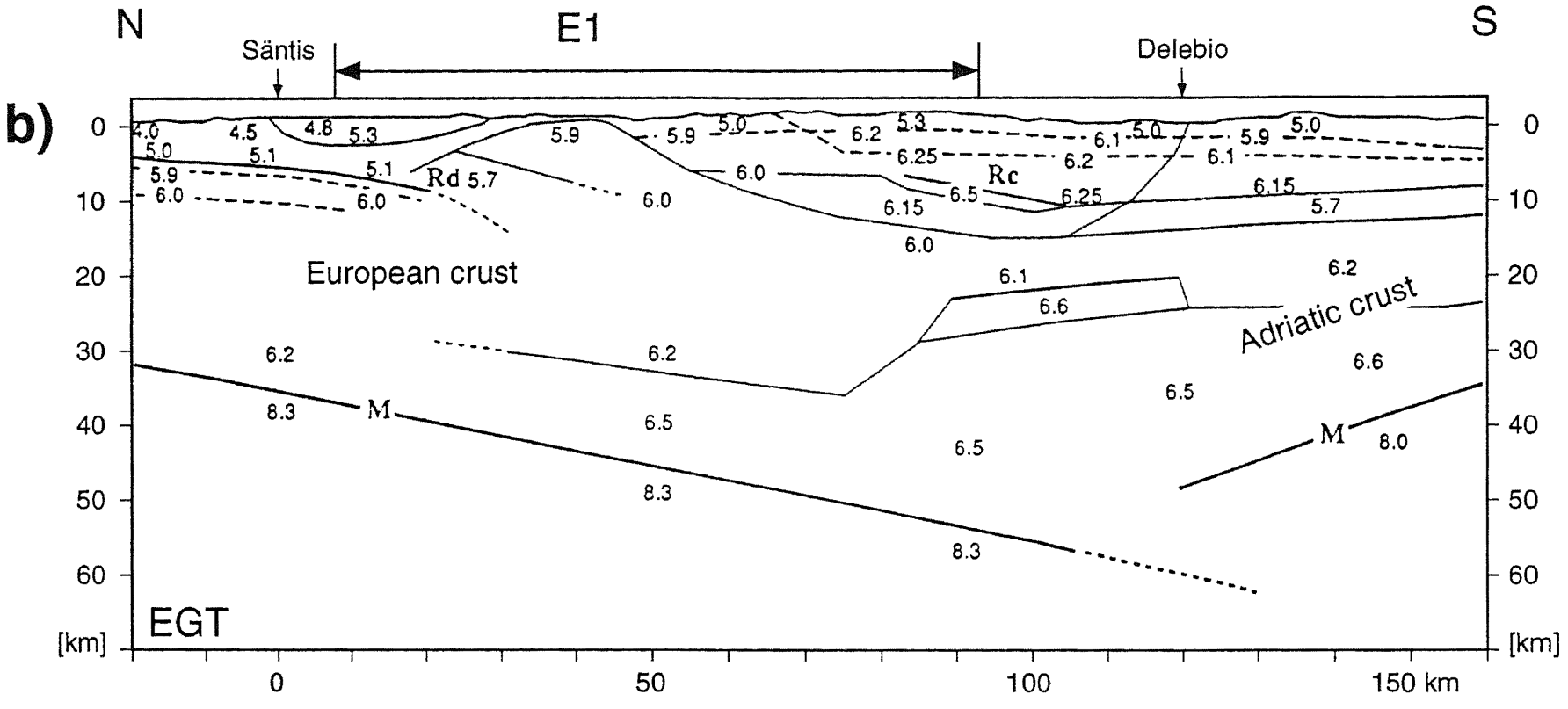

Figure 9-5 b
Refraction derived velocity model (adapted from Ye 1992). Säntis and Delebio are shot points of EGT refraction line. Note mismatch between European and Adriatic Moho.

9.2.2 Geologic interpretation

The crustal structure of this part of the Alps is fairly well known to a depth of 5–10 km due to the easterly axial plunge and the high topographic relief. This makes it possible to calibrate the reflections and to refine and laterally extend the interpretations. The three-dimensional geometry of potential reflectors such as basement-cover contacts has been analyzed using all the available surface data and their projection to depth. These results were presented by Pfiffner et al. (1990 a and b). For the deeper parts of the crust, refraction surveys and wide-angle reflections show low- and high-velocity bodies within the crust and place the Moho at a depth of around 40 km beneath Simmibach and at around 50 km beneath Thusis (Holliger & Kissling 1991, Ye 1992).

The interpretation of the **shallow structures in the North** are discussed in detail by Pfiffner et al. in Chapter 13.1. To the north of line E1 the reflections *B1* in Figure 9-5a at 2.5 and 2.8 sTWT are from the autochthonous sedimentary cover of the foreland, which can be traced all the way across the Molasse Basin (see Pfiffner et al., Chapter 8). The strong, double-cyclic reflections stem from the top of Triassic dolomites (Röti Dolomite). somewhat weaker and less continuous reflections originate from the top of the Mesozoic carbonates. On the northern flank of the Aar massif this cover is shortened by a combination of folding and thrusting. The associated complex geometry of the reflectors leads to defocussing and scattering of the ray paths (Stäuble & Pfiffner 1991, Pfiffner et al., Chapter 13.1) resulting in the loss of coherent reflections. The seemingly "poor quality" seismic data (reflections *B2* in Figure 9-5a) nevertheless delineate the rise of the basement top from 3 sTWT (–8 km) beneath about shot point Altendorf toward the south, where it breaks surface between shot points Valens and Kunkels. Between Valens and Kunkels the basement-cover contact is actually outcropping in the tectonic window of Vättis In contrast to the seismic sections from central Switzerland (line C1, Figure 11-6 a, and Figures 9-13 and 9-14) the Aar massif basement is not seen to override Mesozoic foreland sediments in line E1.

Theshallower groupof reflections (*J* in Figure 9-5a), extending from the northern end of the line (at 1.2 s) to Azmoos, can readily be correlated with the upper and lower interface of Jurassic limestones between the Glarus and Säntis thrusts, i. e. within the Lower Glarus Nappe complex of the Helvetic nappes. The Lower Glarus Nappe complex consists of a series of imbricate thrust sheets grading into folds south of Azmoos (Helbling, 1938; Pfiffner, 1993). The interpretation given in the geologic cross section of Figure 9-8a is a downplunge projection of the surface data outcropping some 10 km farther to the west combined with 3D seismic modeling (Stäuble & Pfiffner 1993).

The basal thrust of the Helvetic nappes, the famous Glarus Thrust (see Funk et al. (1983) for a historic review), is expected immediately below these Jurassic rocks. It puts Permian red beds ("Verrucano") on top of Tertiary North-Helvetic Flysch with a displacement of about 50 km (Pfiffner, 1985) to the west of the line. It is likely that there is no Permian at the base of the Helvetic nappes because going east the basal detachment steps up from the Permian to a higher detachment level (see Pfiffner, 1993). In the transect studied the thrust possibly puts shaly Early Jurassic onto shaly-sandy Tertiary and might, therefore, not express itself seismically.

The few reflections (*Cr* in Figure 9-5a) between 0 and 1.2 s obtained from the Cretaceous limestones and marls of the Upper Glarus Nappe complex or Säntis nappe are difficult to relate to the internal structure of this thrust sheet. The poorer quality of the near-surface data can be attributed to the fact that imaging such shallow structures was not the aim of the seismic experiment. The Tertiary sediments underlying the Helvetic nappes show two types of reflection patterns: numerous short reflections in the north and a more or less transparent section in the south. The boundary between the reflective and the

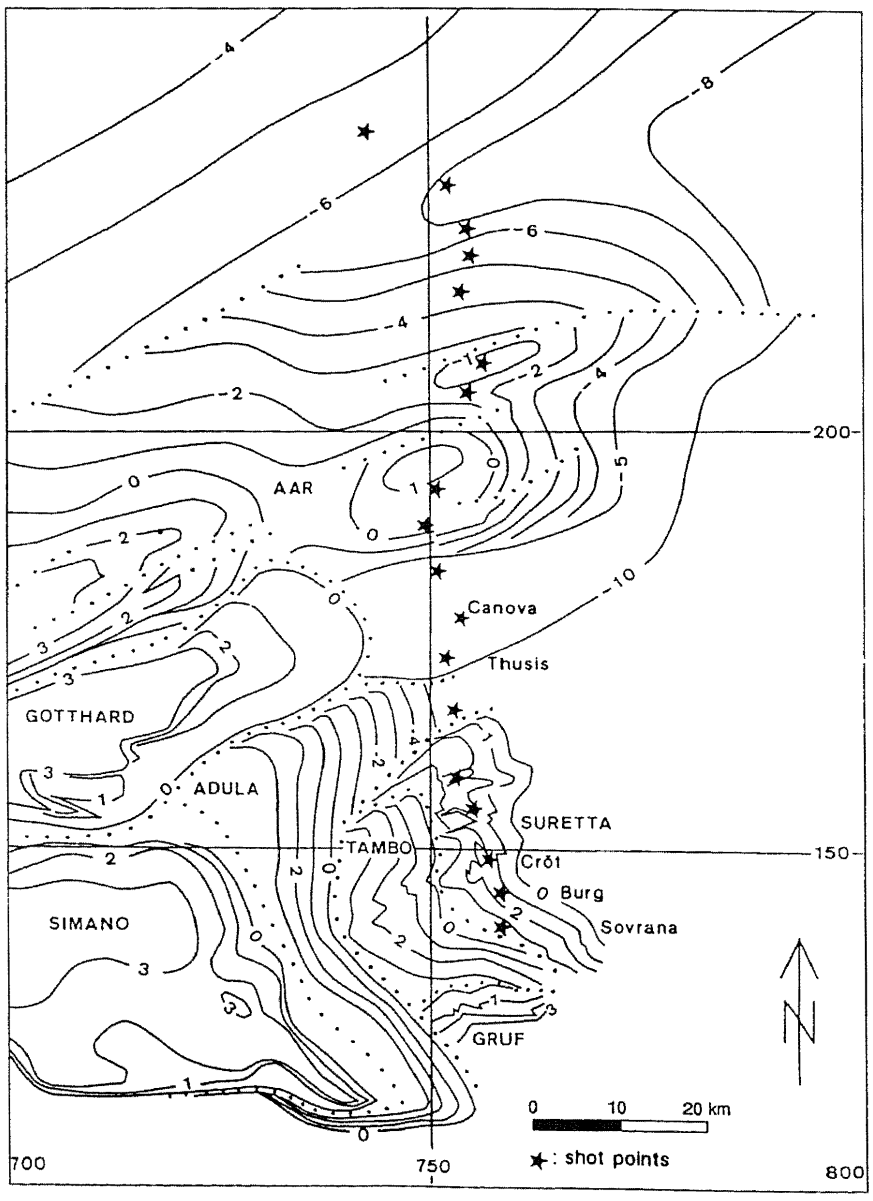

Figure 9-6
Structure contour map of "top crystalline basement" contact based on surface data (from Pfiffner et al. 1990a). Initial model. Stars denote shot points of explosion seismic data of line E1. Note bumby surfaces and cross-dip in southern part resulting in out-of-plane reflections and energy dispersal (defocussung effects).

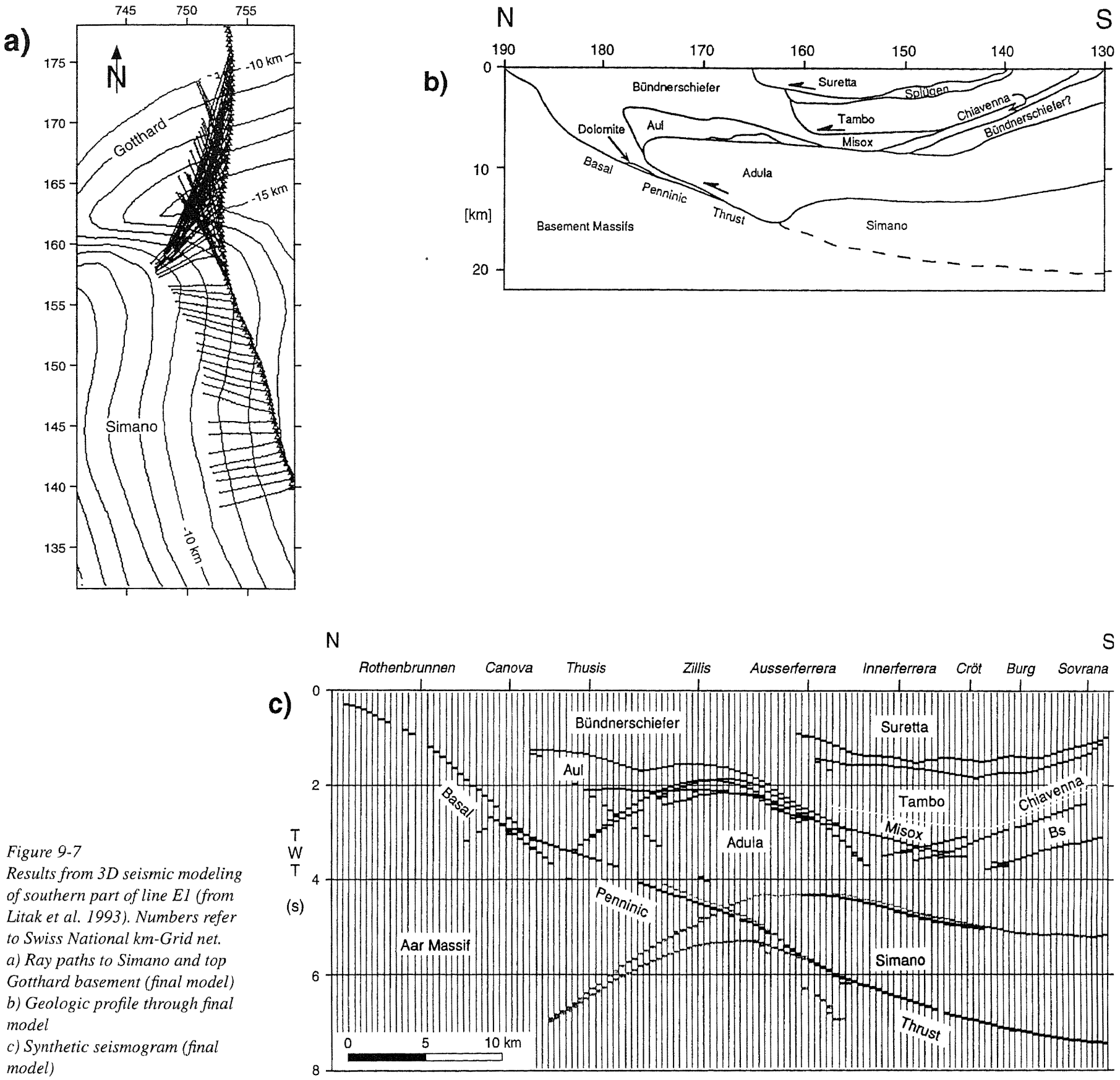

Figure 9-7
Results from 3D seismic modeling of southern part of line E1 (from Litak et al. 1993). Numbers refer to Swiss National km-Grid net.
a) Ray paths to Simano and top Gotthard basement (final model)
b) Geologic profile through final model
c) Synthetic seismogram (final model)

transparent domain is tentatively interpreted as the boundary between the UMM beds of the sub-Alpine Molasse and the North-Helvetic Flysch, as indicated by the different ornaments in Figure 9-8a. The reflective nature of the Molasse can be attributed to its lithologic character: basal turbiditic fan deposits, overlain by fine-grained deposits (shales and shaly marls) grading into a sandy and conglomeratic sequence that characterizes the Oligocene Lower Marine Molasse ("UMM" (Diem, 1986)). The repeated change from fine-grained to coarser-grained sediments at various scales may account for the generally reflective nature of the seismic section. In addition to sedimentary intercalations, tectonic imbrications known to exist farther north at the surface are expected to cause repetitions in the section studied here (see Pfiffner et al., Chapter 8). In contrast, the thick sequence of shales and sandstones of the North-Helvetic Flysch (NHF) is intensively folded (Siegenthaler, 1974), which may explain the seismically more transparent nature of this domain. The transition from flysch to molasse-type sediments is gradual in lithology, age, and location of the depocenter (e. g. Siegenthaler, 1974; Pfiffner, 1986) and therefore unlikely to produce a sharp change in the reflection pattern. In order to balance the shortened Sub-Alpine Molasse section situated farther north, a substantial amount of bedlength of Mesozoic carbonates has to be postulated in the area of the section studied. The structure of the contact between flysch and molasse in the geologic section of Figure 9-8a is intended to account for this. This point is further discussed in more detail by Pfiffner et al. in Chapter 13.1.

The interpretation of the **shallow structures in the south** is more difficult, and in some instances more than one interpretation is plausible and. Hence three models were discussed by Pfiffner et al. (1990b), who based the interpretation on the projection of surface data. Structure contour maps proved to be particularly useful in this context. The interpretation was refined subsequently. First a careful analysis of impedance contrasts based on laboratory measurements (Sellami et al. 1990) and local structure (Pfiffner et al. 1991) was undertaken. The main conclusion which could be drawn from those studies is that very good candidates for potential reflectors are Mesozoic carbonates found as thin layers sandwiched between crystalline basement blocks or within Mesozoic calcareous micaschists (Bündnerschiefer). Finally 3D seismic modeling (Litak et al. 1993) demonstrated the effects of plunging structures and improved the geometric model quantitatively. In Figure 9-7a the lateral offset between the reflection points and the seismic midpoints is about 5 km for the top of the Simano and Gotthard basement blocks. The synthetic spike seismic section shown in Figure 9-7c is derived from the "final" model displayed in 9-7b and matches many of the reflections observable in the seismic line E1 (Figure 9-2 or 9-5a).
The discussion of the individual reflection groups will proceed from top to bottom. Outcropping from south of Zillis to the southern end of the line is the Suretta nappe, a thrust sheet composed essentially of basement rocks topped by a thin cover of Mesozoic quartzites and carbonates (e. g. Milnes and Schmutz, 1978) discussed by Schmid et al. in Chapter 14. At its base the Suretta nappe overlies Mesozoic carbonates of the Splügen zone, which

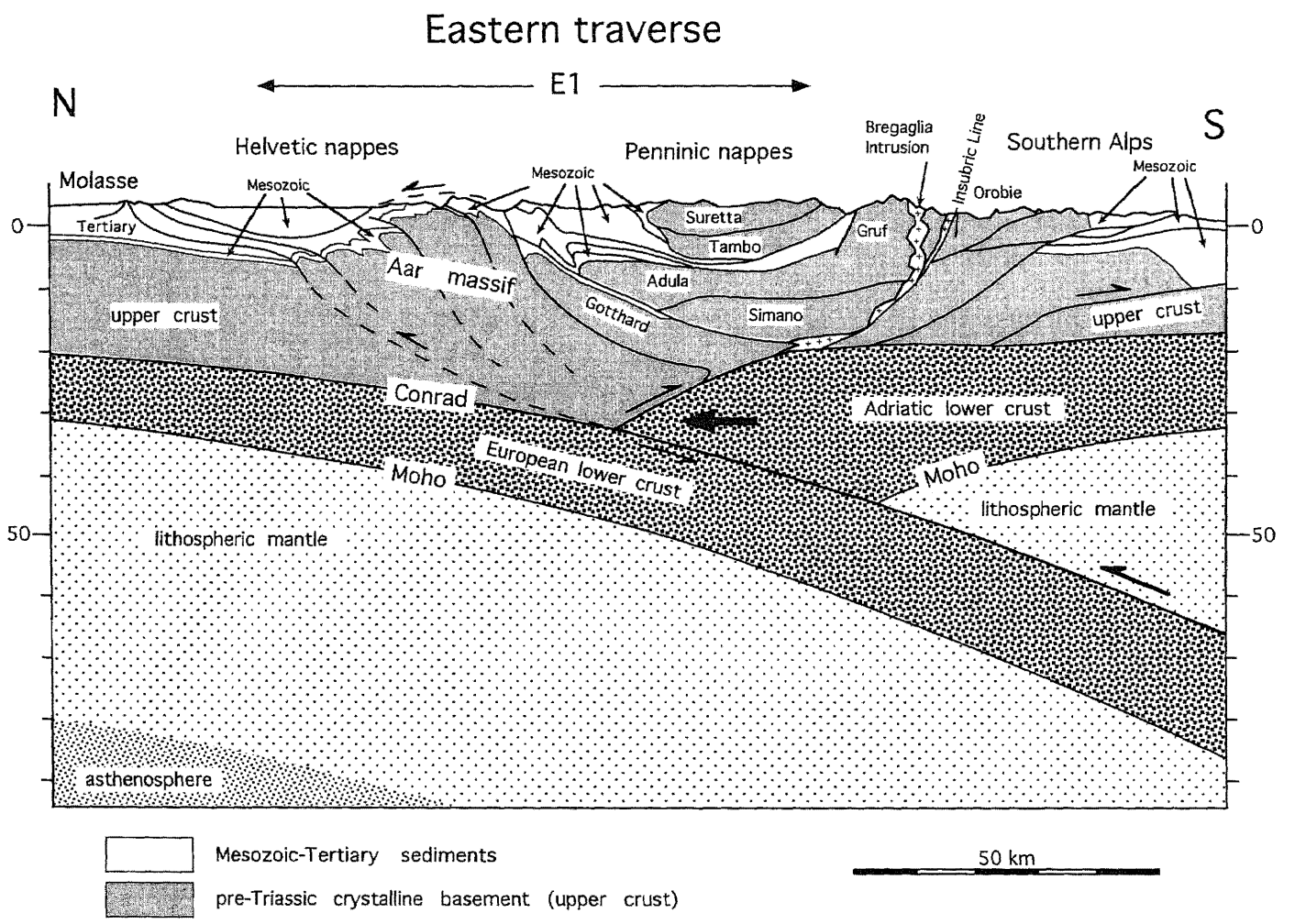

Figure 9-8
General geologic profile across the Alpine orogen, drawn along the trace of line E1, but expanded northwards into the Molasse Basin and southwards into the Po Basin. The profile displays the bivergent stacking of upper crustal flakes and the asymmetric subduction of European lower crust and mantle under the Adriatic plate.

represents a 10- to 500-m-thick layer that extends over a distance of more than 20 km. This Splügen zone can be subdivided into a lower part which represents the autochthonous cover of the Tambo basement and an upper part consisting of slices of allochthonous units (Blanc, 1965; Strohbach, 1965). Considering the regional axial plunges (cf. Pfiffner et al., 1990a), the reflections S*p* in Figure 9-5a at 1 s beneath sovrana extending to the north can readily be correlated with the Splügen zone. Using partial stacks of near-offset traces Pfiffner et al. (1991) could identify individual reflections from the top and the base of the Splügen zone, as well as contacts between ortho- and paragneisses. To the north the base of the Suretta nappe is known to steepen and reaches the surface south of Zillis. Down-plunge projections suggest that reflection S*b* originates from the base of the Suretta nappe.This nappe also contains Triassic carbonates (called "internal Trias" by Milnes and Schmutz (1978)) which form a more or less continuous band separating two basement units within the Suretta nappe and which is the probable source of the reflections S*i* at 1 s beneath Cröt.

The next unit down, the Tambo nappe, consists almost exclusively of basement rocks. It overlies the Misox zone, a thin layer of Mesozoic carbonates and schists which also contain lenses of basement rocks and ophiolitic material (metabasalts). The Misox zone is expected to lie at about 3 s beneath Cröt. Further south it rises toward the surface to overlie the Chiavenna Ophiolites (Schmutz, 1976) 10 km south of Sovrana. The Chiavenna ophiolite body is likely to be triangular shaped in a vertical cross section, but its shape is poorly constrained by surface data. As Schmutz (1976) was able to show, this ophiolite body is in an inverted position. Its northern continuation is likely to be found in the Misox zone, and thus it is possible that the Chiavenna ophiolite body overlies Mesozoic sediments, being responsible for reflection group *Ch* (see also geologic cross section of Figure 9-8a).

The Misox zone widens to the north, being composed of a number of thrust sheets of cover rocks (Gansser, 1937; Nabholz, 1945). The two topmost units, the Tomül and Grava nappes, comprise a thick monotonous sequence of argillaceous to sandy to calcareous sediments, which are called Bündnerschiefer (Nabholz, 1945; Jäckli, 1941, 1944). At their interface, the base of the Tomül unit, consists of a more or less continuous layer made up of a mélange containing carbonates overlain by ophiolitic rocks. This layer is likely to produce reflection group *G* in Figure 9-5a, which is also picked up in line E2 (see Figure 9-11). On line E2, which intersects E1 near shot point Thusis, reflection group *G* has an easterly dip (see also section 9.3). Reflection group *Au* just beneath is likely to stem from the top of the Aul thrust sheet, which consists of massive carbonates interlayered with ophiolitic rocks and which underlies Grava Bündnerschiefer.

The underlying Adula nappe consists of basement rocks topped by remnants of Triassic quartzites and carbonates. Projections of surface data (Pfiffner et al., 1990) 20 km (!) west of the seismic line place the top of the Adula nappe at around 2 s beneath Zillis and 3 s beneath Cröt. The reflections *Ad* observed at these places are thus interpreted as defining this boundary, an interpretation which is consistent with the 3D modeling results by Litak et al. (1993). To the south of the profile the Adula nappe steepens to form large-scale south facing antiforms (see Schmid et al., Chapter 22). The northerly dip of the reflection group *Ad* at 2.7 s beneath Sovrana is an indication of this steepening. Northward the situation is less clear. The Adula nappe has a steep frontal zone, similar to the Tambo and Suretta nappes (see Figure 9-6). But the Adula frontal zone does not have a constant trend and axial projection can thus only place it somewhere between shot points Thusis and Canova. The interpretation shown in Figures 9-5a and 9-8a are consistent with the observed reflections in line E2 (*Ad* in Figure 9-11), which suggests the front to be north of Thusis. According to our interpretation there are a number of reflections within the interior of the Adula nappe (*Adi* in Figure 9-5a). These might arise from strongly foliated paragneisses, contacts between paragneisses and tabular shaped Late-Variscan orthogneisses, and/or thin slabs of Mesozoic (?) carbonates contained within the Adula basement. All of these contacts and the foliation are subparallel to the top of the Adula nappe (see Pfiffner et al., 1990a, and references therein), similar to the reflection pattern, but we refrain from identifying any particular reflection in view of the uncertainties and the considerable projection distance.

The contact between the Adula nappe and the underlying Simano nappe is characterized by a thin zone of Mesozoic amphibolite grade carbonates and schists that thin southward, making the identification of the two nappes very difficult. Projection of surface data (Pfiffner et al., 1990a) places the top of the Simano nappe between 4 and 5 s beneath Ausserferrera-Sovrana and is thus correlated with reflection group *B4*. The Simano nappe is taken to encompass the underlying Leventina granite-gneiss, from which it is separated by small lenses of carbonates in the extreme south and north. To the north the Simano nappe is separated from the Lucomagno basement by the tight Molare syncline, and the Lucomagno basement is in turn separated from the Gotthard massif basement by the steeply dipping Piora zone. Following Milnes (1974), the Gotthard, Lucomagno, and Simano-Leventina basement blocks can be viewed as a single basement complex, the "Subpennine complex." The structural relationships between these basement blocks are observed at outcrop almost 50 km west of the seismic line. It is doubtful that these structures can be projected as far east as the seismic profile, and if so, cylindrical projection has certainly approached its limit (see Pfiffner, 1978, for an evaluation of the lateral continuity of folds and thrust sheets in the adjoining Helvetic zone).

The uncertainty of lateral continuity applies also for the Gotthard massif and the Tavetsch massif. The relevant question for the interpretation of the seismic data is whether or not a subsurface continuation of these basement massifs is to be expected into the area crossed by the seismic profile. The Tavetsch massif is a 5-km-thick sliver of basement rocks situated between the Aar massif and the Gotthard massif. It thins out to the east and represents the original substratum of the Axen nappe of the Helvetic nappes (see Trümpy, 1969). Both units are observed at outcrop 30 km west of the seismic profile.

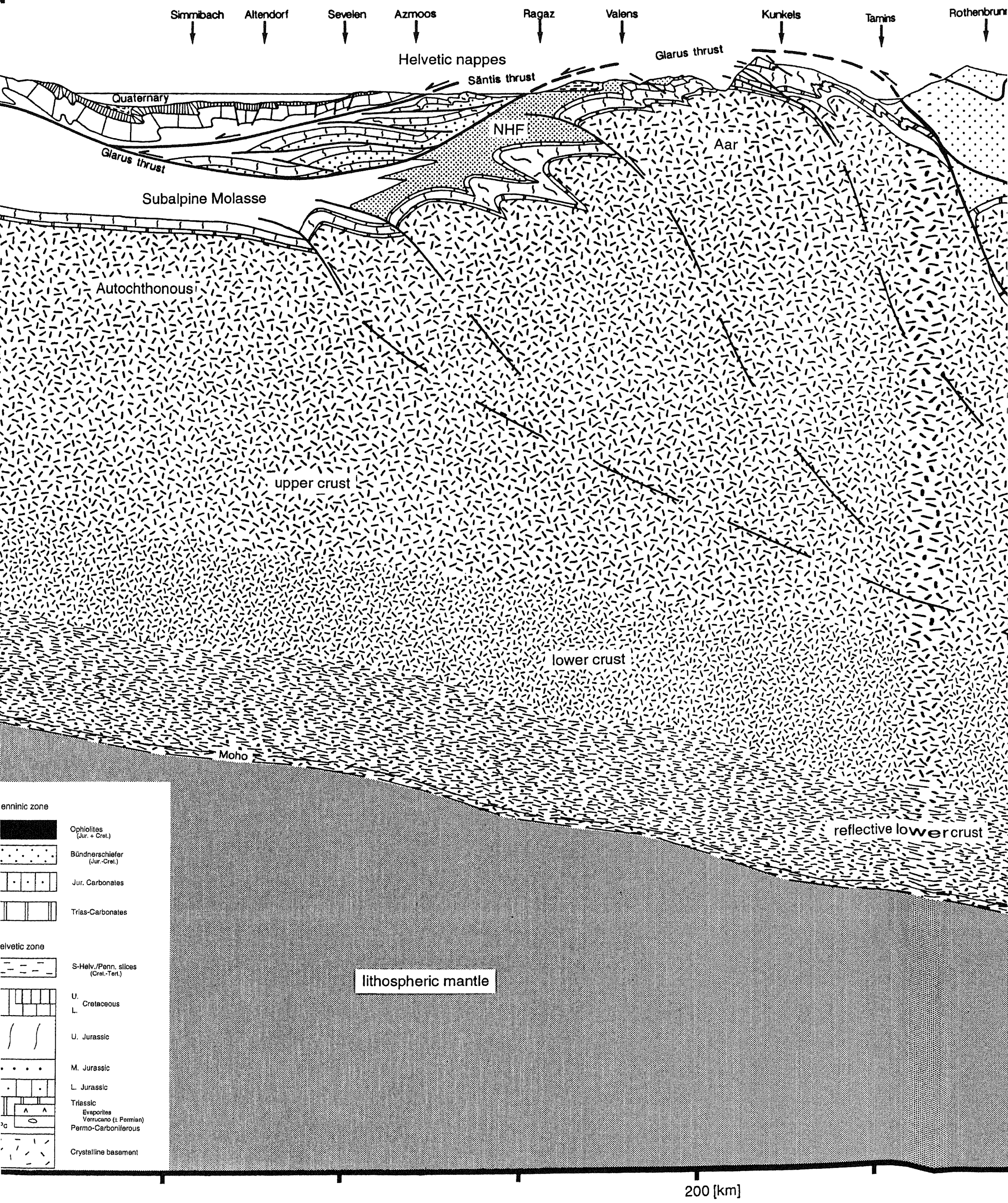

8a

profile along line E1 (drawn on km 755 of Swiss National Grid net) obtained from the combined interpretation of Vibroseis and explosionre-flection ata, and refraction seismic data. The profile is a vertical cross section through the final model obtained from 3D seismic modeling.

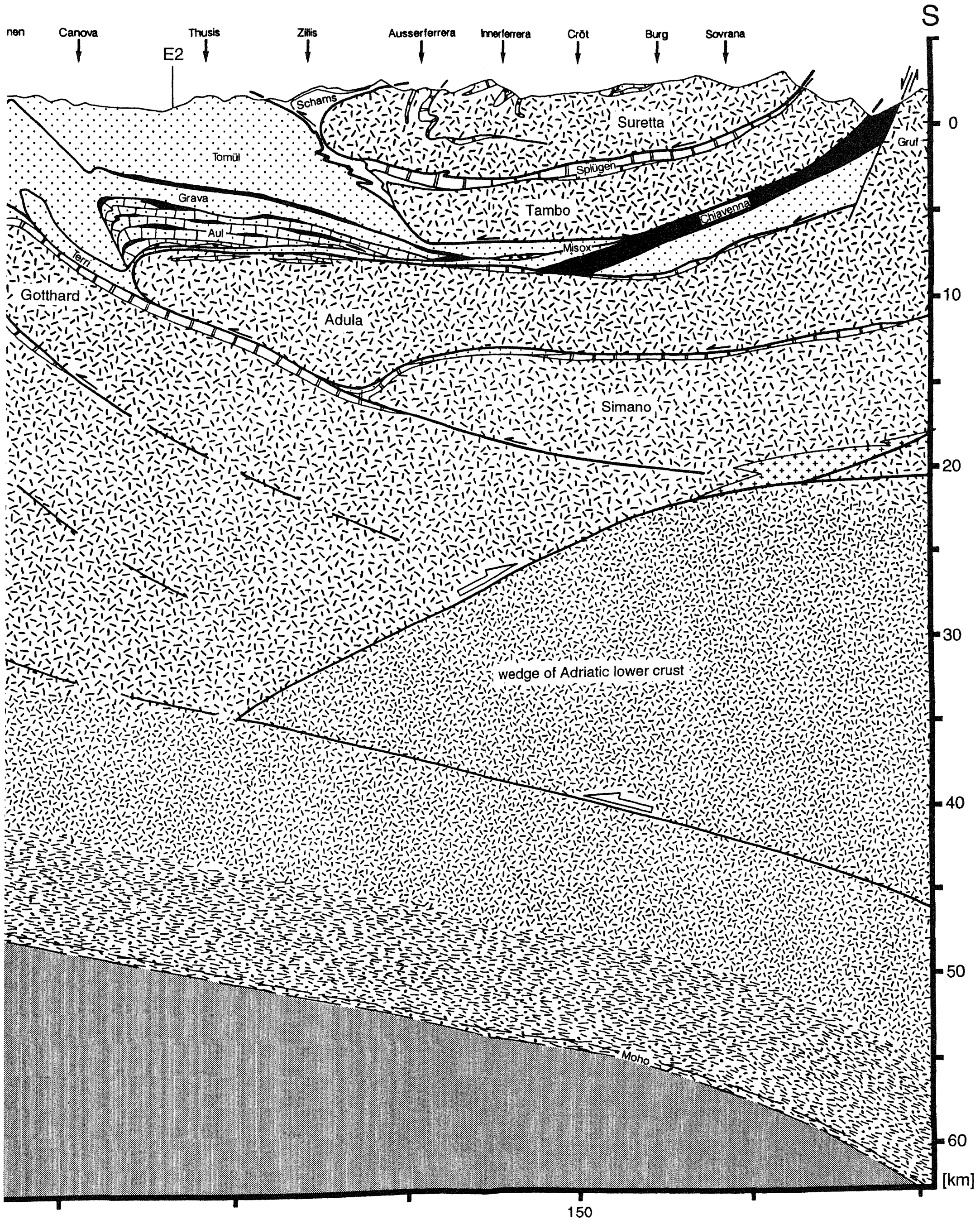
S
nen
Canova
E2
Thusis
Zillis
Ausserferrera
Innerferrera
Cröt
Burg
Sovrana
Schams
Suretta
Gruf
Tomül
Splügen
Grava
Tambo
Chiavenna
Aul
Misox
Terri
Gotthard
Adula
Simano
wedge of Adriatic lower crust
Moho
0
10
20
30
40
50
60
[km]
150

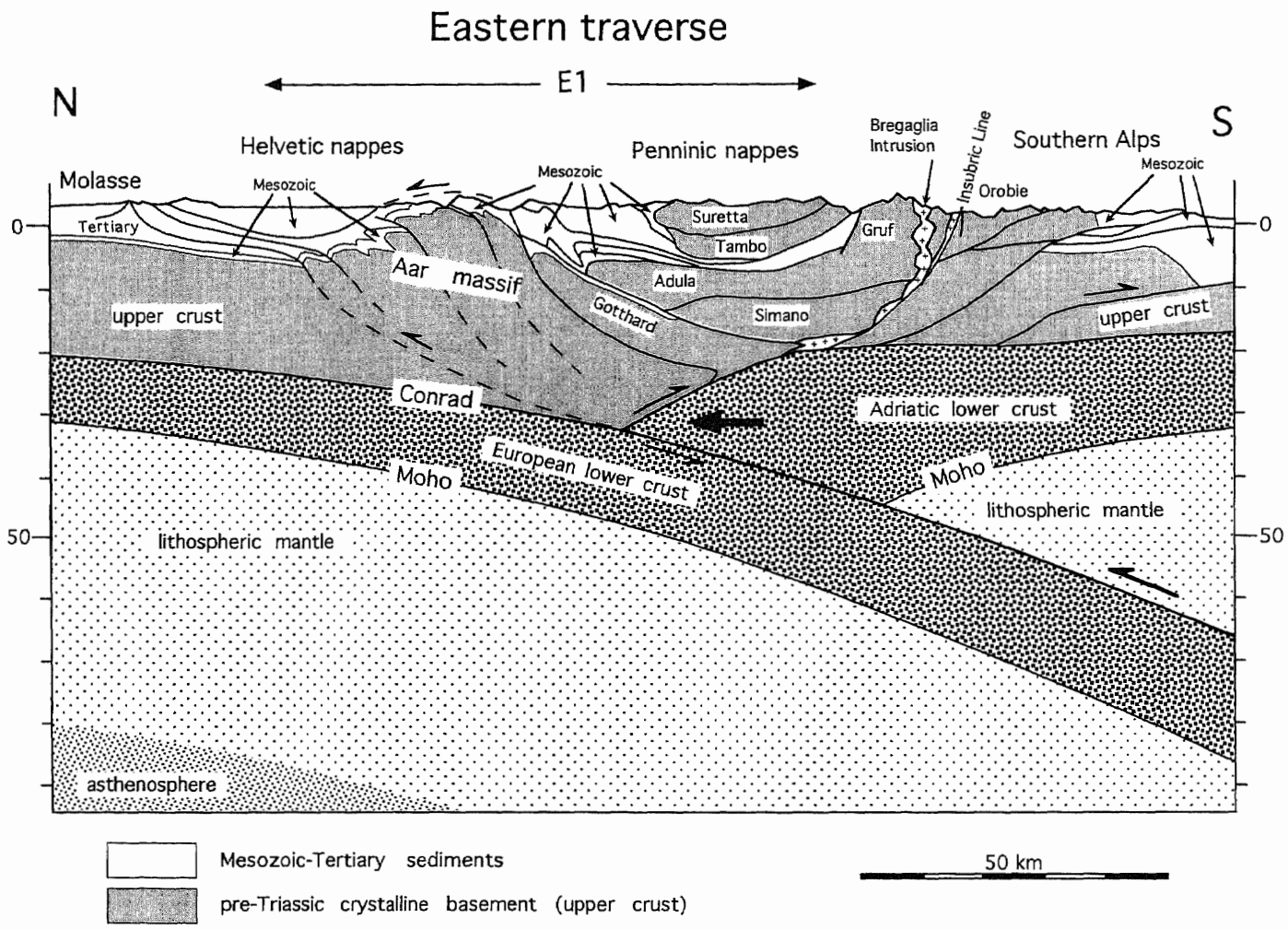

Figure 9-8
General geologic profile across the Alpine orogen, drawn along the trace of line E1, but expanded northwards into the Molasse Basin and southwards into the Po Basin. The profile displays the bivergent stacking of upper crustal flakes and the asymmetric subduction of European lower crust and mantle under the Adriatic plate.

represents a 10- to 500-m-thick layer that extends over a distance of more than 20 km. This Splügen zone can be subdivided into a lower part which represents the autochthonous cover of the Tambo basement and an upper part consisting of slices of allochthonous units (Blanc, 1965; Strohbach, 1965). Considering the regional axial plunges (cf. Pfiffner et al., 1990a), the reflections S*p* in Figure 9-5a at 1 s beneath sovrana extending to the north can readily be correlated with the Splügen zone. Using partial stacks of near-offset traces Pfiffner et al. (1991) could identify individual reflections from the top and the base of the Splügen zone, as well as contacts between ortho- and paragneisses. To the north the base of the Suretta nappe is known to steepen and reaches the surface south of Zillis. Down-plunge projections suggest that reflection S*b* originates from the base of the Suretta nappe.This nappe also contains Triassic carbonates (called "internal Trias" by Milnes and Schmutz (1978)) which form a more or less continuous band separating two basement units within the Suretta nappe and which is the probable source of the reflections S*i* at 1 s beneath Cröt.

The next unit down, the Tambo nappe, consists almost exclusively of basement rocks. It overlies the Misox zone, a thin layer of Mesozoic carbonates and schists which also contain lenses of basement rocks and ophiolitic material (metabasalts). The Misox zone is expected to lie at about 3 s beneath Cröt. Further south it rises toward the surface to overlie the Chiavenna Ophiolites (Schmutz, 1976) 10 km south of Sovrana. The Chiavenna ophiolite body is likely to be triangular shaped in a vertical cross section, but its shape is poorly constrained by surface data. As Schmutz (1976) was able to show, this ophiolite body is in an inverted position. Its northern continuation is likely to be found in the Misox zone, and thus it is possible that the Chiavenna ophiolite body overlies Mesozoic sediments, being responsible for reflection group *Ch* (see also geologic cross section of Figure 9-8a).

The Misox zone widens to the north, being composed of a number of thrust sheets of cover rocks (Gansser, 1937; Nabholz, 1945). The two topmost units, the Tomül and Grava nappes, comprise a thick monotonous sequence of argillaceous to sandy to calcareous sediments, which are called Bündnerschiefer (Nabholz, 1945; Jäckli, 1941, 1944). At their interface, the base of the Tomül unit, consists of a more or less continuous layer made up of a mélange containing carbonates overlain by ophiolitic rocks. This layer is likely to produce reflection group *G* in Figure 9-5a, which is also picked up in line E2 (see Figure 9-11). On line E2, which intersects E1 near shot point Thusis, reflection group *G* has an easterly dip (see also section 9.3). Reflection group *Au* just beneath is likely to stem from the top of the Aul thrust sheet, which consists of massive carbonates interlayered with ophiolitic rocks and which underlies Grava Bündnerschiefer.

The underlying Adula nappe consists of basement rocks topped by remnants of Triassic quartzites and carbonates. Projections of surface data (Pfiffner et al., 1990) 20 km (!) west of the seismic line place the top of the Adula nappe at around 2 s beneath Zillis and 3 s beneath Cröt. The reflections *Ad* observed at these places are thus interpreted as defining this boundary, an interpretation which is consistent with the 3D modeling results by Litak et al. (1993). To the south of the profile the Adula nappe steepens to form large-scale south facing antiforms (see Schmid et al., Chapter 22). The northerly dip of the reflection group *Ad* at 2.7 s beneath Sovrana is an indication of this steepening. Northward the situation is less clear. The Adula nappe has a steep frontal zone, similar to the Tambo and Suretta nappes (see Figure 9-6). But the Adula frontal zone does not have a constant trend and axial projection can thus only place it somewhere between shot points Thusis and Canova. The interpretation shown in Figures 9-5a and 9-8a are consistent with the observed reflections in line E2 (*Ad* in Figure 9-11), which suggests the front to be north of Thusis. According to our interpretation there are a number of reflections within the interior of the Adula nappe (*Adi* in Figure 9-5a). These might arise from strongly foliated paragneisses, contacts between paragneisses and tabular shaped Late-Variscan orthogneisses, and/or thin slabs of Mesozoic (?) carbonates contained within the Adula basement. All of these contacts and the foliation are subparallel to the top of the Adula nappe (see Pfiffner et al., 1990a, and references therein), similar to the reflection pattern, but we refrain from identifying any particular reflection in view of the uncertainties and the considerable projection distance.

The contact between the Adula nappe and the underlying Simano nappe is characterized by a thin zone of Mesozoic amphibolite grade carbonates and schists that thin southward, making the identification of the two nappes very difficult. Projection of surface data (Pfiffner et al., 1990a) places the top of the Simano nappe between 4 and 5 s beneath Ausserferrera-Sovrana and is thus correlated with reflection group *B4*. The Simano nappe is taken to encompass the underlying Leventina granite-gneiss, from which it is separated by small lenses of carbonates in the extreme south and north. To the north the Simano nappe is separated from the Lucomagno basement by the tight Molare syncline, and the Lucomagno basement is in turn separated from the Gotthard massif basement by the steeply dipping Piora zone. Following Milnes (1974), the Gotthard, Lucomagno, and Simano-Leventina basement blocks can be viewed as a single basement complex, the "Subpennine complex." The structural relationships between these basement blocks are observed at outcrop almost 50 km west of the seismic line. It is doubtful that these structures can be projected as far east as the seismic profile, and if so, cylindrical projection has certainly approached its limit (see Pfiffner, 1978, for an evaluation of the lateral continuity of folds and thrust sheets in the adjoining Helvetic zone).

The uncertainty of lateral continuity applies also for the Gotthard massif and the Tavetsch massif. The relevant question for the interpretation of the seismic data is whether or not a subsurface continuation of these basement massifs is to be expected into the area crossed by the seismic profile. The Tavetsch massif is a 5-km-thick sliver of basement rocks situated between the Aar massif and the Gotthard massif. It thins out to the east and represents the original substratum of the Axen nappe of the Helvetic nappes (see Trümpy, 1969). Both units are observed at outcrop 30 km west of the seismic profile.

At its eastern end the Tavetsch massif cores an anticlinal structure in the Permian Verrucano unit. Its fold axis changes trend from WSW-ENE to WNW-ESE going east. In addition, the basal detachment of the Helvetic nappes steps up from the basement into the Mesozoic cover going east. It is probably situated in shaly Jurassic sequences along the seismic profile. All these points suggest that the Tavetsch massif is unlikely to be expected in the transect of the seismic profile E1 and does therefore not appear in our interpretation shown in Figure 9-8a. The Gotthard massif, on the other hand, probably represents the substratum of the higher Säntis-Drusberg nappe (Pfiffner, 1985; Wyss, 1986) and is more likely to be encountered in the E1 transect. Reflection group *B3* is thus interpreted to stem from the top of the Gotthard massif, the high density package at 3.5 sTWT beneath Thusis possibly representing slivers of Mesozoic carbonates which are known to occur at similar structural positions. This reflection package *B3* is also identifyable on line E2 (see Figure 9-11).
In line E1 reflection groups *B3* and *B4* are crossing each other. The N-dipping reflection group *B4* has been explained by back-thrusting in interpretation C of Pfiffner et al. (1990b). Similarly, N-dipping reflections observed in the western traverse have been interpreted to represent large scale backfolds by Steck et al. (Chapter 12), Escher et al. (Chapter 16) and Marchant & Stampfli (Chapter 24). We prefer an interpretation without large scale backfolding for the following reasons:
1) 3D seismic modeling by Litak et al (1993) suggest that the crossing of reflection groups *B3* and *B4* (beneath Zillis in Figure 9-5a) could equally well be part of a bow-tie structure resulting from a shallow synformal structure between Gotthard massif and Simano nappe (see Figure 9-7).
2) The top of the basement blocks (Aar, Gotthard and Penninic nappes) are affected by back-folding or back-thrusting which locally overturned some nappe contacts and early foliations. In the case of the Suretta nappe, a higher unit, back-folding produced even "south-verging" antiforms as discussed in more detail by Schmid et al. (Chapter 14). But the Bündnerschiefer units encountered along line E1 do not point to any significant back-folding. Also the back-folds affecting the top of the Gotthard basement farther west (along lines C1–C2 of the central traverse and in the Piora-Olivone area) seem to lose amplitude going east.
Thus, in Figures 9-8a and b the top of the Aar massif beneath Tamins-Rothenbrunnen is taken to dip steeply south. This geometry corresponds to the one observed in the Urseren zone farther west (see Pfiffner & Heitzmann, Chapter 11). This steep subsurface continuation of the Aar massif (south of Tamins in Figure 9-8a) is indicative of some sort of back-flow associated with shortening and uplift of the Aar massif basement block. Pfiffner et al. discuss the tectonic evolution of this external basement massif in Chapter 13.1 and emphasise that its structure varies along strike, the western part having been subjected to more extensive shortening in a late phase. We thus feel that the difference between the geologic profiles along the western and eastern traverse reflects in part a true difference in geologic structure.

The most prominent feature of the **deep structure** is the reflection band M in Figures 9-2 and 9-5a at 11–12 s TWT observed at the northern end and extending southward to greater depths (14.5-15.5 s TWT beneath Canova). Converting the refraction data (Holliger & Kissling 1991, Ye 1992) to a time section places the crust-mantle boundary at around 12.5 s TWT at the northern end of the section and at around 16 s TWT beneath Canova, i. e., the velocity jump associated with the refraction Moho corresponds to the bottom limit of the reflection band seen in the reflection experiment. As pointed out by Pfiffner et al. (1988), this reflection band might represent a transition zone from lower crustal to upper mantle velocities which would be beyond the resolution of refraction seismology. This reflection band, representing a reflective lowermost crust is apparent as far south as Thusis, where it disappears at 15–16 s TWT with a relatively steep southerly dip. As discussed in section 9.3. a similar observation can be made along strike line E2, where corresponding reflections from the lowermost crust disappear in an easterly direction. The EGT refraction experiment (Blundell et al. 1992, Ye & Ansorge 1990, Ye 1992), which runs parallel to E1 allows the refraction Moho to be traced farther south (see Figure 9-5b). The EGT refraction experiments indicate that the European Moho extends southward to greater depths and that a discontinuous crust-mantle boundary at a shallower depth just south of line E1 points to a crustal imbrication (see also Valasek et al. 1991, Ye 1992). Hereby a wedge of lower Adriatic crust was forced into the European crust, splitting it apart and delaminating it. The wedge of lower Adriatic crust reaches about as far north as Thusis along line E1 (see Figure 9-8a). Complex deformation is to be expected at the northern tip of this wedge and may lead to scattering and defocussing of reflected seismic rays. In the EGT-refraction experiment on the other hand, the European crust-mantle boundary has been sampled by undershooting this complex zone.
The sparse, discontinuous reflections at around 8–9 s TWT in the northern part of the section (**C** in Figure 9-5a) occur at an increase in refraction determined velocities (cf. Ye & Ansorge 1990; Valasek 1992; Ye 1992) from 6.2 to 6.5 km/s. An origin of these reflections due to the presence of fluids released in devolatilization reactions was evoked by Pfiffner et al. (1988). Some of these events are shorter than the diameter of the first Fresnel zone (limit of horizontal resolution) and may thus be due to diffractions from lateral inhomogeneities caused by irregularly shaped rock bodies rather than from horizontal layering. This velocity discontinuity, representing most likely the transition to the lower crust (Conrad discontinuity), can be traced southward to about shot point Thusis, i. e. the intersection point with line E2 (see section 9.3.). This point coincides also with the northern tip of the Adriatic wedge. The Conrad discontinuity, which is constrained by refraction seismic data, can be followed eastwards, a point discussed in more detail in section 9.5 of this chapter. Note that the position of this discontinuity as shown in Figures 9-8a and b differs from the one given by Marchant & Stampfli in Chapter 24 (Figure 24-7).
In the southern part of line E1 reflections at around 7 sTWT (*CA* in Figure 9-2) also coincide with a velocity discontinuity from 6.1 to 6.6 km/s (op. cit.). Farther north, beneath shot points Ausserferrera and Thusis this Adriatic Conrad dicontinuity dips steeply northward and is therefore not sampled in the reflection experiment.

9.2.3 Discussion and conclusion

Although the seismic line E1, which crosses a major part of the Alps, has considerably added to the knowledge of the deep structure of the Alps, additional insight was gained from the companion seismic lines through the Alps of western central and southern Switzerland. Thus, rather than trying to discuss the Alps as whole, the following discussion will focus on implications for which E1 is particularly relevant. But in order to place line E1 into the larger scale Alpine framework, the cross section of Figure 9-8a is expanded to the north, using the insight gained from the seismic lines E4, E5 and E6 crossing the Molasse basin, which are discussed in detail by Pfiffner et al. in Chapter 8, and to the south using cross sections through the Southern Alps by Schönborn (1992). The resulting, schematic geologic cross section in Figure 9-8b serves as basis for this short discussion. A more detailed discussion of this eastern transect is given by Schmid et al. in Chapter 22.

The Tertiary sedimentary infill of the North-Alpine Foredeep has been significantly shortened in its southern part, the Sub-Alpine Molasse (see Pfiffner et al., Chapter 8). The associated thrust faults level off at depth going southward and are most probably linked to shortening and uplift of the **Aar massif** (see Pfiffner et al., Chapter 13.1). In the cross section of Figure 9-8b this basement shortening is accomodated by a set of structures representing a combination of folding and faulting. The magnitude of the basement uplift from about 7 km below to 1 km above sea level requires a crustal-scale balance. It has to be noted that the amount of basement uplift becomes even more important in central Switzerland (see Pfiffner et al., Chapter 13.1); there shortening of the Jura Mountains is also related to the Aar massif basement uplift.
Balancing the geologic profile of Figure 9-8b (or 9-8a) suggests that bedlengths of Mesozoic strata are shortened by about 28.5 km to an actual length of 62.5 km, as measured between a point situated at the northern end of the profile and the point beneath shot point Canova on the southern flank of the Aar massif in the south. Comparing the area of structural relief defined by the Aar massif bulge to the curvimetric shortening of the Mesozoic strata suggests a detachment of the Aar massif at some 12 km below the basement top. Going down these 12 km from the southern flank of the Aar massif puts the detachment level at the top of the Adriatic wedge. It is thus plausible that the thrust fault at the base of the Adriatic wedge which must extend northward and upward because of its significant displacement, is kinematically linked to the basal detachment of the Aar massif. It could be envisaged that the imbricate structure of the Aar massif evolved in sequence, i. e. propagated northward at the tip of the Adriatic wedge. The north-dipping thrust fault at the top of this wedge is kinematically linked to basement shortening in the Southern Alps (with south-directed thrusting of Miocene age) and to Oligo-Miocene steep south-directed thrusting on the Insubric Line. Comparing the uplift history of the Aar massif (Pfiffner et al., Chapter 13.1) and the Insubric Line (Schmid et al., Chapter 22), and considering that shortening of the Aar massif is kinematically linked to shortening of the Sub-Alpine Molasse which contains Early Miocene sediments, it follows that in Oligocene/ Miocene times, both Aar massif and Insubric Line were sites of rapid uplift under ductile conditions. On the other hand much of the northward movement of the tip of the wedge is probably related to Late Miocene shortening in the Southern Alps. It thus follows that uplift of the Aar massif and along the Insubric line in this transect of the Alps was coeval and occurred as a pop-up structure, bordered by conjugate thrust faults, and that it took place at some distance ahead of the northward moving Adriatic wedge.

Inspection of the **Penninic nappes** shown in Figure 9-8b reveals that the upper crustal basement nappes form a four (or more) fold stack and thus require a substantial volume of lower crust for reasons of volumetric balancing. This volume is apparently not available in this cross section. Instead, one is forced to conclude that lower crustal material has been subducted. Subduction of lower crust has already been postulated by Laubscher & Bernoulli (1982) and Trümpy (1988). An accurate mass balance is, however, rendered difficult for the following reasons:

1. Unlike the Helvetic zone, where nappe transport was directed approximately south to north (Pfiffner, 1981, 1985), in the Penninic zone transport directions were less regular and include E-W components (see Schmid et al., Chapter 14) i. e., in and out of the section plane.
2. The thickness of the crust prior to Alpine orogeny is not yet well constrained, but it is likely that the crust had been thinned during Mesozoic rifting associated with the formation of the Tethys ocean.
3. The Moho may not behave purely as a passive interface but rather may undergo postorogenic "ordering processes" (Trappe et al., 1988). This point is particularly important for those parts of the Alps which underwent the Cretaceous to Eocene orogenic phases (Penninic, Austroalpine, and South-Alpine domains). It is possibly less relevant for the European crust of the Helvetic zone which was mainly deformed in Oligocene-Miocene times.
4. An accurate material balance should incorporate effects associated with the complex metamorphic history of the rocks involved (e. g., high-pressure metamorphism in the Adula nappe) and of the geometry of the subduction suture which is truncated by the Insubric Line near the Bergell Intrusion but which must have a continuation at depth.

The Penninic basement nappes shown in Figure 9-8b are each about 5 km thick. Considering the nappe-internal strain and structure, the original thicknesses can be estimated at 4 km (Suretta), 8 km (Tambo), 5-15 km (Adula), 15 km (Simano), which compares with the depth-to-detachment of the Gotthard (10 km) and the one derived for the Aar massif (12 km). Surface observations suggest that the geometry of these basement nappes are often controlled by lithologic contrasts, late-Variscan granitoid bodies often marking the front of such nappes. The base of these nappes, where the detachment horizon was sub-parallel to the overlying Mesozoic cover rocks, are not obviously related to lithologic contacts. Considering the evolution of the thrust belt it may be argued that the detachment level rather is controlled by temperature (weakening quartz e. g.), pressure and/or weakening due to fluid release.

In a general way **crustal shortening** within the European plate thus can be envisaged as an imbrication of upper crustal flakes detached along or slightly above the Conrad discontinuity in response to the northward moving Adriatic wedge. The lower European crust was subducted, i. e. overriden by the Adriatic wedge. Crustal thickening is thus essentially due to thickened, imbricated upper crust. The lower crust, however, also thickens slightly across line E1 according to the velocity analyses by Valasek (1992) and Ye (1992). This thickness increase is shown schematically in the geologic profile of Figure 9-8b. The southern, overriden part of this lower crust represents the substratum of the upper crustal flakes that now form the Penninic basement nappes. The latter in turn form the substratum of the Penninic cover nappes. As discussed by Schmid et al. in Chapter 14, however, this part of the European crust was stretched and thinned during the Mesozoic. These seemingly contradicting observations could be explained by shortening and imbrication of thinned lower crustal units in the footwall of the Adriatic wedge. There are, however, no reflections discernible which would highlight structures associated with this underplating.

A structure with south-directed thrusting and imbrication exists in the Southern Alps (see Schumacher et al., Chapters 10 and15, and Schmid et al. Chapter 22). Some of the north-dipping reflections beneath shot point Sovrana might in fact stem from ductile shear zones associated with South-Alpine basement flakes. On line C3 (Pfiffner & Heitzmann, Chapter 11) distinct south-dipping reflections are recognized that are likely to stem from South-Alpine thrust faults. In contrast to the northern, European part, the Adriatic lower crust beneath the Southern Alps is also thickened. This is evident from Figure 9-5b, where the top of the **Adriatic wedge**, or more precisely, the Conrad discontinuity forms a bulge. Reflections beneath reflection group *N* in Figure 9-5a are from within the Adriatic wedge and may well be related to its shortening. In any case the wedge of Adriatic lower crust which was forced into the European crust in the late stages of the Alpine collision was internally deformed. Complex deformation within the tip of the wedge may defocus and scatter seismic rays, which may explain the southward disappearance of reflections from the lowermost European crust in the near-vertical seismic profiling. The wedge overrode a slab of lower European crust in the process of collsion, peeling off and shortening the upper crust. The latter's internal deformation occurred at least in part some distance ahead of the tip of the wedge.

9.3 Interpretation of line E2: The crustal structure along strike in the eastern Swiss Alps

L. Hitz & O. A. Pfiffner

In this part of chapter 9, results of a deep seismic reflection survey located in the eastern Swiss Alps are presented. The survey was carried out in 1990 and consists of Vibroseis and dynamite recordings. The composite transect is termed E2. In contrast to the majority of the NRP 20 profiles which were recorded perpendicular to the Alpine strike, the profile E2 was recorded from WSW to ENE, parallel to the Alpine strike. It runs from Thusis to just E of Scuol in the Lower Engadine Valley (Figure 9-9b). At Thusis, line E2 intersects with line E1 (Figure 9-1) and near Scuol it intersects with line E3 (Figure 9-15) providing thus a lateral connection to the N-S trending E1 and E3 profiles as well as to the fan profiles E7 to E9. In addition, the earlier acquired seismic refraction profile ALP75 (Alpine Longitudinal Profile, Figure 9-9a) is oriented parallel to line E2. Its results are integrated in the interpretation of line E2.

9.3.1 The data

Profile E2 consists of a 21 km long Vibroseis line and an overlapping 70 km long dynamite line. Vibroseis recordings with a penetration to approximately 6 s cover the western third of the transect.

The processed dynamite and Vibroseis sections are shown in Plates 9-3 and 9-4. Both lines show a rather poor data quality for several reasons. First, the lines had to follow narrow valleys with high traffic density and railways, which results in a high ambient noise level and in a decrease of the signal/noise ratio. Second, the source energy was low, especially in the Vibroseis measurements with only 1 sweep/vibration point. Third and probably most important, the crustal structure of the Alps in N-S transects is complex with steeply N- and partly also S-dipping reflectors. The consequence of this for a seismic strike-line is strong energy scattering and the presence of out-of-plane reflections both contributing to poor data quality. Nevertheless, coherent reflected energy can be observed in both data sets. The E2 dynamite data (see Plate 9-3) are characterized by several distinctive reflection bands from

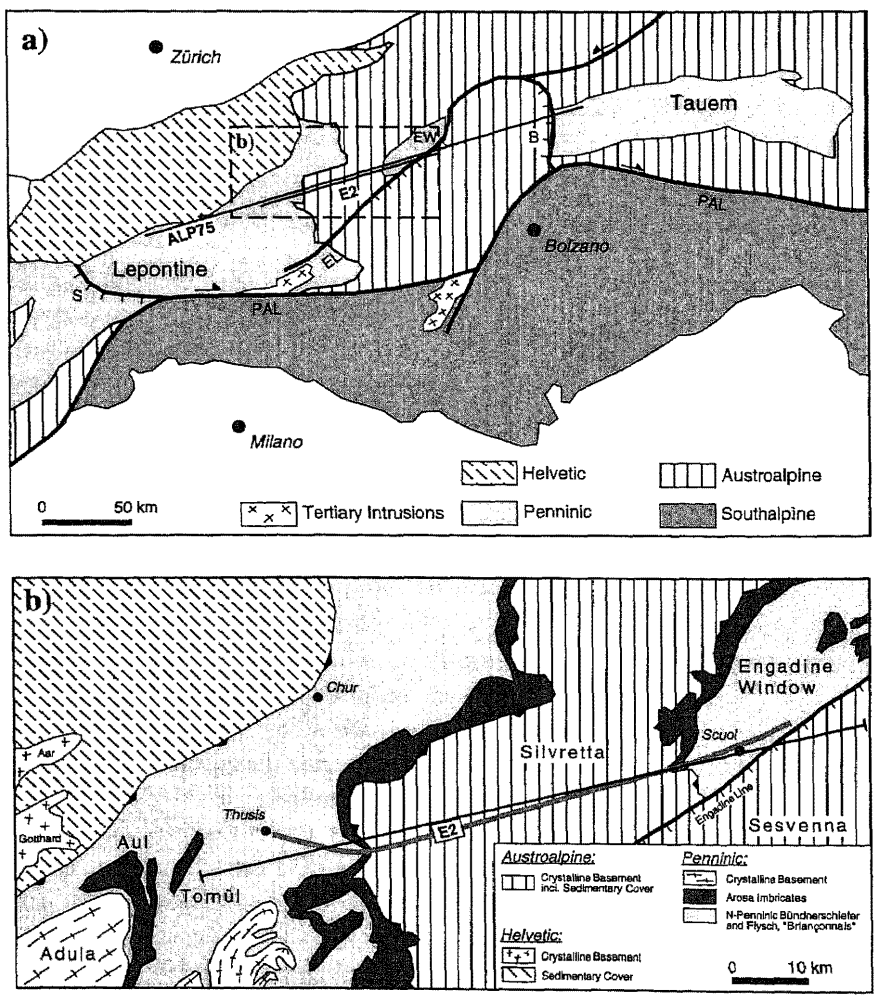

Figure 9-9
Location maps. (a) Simplified geological map of the Alps showing the locations of the E2 seismic reflection profile and the central part of the ALP75 seismic refraction profile (cf. Yan & Mechie 1989). PAL = Periadriatic lineament, EL = Engadine line, B = Brenner line, S = Simplon line, EW = Engadine window. (b) Enlarged area of (a) showing the location of the E2 processing line (dashed line) and the trace of the geological cross-section of Figure 9-12 (solid straight line).

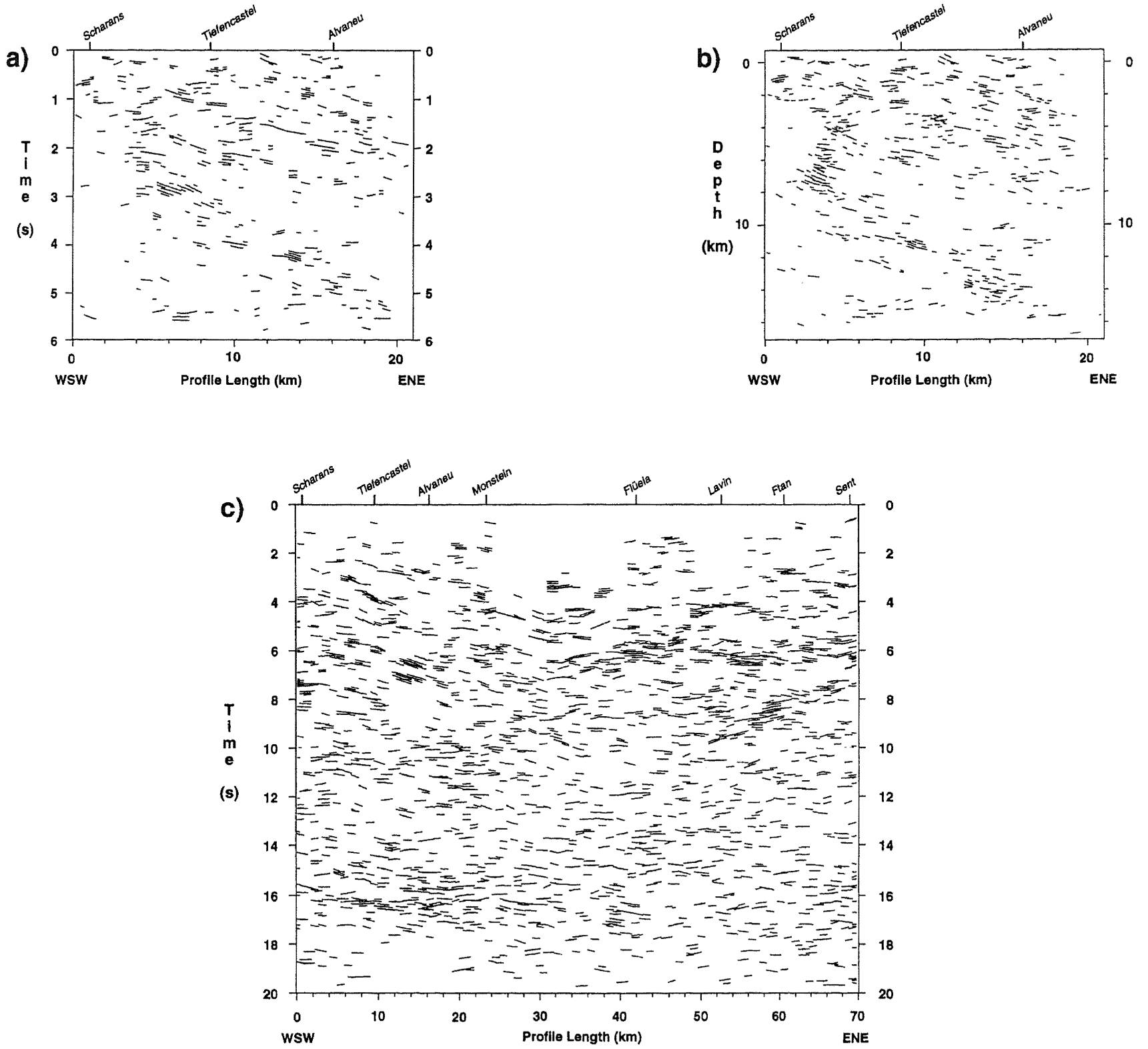

Figure 9-10
Automatic line drawings (cf. Valasek 1992) of E2 Vibroseis and E2 dynamite data. (a) E2 Vibroseis unmigrated. (b) E2 Vibroseis depth-migrated. (c) E2 dynamite unmigrated. (d) E2 dynamite depth-migrated. Horizontal to vertical scale = 1:1.
Note the increase in the dynamite profile length due to updip migration of dipping line elements.

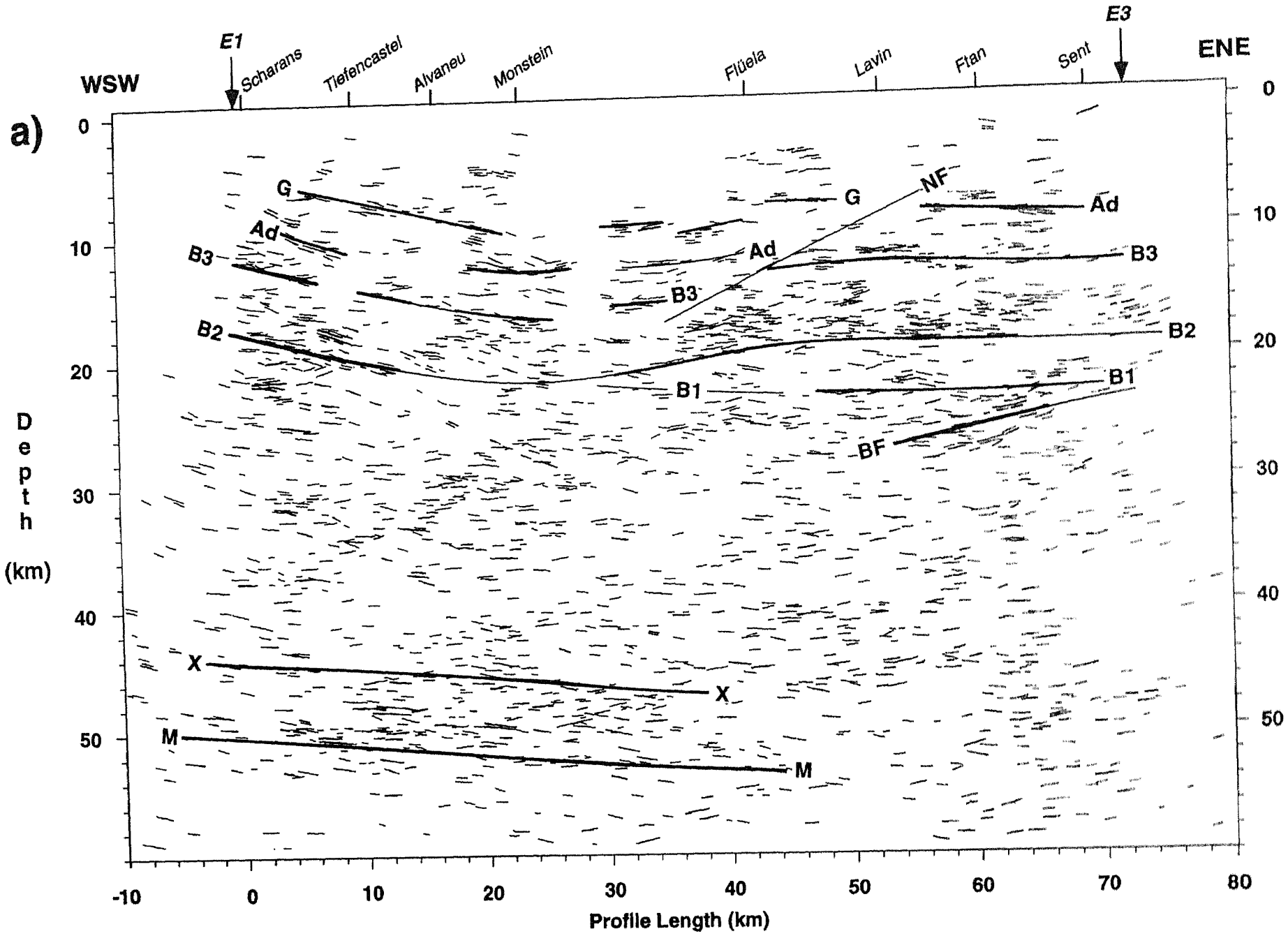

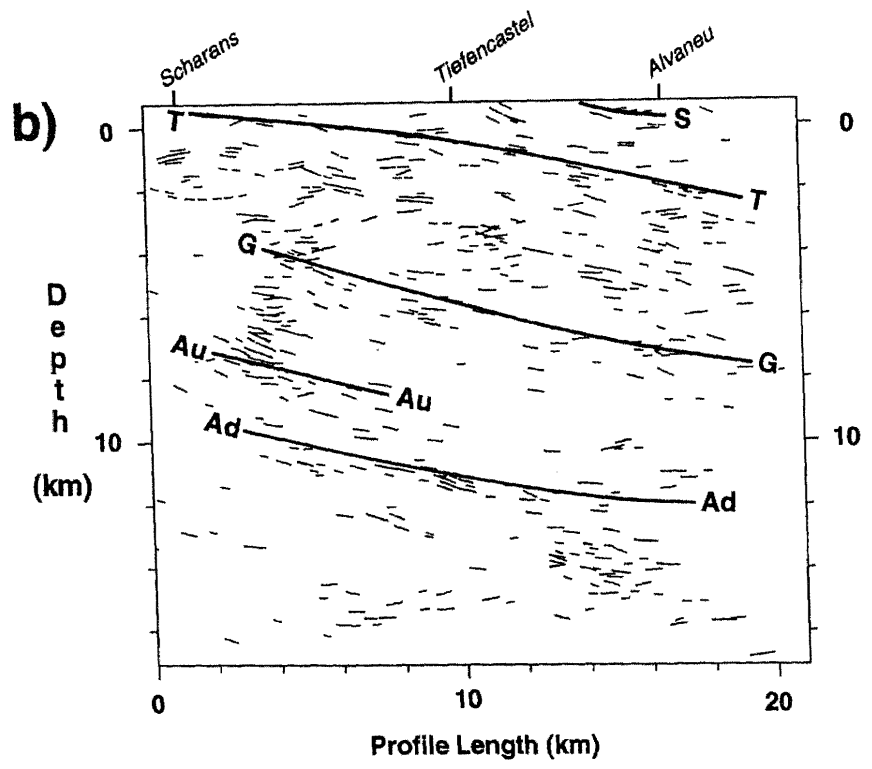

Figure 9-11
Interpretation of (a) E2 dynamite and (b) E2 Vibroseis depth-migrated line drawings. Thick lines correspond to clearly coherent reflection groups, thin lines to less "certain" reflection groups. Horizontal to vertical scale = 1:1. S = base Silvretta nappe, T = top Tomül thrust sheet, G = top Grava thrust sheet, Au = top Aul thrust sheet, Ad = top N-Penninic basement (Adula), B3 = top S-Helvetic basement (Gotthard), B2 = top Helvetic basement (Aar), B1 = top local Helvetic basement slice, NF = low-angle normal fault, BF = Brenner mylonites, X = top reflective lower crust, M = base reflective lower crust (Moho).

1 to about 9 s. The reflection geometry is characterized by a general change in reflection-dip between shotpoints Monstein and Flüela. To the west of this area, reflections predominantly dip to the E, whereas they are subhorizontal to W-dipping to the east. Below 9 s reflectivity is predominantly incoherent with the exception of a 1.5 to 2 s thick reflection band in the W starting at approximately 15 s. The E2 Vibroseis data (see Plate 9-4) show a reflective upper crust to a depth of approximately 6 s. As deeper reflection packages are encountered in the dynamite section, but are not visible in the Vibroseis line, the lack of coherent reflectivity below 6 s is attributed to the low signal strength. On the Vibroseis section several more or less coherent reflection groups can be distinguished. Their overall geometry closely corresponds to the reflection geometry in the western part of the dynamite section with individual reflection groups dipping predominantly to the E.

For the purpose of depth-migration, the seismic data presented in Plate 9-4 were transformed into line drawings using a computer-based line drawing technique (Valasek & Frei, chapter 4). The unmigrated line drawings are shown in Figures 9-10a and 9-10c. Comparison with the actual seismic data shows that the computer-based method depicts individual reflections very accurately including also minor dip-changes within one single reflection. Upon subsequent ray theoretical depth-migration (cf. Holliger 1991), curved or wavy line segments representing single reflections are torn apart by the migration process. The effects can be seen in the migrated line drawings of Figures 9-10b and 9-10d where individual migrated reflection elements are shorter as compared to unmigrated reflections. Thus, migration gives at least at first sight an overall less coherent image. Another migration effect is the increase in profile length due to updip migration of dipping line elements which in the case of the dynamite section adds another 20 km to the initial profile (Figure 9-10d). Depth-migration was performed using a velocity structure based on the results of the nearby ALP75 refraction profile (cf. Yan & Mechie 1989, Figure 9-13).

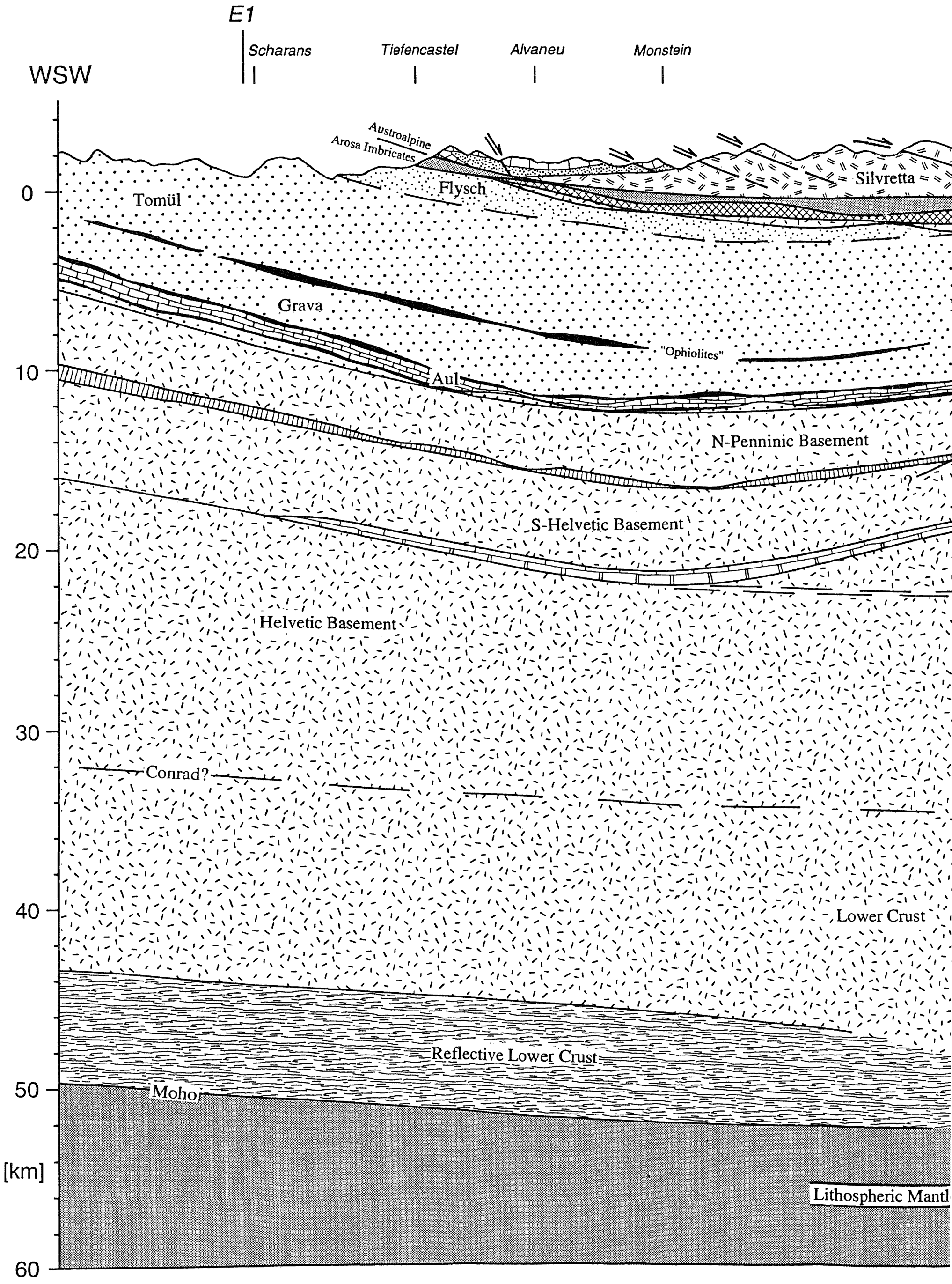

Figure 9-12
Crustal-scale cross-section based on the interpretation of the E2 dynamite and Vibroseis data, the parallel oriented ALP75 refraction profile, the intersecting reflection profiles E1 and E3, and surface geology. The cross-section follows the straight line indicated in Figure 9-9b. No vertical exageration. Coordinates correspond to the Swiss National grid net.

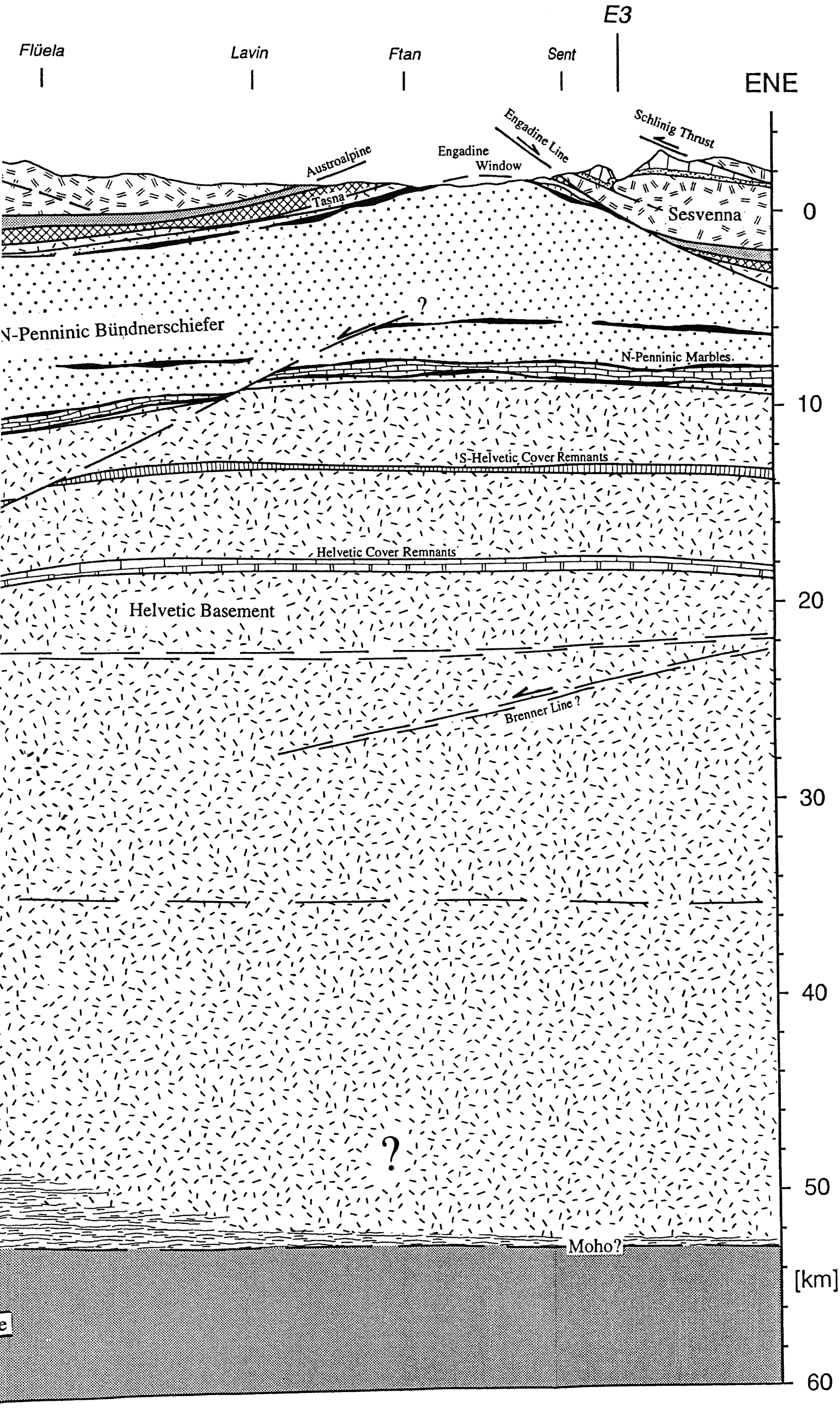
E3
Flüela
Lavin
Ftan
Sent
ENE
Engadine Line
Schlinig Thrust
Austroalpine
Engadine
Window
Tasna
Sesvenna
0
?
N-Penninic Bündnerschiefer
N-Penninic Marbles
10
S-Helvetic Cover Remnants
Helvetic Cover Remnants
Helvetic Basement
20
Brenner Line ?
30
40
?
50
Moho?
[km]
60

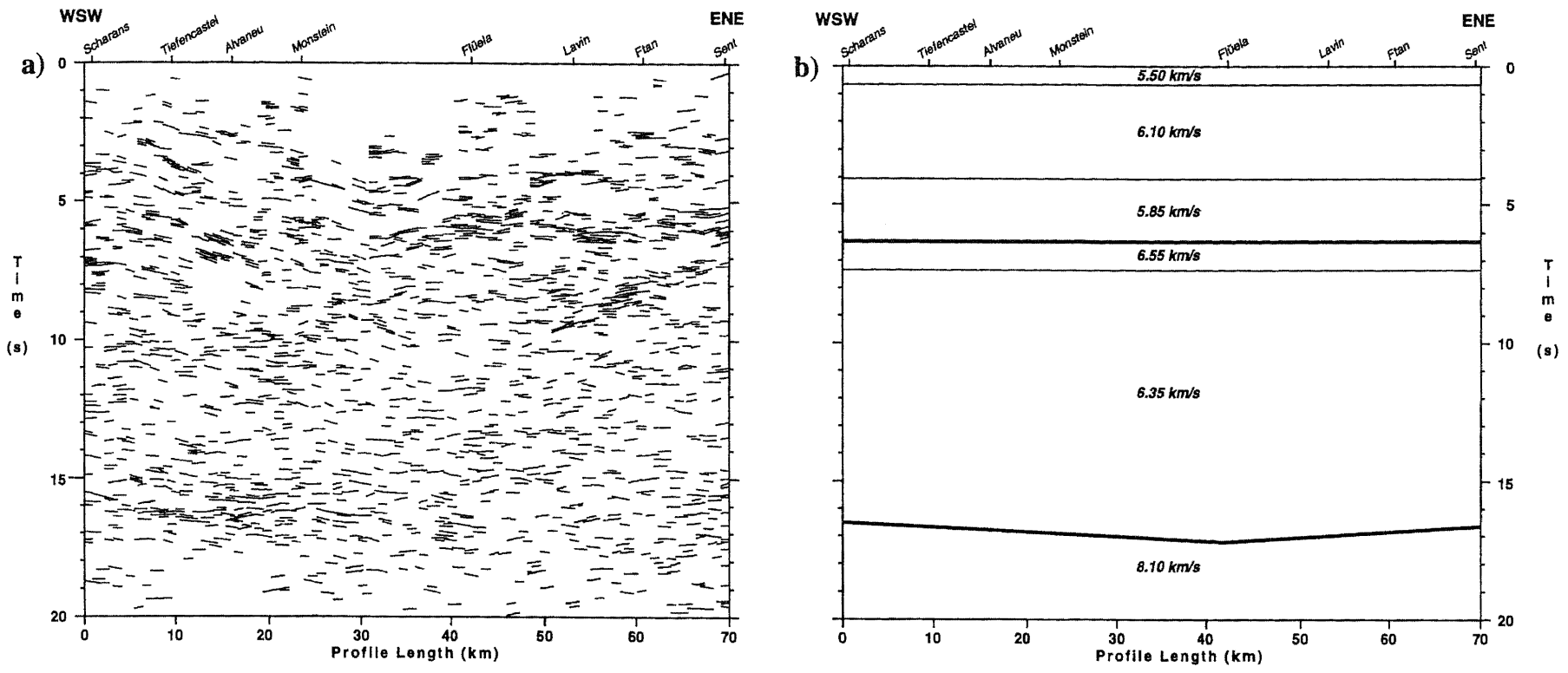

Figure 9-13
Comparison between (a) unmigrated E2 reflection data and (b) the corresponding extract of the parallel oriented ALP75 velocity-depth model by Yan & Mechie (1989). The base of the reflected energy at around 6 s and the base of the reflective lower crust at approximately 16.5 s correspond well to two pronounced velocity discontinuities in the velocity-depth model (thick lines). Horizontal to vertical scale = 1:1 at an average crustal velocity of 6 km/s.

9.3.2 Geologic interpretation

The test of a good interpretation is consistency. This statement is especially valid for the deep seismic reflection data of line E2 with its low signal/noise ratio. Accordingly, the following information was used for the interpretation of the E2 data: (1) reflection geometry; (2) surface geology along the transect based on the works by Brauchli & Glaser 1924, Willhelm 1929, Eugster & Leupold 1930, Bearth et al. 1935, Spaenhauer et al. 1940, Jäckli 1941, Nabholz 1945, Cadisch 1953, Cadisch et al. 1963, Trümpy 1980, Stutz & Walter 1983, Eichenberger 1986, Behrmann 1988, Selverstone 1988, Schmid & Haas 1989, Schmid & Froitzheim 1993, Pfiffner et al. 1990a; (3) interpretations of line E1 by Pfiffner et al. 1988, 1990b, 1991, Frei et al. 1989, Mueller 1990, Valasek 1992 and Litak et al. 1991, 1993; and (4) refraction derived velocity-depth models by Egloff 1979, Noack 1984, Yan & Mechie 1989 and Ye 1992. In a first interpretative step, migrated reflections forming coherent reflection groups were identified (Figure 9-11, thick lines). Then, the identified reflection packages were, if possible, joined together over the entire profile length considering also less "certain" reflection groups (Figure 9 -11, thin lines). Finally, the resulting structural interpretation was iteratively compared with the above-mentioned geological and geophysical data base in order to obtain maximum consistency. In the following, the results of this interpretation procedure are presented starting with the structurally highest tectonic unit and proceeding downwards to the base of the crust. The interpretation is summarized in the geological cross-section of Figure 9-12.

Austroalpine, Arosa imbricate and Briançonnais units: As mentioned earlier, the WSW–ENE running E2 profile parallels the general strike of the Alpine chain. As a consequence, only two major Alpine tectonic units, the Austroalpine zone (represented by the Silvretta and Sesvenna nappes) and the underlying Penninic zone (represented by the Arosa imbricate, Briançonnais (Tasna nappe in the E) and N-Penninic Bündnerschiefer and Flysch units) are exposed along the line (Figure 9-9b). Surface correlation indicates that the base of the Austroalpine Silvretta nappe lines up with shallow reflections between shotpoints Tiefencastel and Alvaneu in the Vibroseis data (*S* in Figure 9-11b). In the dynamite data, the Austroalpine base is not imaged due to the large-offset recordings. The seismic record of this discontinuity is hence very sparse and its construction in the crustal cross-section of Figure 9-12 is predominantly based on geological surface maps (cf. Willhelm 1929, Bearth et al. 1935, Spaenhauer et al. 1940, Cadisch et al. 1963) and a structure contour map specifically constructed thereof. The position of the underlying Arosa imbricates, marking the oceanic suture between Briançonnais and Austroalpine units, and the position of the Briançonnais units themselves are again poorly constrained by the seismic data, although a velocity increase in the ALP75 seismic refraction profile from 5.5 km/s to 6.1 km/s (Figure 9-13, Yan & Mechie 1989) might be attributed to ophiolitc rocks found within the Arosa imbricates as well as in the topmost Bünderschiefer units of the Engadine window (Figure 9-9b). It can however not be used for constructing structural details. As a consequence, the geometry of the Arosa and Briançonnais units is again based on surface geological data and thus somewhat speculative at depth.

N-Penninic cover nappes and basement: Updip projections of reflection packages *T*, *G* and *Au* (Figure 9-11) suggest that these reflections stem from the N-Penninic Bündnerschiefer unit. The latter consists of several tectonic subunits or thrust sheets, which contain predominantly shaly-sandy calcareous micaschists with intercalated layers of marbles and ophiolitic rocks (cf. Jäckli 1941, 1944, Nabholz 1945, Cadisch 1953). Using laboratory P-wave velocity measurements by Sellami et al. (1990) and first arrivals, Pfiffner et al. (1991) argued that high reflection coefficients result from juxtaposition of these rock types. On the other hand, complexely deformed lenses of dolomites and ophiolitic rocks, as they are observed at surface, are expected to scatter the seismic energy and thus decrease the signal coherency. Only regular and larger scale structures within the N-Penninic Bündnerschiefer are therefore likely to produce coherent reflected energy. One such structure are massive carbonates found at the top of the Tomül thrust sheet (Willhelm 1929, Jäckli 1944) and westward up-dip projection of reflection group *T* is consistent with this interpretation. In a similar way, reflection group *G* can be attributed to the marble-basalt layer seperating the Tomül thrust sheet from the underlying Grava thrust sheet. This interpretation is consistent with the E1-interpretations by Pfiffner et al. (1990b, 1991) and Litak et al. (1991, 1993). Reflection group *Au*, being again in good agreement with the E1-interpretations, may well stem,from the Aul thrust sheet (Figure 9-9b) which contains large bodies of marbles and several slivers of ophiolitic rocks (Nabholz 1945). Due to the lower resolution of the dynamite data, *Au* cannot be clearly seperated from the next deeper reflection group *Ad*. For the geologic interpretation, the top of the Aul thrust sheet along the dynamite section is thus placed at the top of reflection group *Ad*, which is attributed to the top of the N-Penninic Adula basement nappe directly underlying the Aul thrust sheet. This interpretation results from the correlation with the E1-interpretations by Pfiffner et al. (1990b), which itself was derived from surface data (structure contour maps by Pfiffner et al. 1990a), as well as by Litak et al. (1993) who validated the interpretation by 3D seismic modeling. The observed lateral discontinuity of the described reflection groups is explained by variations in subsurface geology and by strong local energy scattering along complex structures.

Helvetic Basement: Based on the correlation with the top of the of the S-Helvetic basement in line E1 (*B3* in Figure 9-5a), reflection group *B3* (Figure 9-11a) is interpreted as the top of the S-Helvetic Gotthard "massif". Reflectivity of this discontinuity is explained by remnants of autochthonous Mesozoic sediments and by a mylonitic fabric due to thrusting along the basal Penninic thrust. Also based on E1, reflection group *B2* (Figure 9-11a) is attributed to the top of the Helvetic Aar massif basement. Along the E1 transect, the contact between the Helvetic Aar massif and the overlying S-Helvetic Gotthard thrust-sheet puts basement rocks onto basement rocks. This configuration lacks the appropriate impedance contrast to generate strong reflections in the E1 data. The marked difference in the seismic ex-

pression of the southern top of the Helvetic basement in lines E1 (non-reflective) and E2 (strongly reflective) is attributed to difference in structural style: the basal Helvetic thrust in line E1 is located at the base of the Permian "Verrucano" clastics, whereas towards the E, i. e. in the area of line E2, the basal thrust ramps laterally up into middle Jurassic shales (Trümpy 1969, Pfiffner 1993). Therefore, in the area of line E2, Triassic to lower Jurassic sediments presumably remained attached to their crystalline substratum and were overridden by the S-Helvetic basement unit. Such lithologic layering can easily explain the comparatively strong reflectivity of the top of the Helvetic basement in line E2. Moreover, in the velocity-depth model derived from the ALP 75 profile (Yan & Mechie 1989), reflection group *B2* coincides with a thin high-velocity layer (6.55 km/s, see Figure 9-13). This layer might correspond to carbonates sandwiched between the crystalline basement units as described above. There is, however, a big discrepancy in the thickness of the Triassic to lower Jurassic Helvetic sediments (max. est. 500 m) and the thickness of reflection group *B2* (max. 2 km). This discrepancy is possibly due to geometrical ray focussing and will be further discussed in the following section. Finally, the weakly defined reflection group *B1* in the eastern part of line E2 (Figure 9-11a) is interpreted as originating from a slab of Mesozoic rocks contained within the Helvetic basement. As is the case with *B2*, reflectivity is likely to stem from lithologic layering. Reflection group *B1* is clearly registered in line E3 (see section 9.4) where it is strongly S-dipping (approx. 25°) and ends approximately 10 km N of the intersection with E2. We therefore conclude that *B1* represents an out-of-plane reflection and that the Mesozoic sediments which caused the reflections are probably absent vertically beneath E2. In the geological cross-section of Figure 9-12, the base of the overlying Helvetic basement slice is thus drawn as a discrete shear zone.

Normal Faults: Updip projection of reflection group *BF* (Figure 9-11a) yields a surface position near the western end of the Tauern window. This western margin is defined by a W-dipping low-angle normal fault (Figure 9-9a), termed Brenner Line (Selverstone 1988) or Sterzing-Steinach mylonite zone (Behrmann 1988). The normal fault shows a minimum vertical throw of 10 km (Lammerer 1988) and is related to final movements in the unroofing history of the Tauern window, which started at latest in the Early Oligocene (Selverstone 1988). Displacements along the Brenner Line are associated with strong mylonitization in an up to 400 m thick mylonite belt (Behrmann 1988). Reflection group *BF* could thus be tentatively interpreted as acoustic response to the Brenner mylonites. Another possibility, not implying such large distance correlations, would be to consider reflection group *BF* as a side swipe associated with the Adriatic wedge, since the lack of lower crustal reflectivity beneath *BF* could be the consequence of deep crustal deformation by the indenting wedge (see below). When following the upper crustal reflections over the entire profile length, a W-dippinig zone offsetting reflection groups *Ad* and *B3* can be noted (*NF* in Figure 9-11a). With the exception of some W-dipping reflections, this zone lacks reflectivity (Figure 9-10d). Correlation of reflection groups *Ad* and *B3* across *NF* suggests a normal fault displacement. These observations lead us to the postulation of a W-dipping low-angle normal fault cutting across the upper crustal nappe stack. At the surface, this fault zone might be related to a system of NNW–SSE trending brittle faults cutting all the tectonic units of the Engadine window. Kläy (1957) suggests that this fault system plays an important role in the uplift and formation of the Engadine window. If this correlation between the postulated normal fault and the brittle faults observed at surface is correct, it may be argued that the shear zone flattens towards the E and that the brittle faults represent associated high-angle faults in the hanging wall. This structural relation can also be observed in the Turba mylonite zone where high angle brittle faults cut across the hanging wall of the mylonite zone (Nievergelt et al. 1996).

Lower Crust and Moho: In line E2, clearly coherent reflectivity in the lower crust is only found between *X* and *M* (Figure 9-11a). This stands in contrast to the intersecting line E1 and the EGT refraction profile where besides a reflective lowermost crust, a reflective Conrad discontinuity (C in Figure 9-5a) and a corresponding velocity increase from 6.2 to 6.5 km/s (Figure 9-5b) can be observed. The lack of a reflective Conrad discontinuity in line E2, however, is in agreement with ALP75 velocity-depth models (Yan & Mechie 1989, Noack 1984) and with the intersecting line E3, where a well-defined Conrad discontinuity is absent, too. We can therefore conclude that the Conrad discontinuity along E2 is not a sharp boundary and generates neither coherent near-vertical nor wide-angle reflections. In order to distinguish nevertheless between upper and lower crust in the E2-interpretation, we extrapolated the Conrad discontinuity from the N and W, where it is defined by both seismic methods (section 9.5, Egloff 1979, Ye 1992).
As mentioned above, coherent reflectivity in the lower crust is observed in the western part of line E2, where it forms an approximately 6 km thick reflective zone between *X* and *M* (Figure 9-11a). The comparatively strong reflectivity corresponds to the seismic character of the lowermost crust in line E1 near the intersection, as well as to lower crust sampled in many other areas (cf. Klemperer et al. 1986). Numerical modeling shows that a subhorizontal layering of laminae with low and high seismic velocities explains best the high reflectivity of the lower crust (cf. Sandmeier & Wenzel 1986). In the case of the Alps, Rey (1993) suggested that the layering might have been produced by Variscan post-thickening crustal extension and low-P granulite facies metamorphism of the lower crust in late Carboniferous to Permian times. The characteristic lower crustal reflectivity, however, diminishes towards the E (Figure 9-11a). The decrease in reflectivity could be the effect of (1) recording conditions (cf. Smithson 1986), (2) scattering of the seismic wave front in a structurally complex overburden (cf. Raynaud 1988, Carbonell & Smithson 1990) or (3) scattering of the seismic energy within a complex lower crust (cf. Valasek et al. 1991, Pfiffner et al.1991). Argument (1) can be excluded, as recording conditions did not change significantly along the E2 transect. Arguments (2) and (3) are discussed in the following section. The base of the crust in the E2 transect, i. e. the reflection Moho, is placed at the bottom of the reflection group between *X* and *M* (Figure 9-11a). This is in good agreement with the Moho depth derived from the ALP75 refraction profile in this area (Yan & Mechie 1989, Noack 1984). Moreover, at the intersection, it coincides with the reflection Moho of line E1 (Pfiffner et al. 1990b, Valasek 1992) and with the refraction Moho derived from the EGT data (Ye 1992). As the reflection Moho is not defined in the eastern part of E2, the Moho depth in this area is entirely based on the southward extrapolation of strong Moho reflections from line E3 (see section 9.4).

9.3.3 Discussion and conclusion

Data quality: In comparison to the intersecting lines E1 and E3, the seismic data quality of line E2 is poor. Low signal/noise ratio due to a high ambient noise level and intense energy scattering along complex structures is an inherent problem for all three deep seismic surveys, although probably not everywhere to the same degree (ambient noise is lowest in line E3). However, what clearly distinguishes line E2 from the other profiles is the fact that it runs parallel to the Alpine strike. In the area of intersection between lines E1 and E2, steeply S- and partly also N-dipping potential reflectors are very likely to exist (Figure 9-8a). Thus, significant out-of-plane energy is to be expected in line E2. If interfering destructively, such out-of-plane reflections can break up the recorded wave fronts significantly, resulting in a loss of signal coherency. In special geometrical configurations, however, constructive interference might result in thick zones of multcyclic reflections. This might well be the case for the southern Aar massif with its concave-like geometry (Figure 9-8a or b) and could explain the difference in thickness between reflection group *B2* (up to 2 km) and the thickness of the sandwiched Triassic to Lower Jurassic cover sediments (up to 500 m) responsible for the reflections.

Comparison between seismic reflection and refraction data: Comparison of the E2 reflection data with the velocity model derived from the ALP 75 refraction profile by Yan & Mechie (1989) reveals good agreement in two major crustal boundaries (Figure 9-13): (1) comparison reveals a good fit between the base of the reflective lower crust and the refraction Moho, defined by a velocity jump from 6.35 km/s to 8.1 km/s and (2) the band of reflected energy at approximately 7 s correlates well with a thin high-velocity layer of 6.55 km/s underlying a velocity inversion zone of 5.85 km/s. The remaining velocity discontinuities cannot be clearly linked to the E2 reflectivity pattern. From this comparison it can however be concluded, that velocity discontinuities with velocity contrasts > 5% in the ALP75 refraction profile are indeed reflective in the E2 reflection profile.

Partial lack of lower crustal reflectivity: As pointed out in the previous paragraph, the poor lower crustal reflectivity in the eastern half of line E2 is most probably related to strong energy scattering along complex structures. A comparison of the upper crustal architecture of line E1 (intersecting E2 in the W) and line E3 (intersecting E2 in the E) reveals a similarly complex upper crustal structure. It thus seems unlikely that an increase in the complexity of the upper crust, i. e. scattering of the seismic energy in the overburden, could explain the observed disappearance of lower crustal reflectivity. On the other hand, a southward decay of lower crustal reflections is also observed in line E1 (S of the intersection with E2). There, it coincides with the northern front of the Adriatic wedge consisting of lower crust. The disappearance of a reflective lower crust in E1 has thus been attributed to energy scattering in a complexly deformed lower crust associated with this indenting wedge (Pfiffner et al. 1991, Valasek et al. 1991). Between the western and the eastern NRP 20 transects, Valasek (1992) deduced a WSW–ENE strike for the northern front of the wedge. Its further continuation towards the E can be indirectly assessed from the shortening within the Southern Alps (as argued by

Pfiffner et al. 1991, the wedge's length should balance with the length of the upper crustal flakes stacked up in the Southern Alps). Judging from the shortening estimates gathered from balanced N–S profiles across the Southern Alps (Schönborn 1992), the wedge's northern front may well retain its WSW–ENE strike and may even extend farther N than the eastern end of line E2. The disappearance of the lower crustal reflections towards the E in line E2 may thus also be explained by scattering of the seismic energy due to deep-crustal deformation by the indenting Adriatic wedge.

Geologic interpretation: It has to be stressed that, given the relatively poor data quality of line E2, the geologic interpretation presented here is certainly not the only possible solution, although the integration of complementary data like the intersecting profiles E1 and E3, the refraction profile ALP 75 and surface geology presents strong constraints. Moreover, it has to be kept in mind that any crustal geologic cross-section represents a strongly simplified image of the crust, because of the limited resolution of the available geological and geophysical data. With these restrictions in mind, the most important information in the geologic context gathered through line E2 are (Figure 9-12): (1) The S-Helvetic and N-Penninic basement units appear to be continuous along strike. (2) The axial dip of upper crustal units, which is also observed at surface, rapidly decays towards the E. This decay may be attributed to the presence of a Helvetic basement slice underneath the Engadine tectonic window, which induces an uplift of of the overlying units. (3) The domal antiform forming the Engadine window does not seem to affect the underlying basement. This means that the N-Penninic Bündnerschiefer units must be detached from their crystalline substratum. (4) Both the Brenner line (if this interpretation is followed) and the postulated normal fault in the upper crust along line E2 indicate E–W extension. Seismic refraction data (Yan & Mechie 1989) do not point to a significant uplift of the crustal base associated with this extension. Consequently, extension might be related to N-S shortening and vertical thickening. Based on surface observation, syncompressional E-W extension in the Eastern Alps was already postulated by Behrmann (1988), Selverstone (1988) and Ratschbacher et al. (1991b) and was modeled by Ratschbacher et al. (1991a). The extension recorded in E2 can be dated as "post-nappe" as it affects e. g. the basal Penninic thrust (Figure 9-12). Since the latter is post Early Eocene (see Schmid et al., Chapter 14), E-W extension along E2 is dated as Late Eocene or younger, i. e. coeval with extension linked to the Tauern uplift (Selverstone 1988). (5) The NE part of the Engadine line (Figure 9-9b) is a normal fault with an estimated minimum vertical throw of 4 km in the area of scuol (Schmid & Haas 1989, schmid & Froitzheim 1993). If the Brenner line is taken to be responsible for reflection group *BF*, the Engadine and Brenner lines would form a set of conjugate normal faults. In this case, the Austroalpine crustal lid situated between these two faults is essentially downfaulted, accentuating the structural highs of the Engadine and Tauern windows (Figure 9-14). Note that a conjugate fault geometry does not necessarily imply contemporaneous activity.

Summarizing, the following conclusions can be drawn:

(1) The seismic data quality in the E2 strike-line is poor as compared to N–S oriented seismic dip-lines. The difference in data quality is attributed to the destructive interference of reflected out-of-plane energy.

(2) Velocity contrasts in excess of 5% in the ALP75 refraction profile proved to be reflective in the E2 reflection profile. Consequently, where available, seismic refraction results should be integrated in the interpretation of deep-seismic reflection data.

(3) Reflectivity of the lowermost crust is poor in the eastern half of line E2 as compared to the western half. This is speculatively attributed to scattering of the seismic energy due to deformation of the lower crust by the indenting Adriatic wedge.

(4) The S-Helvetic and N-Penninic basement units appear to be continuous along strike.

(5) The axial dip of upper crustal units rapidly decays towards the east. This might be attributed to the presence of a Helvetic basement slice underneath the Engadine window, which induces an uplift of the overlying units.

9.4 Interpretation of line E3: The deep structure of the Engadine window

L. Hitz & O. A. Pfiffner

This section presents the results of a deep seismic reflection survey located at the eastern margin of the Engadine tectonic window (Figure 9-15). The survey consists of two short dynamite lines which are combined into a composite transect termed E3. Line E3 crosses all the major tectonic units of the lower Engadine valley including the so-called Engadine line, a major structural discontinuity in the eastern Swiss Alps. In addition, line E3 intersects line E2 just east of Scuol (Figure 9-15). Combined with the E2 transect, line E3 was intended to clarify the deep structure of the Engadine window, a tectonic window which Termier (1904) referred to as "the most beautiful example to cite".

9.4.1 The data

Line E3 was recorded in the fall of 1991 in a joint operation of the Geophysical Institutes of Clausthal (FRG), Munich (FRG), Münster (FRG), Leoben (A), Zürich (CH) and a private Swiss company. A total of 6 dynamite shots were fired, each with a 30 kg charge. They were recorded by a 14.3 km long receiver spread consisting of five different registration units in the Uina and Sinestra valleys (Clausthal, Munich, Münster, Zürich and GeoExpert), and by a separate 4.8 km long receiver spread in the Fimber valley (Leoben). This configuration resulted in two separate CDP-processing lines (Figure 9-15),

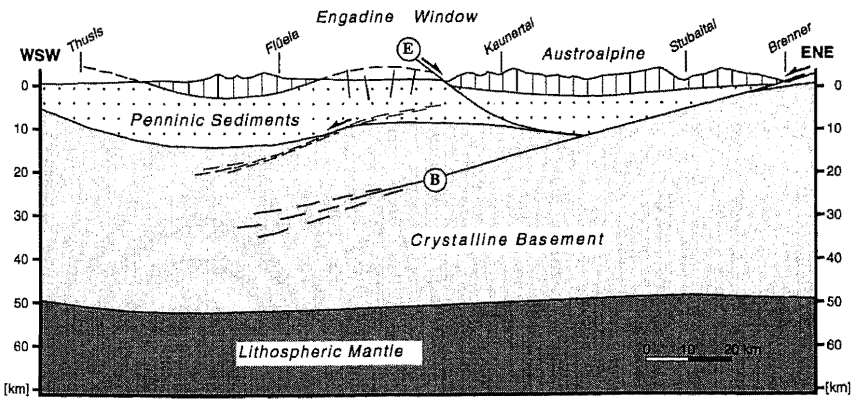

Figure 9-14
Tectonic model along strike showing a possible relationship between the Engadine line (E) with the Brenner line (B) as a set of conjugate normal faults. Normal faulting leads to the formation of a downfaulted Austroalpine crustal block situated between the two faults.
The model follows the ALP75 trace indicated in Figure 9-9a and includes data from Kläy (1957), Behrmann (1988), Selverstone (1988), Yan & Mechie (1989) and Schmid & Froitzheim (1993).

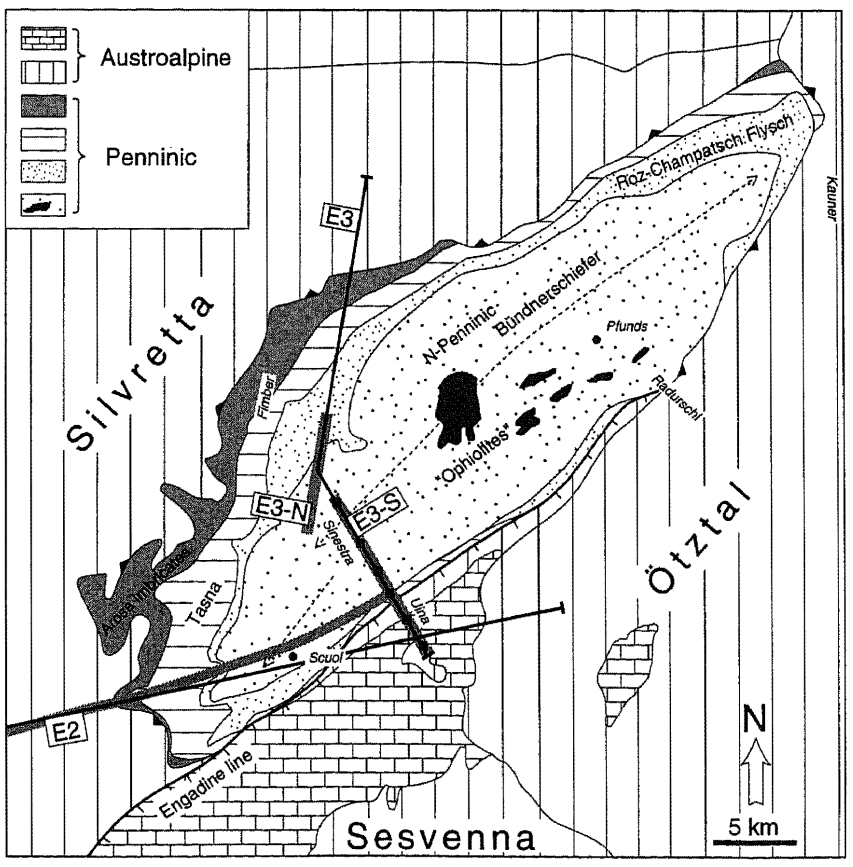

Figure 9-15
Simplified tectonic map of the Engadine tectonic window showing the location of the E3 transect consisting of the seismic reflection profiles E3-North (E3-N) and E3-South (E3-S), and part of the intersecting seismic reflection profile E2.
Grey lines = CDP-processing lines, black squares = shot locations, black straight lines = traces of geological cross-sections, dashed lines with arrows = crest-lines of the Engadine antiform (cf. Cadisch et al. 1963).

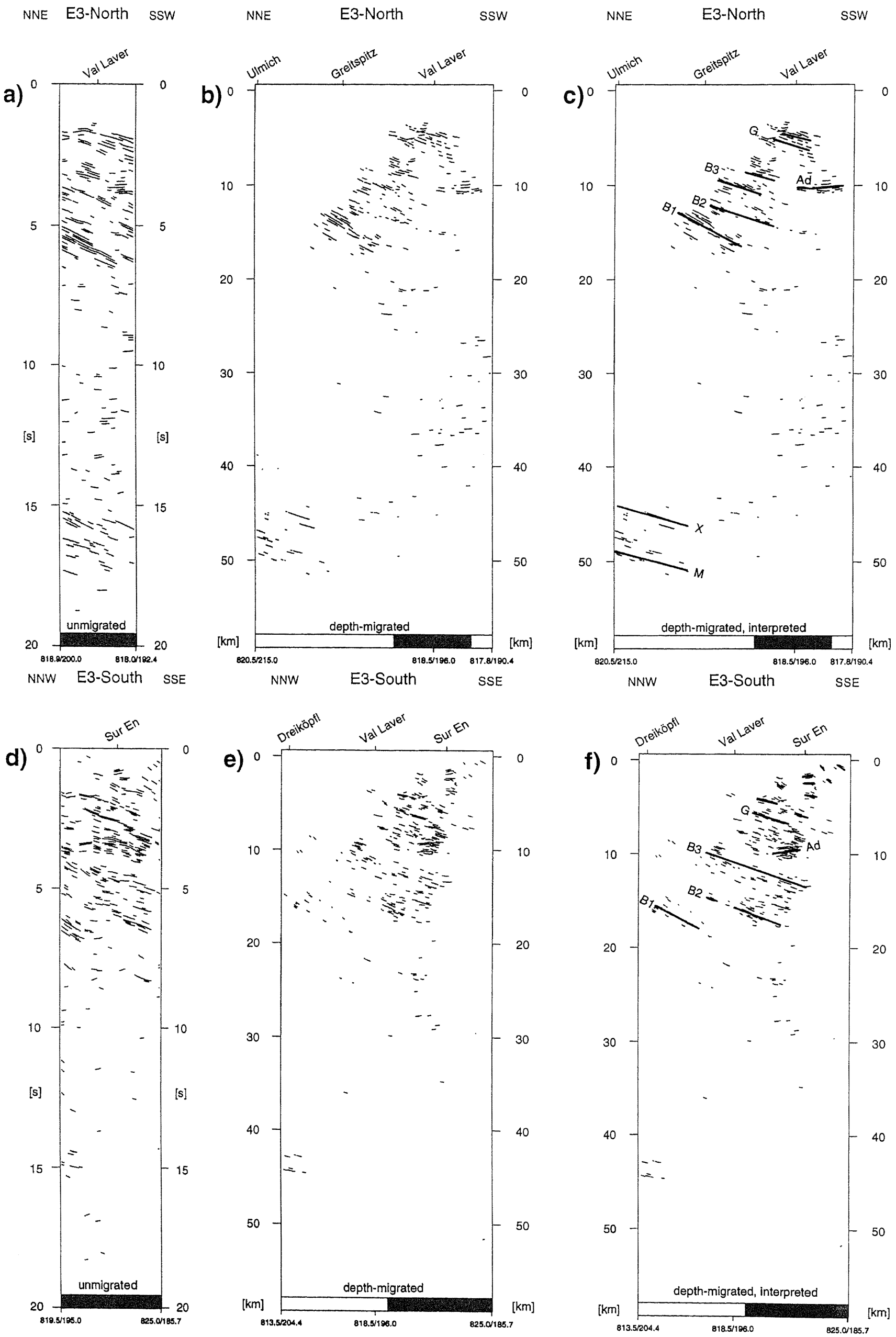

Figure 9-16
Automatic line drawings of the E3 seismic reflection data. Data are shown in unmigrated (a and d), depth-migrated (b and e) and interpreted form (c and f). Lettered reflection groups are discussed in the text. Horizontal to vertical scale = 1:1.
Note the increase in profile length due to up-dip migration of dipping line elements.

one oriented SSE–NNW (E3-South), and one oriented SSW–NNE (E3-North). The data were treated at the processing center of the ETH Zürich using standard processing procedures troughout. Due to the unique character of every individual shot-gather and the low CDP coverage (max. 5), however, special processing parameters and methods of determing them had to be designed (cf. De Haas 1992). The processed data are presented in Plates 9-5 and 9-6.

E3-South (Plate 9-6, see also Figure 9-16d) shows strong reflections in the upper 8 s dipping predominantly to the SSE. Below 8 s, reflectivity is very poor. The most prominent reflection group is characterized by two-cyclic, high-amplitude reflections dipping from 2.0 s in the NNW to 3.5 s in the SSE. Below this group, a subhorizontal to slightly NNW-dipping reflective zone can be observed. The latter is followed by two SSE-dipping reflection groups, one from 4 to 5.5 s in the SSE, the other from 5 to 6.5 s in the SSE. Upper crustal reflectivity ends with a strongly SSE-dipping reflection group at 6 s in the NNW. Reflectivity in the shallowmost part of line E3 between 0 and 1.5 s is rather erratic. Note, however, a change in reflection geometry from subhorizontal to NNW-dipping in the central part to SSE-dipping in the southern part of the line.

Similar to E3-South, E3-North (Plate 9-5, see also Figure 9-16a) shows a strongly reflective upper crust starting with an approximately 1 s thick reflective zone from 2 s in the NNE to 3 s in the SSW. This is followed by a reflection group with a marked change in reflection geometry: in the SSW, reflections are subhorizontal to NNE-dipping, whereas towards the NNE they are SSW-dipping. Below the latter, a 2 s thick zone with constantly SSW-dipping reflection packages can be observed marking the base of the reflective upper crust. In contrast to the similarity of upper crustal reflectivity, E3-North shows strong SSW-dipping reflections also in the lowermost crust between 15 and 17 s.

For the purpose of depth-migration, the seismic data (Plates 9-5 and 9-6) were transformed into automatic line drawings (Figure 9-16a and d) using a program developed by Valasek (1992; see Valasek & Frei, chapter 4). Ray-theoretical depth-migration (cf. Holliger 1991) was done using a velocity structure derived from the ALP 75 velocity-depth model by Yan & Mechie (1989). The depth-migrated line drawings are shown in Figure 9-16b and e. Note that up-dip migration of dipping line elements increased the profile length considerably and that the identification of the above described reflection groups, which is easy in Figure 9-16a and d, is less evident in the depth-migrated line drawings of Figure 9-16b and e.

9.4.2 Geologic interpretation

In a first interpretative step, depth-migrated coherent reflection groups were laterally correlated and labeled (Figure 9-16c and f). In a second step, these reflection groups were projected parallel to the regional strike (WSW-ENE, see inset in Figure 9-17) onto a common trace termed E3 (Figure 9-15). The result of this procedure can be seen in the simplified line drawing of Figure 9-17. Note that the projected reflection groups line up smoothly, indicating that distortions due to projection are moderate. The next step in the interpretation involved the correlation of the simplified line drawing with the geophysical and geological database available for the study area. The geophysical database consists of the intersecting E2 seismic reflection profile (section 9.3), the intersecting ALP 75 seismic refraction profile (cf. Yan & Mechie 1989, Noack 1984) and two seismic experiments in the area E of Pfunds (Scheliga 1971, Giese & Prodehl 1976). Geologic data include geologic and tectonic maps (Kläy 1957, Cadisch et al. 1963, Trümpy 1972, Oberhauser 1980), structure contour maps (Stutz & Walter 1983) and various other studies regarding the geology of the Lower Engadine valley (cf. Cadisch 1953, Trümpy 1980, Schmid & Haas 1989, Mattmüller 1991, Schmid & Froitzheim, 1993). It should be noted that the domal structure of the Engadine window prohibits reflection correlation with geologic outcrops by means of projections, as done in the case of E1. The identification of individual reflections is thus mainly based on the correlation with the intersecting line E2 and the ALP 75 velocity-depth model. In the following, the results of the geologic interpretation, summarized in the geologic cross-section of Figure 9-19, are presented.

Shallow crust: Due to large off-set recordings and low CDP-coverage, reflections from the shallowmost crust are predominantly absent. Only in the southernmost part of line E3 where offsets are smallest, shallow reflectivity can be observed (Figure 9-17). There, line E3-South shows some faint strongly SSE-dipping reflections at 1 to 1.5 s at the line's southern end (Figure 9-18). By up-dip projection, they match with the Engadine line, a normal fault with an estimated vertical throw of 4 km in the area of Scuol (Schmid & Haas 1989). Reflectivity might stem from the juxtaposition of contrasting lithologies, as downfaulting along the Engadine line places Austroalpine basement (Sesvenna) next to Penninic sediments (Bündnerschiefer unit). The interpretation of the Austroalpine units, the Arosa imbricates and the Briançonnais unit (Tasna nappe) as shown in Figure 9-19 is mainly based on surface data by Kläy (1957) and Oberhauser (1980) for the northern part, and Cadisch et al. (1963), Stutz & Walter (1983), Schmid & Haas (1989) and Schmid & Froitzheim 1993 for the southern part. At the NE margin of the Engadine window, Scheliga (1971) reported strong reflections at 1.1 s TWT (~1.5 km b.s.l.) from a seismic reflection experiment in the Kauner valley (Figure 9-15). Giese & Prodehl (1976) attributed these reflections to the contact between Penninic Bündnerschiefer and Austroalpine basement.

N-Penninic cover nappes and basement: Extrapolation of surface data suggests that the short, predominantly SSE-dipping reflections between 2 and 7 km depth (Figure 9-17) originate from within the N-Penninic Bündnerschiefer unit. Reflectivity is likely to stem from intercalated large-scale lenses of ophiolitic rocks observed also at surface (cf. Koller & Höck 1987). Reflections labeled *G* in Figure 9-17 are speculatively attributed to a more or less continuous ophiolitic layer, similar to the one encountered in lines E1 and E2. In the W, this layer is correlated with the Grava thrust sheet, a subunit of the N-Penninic Bündnerschiefer unit (see sections 9.2 and 9.3).

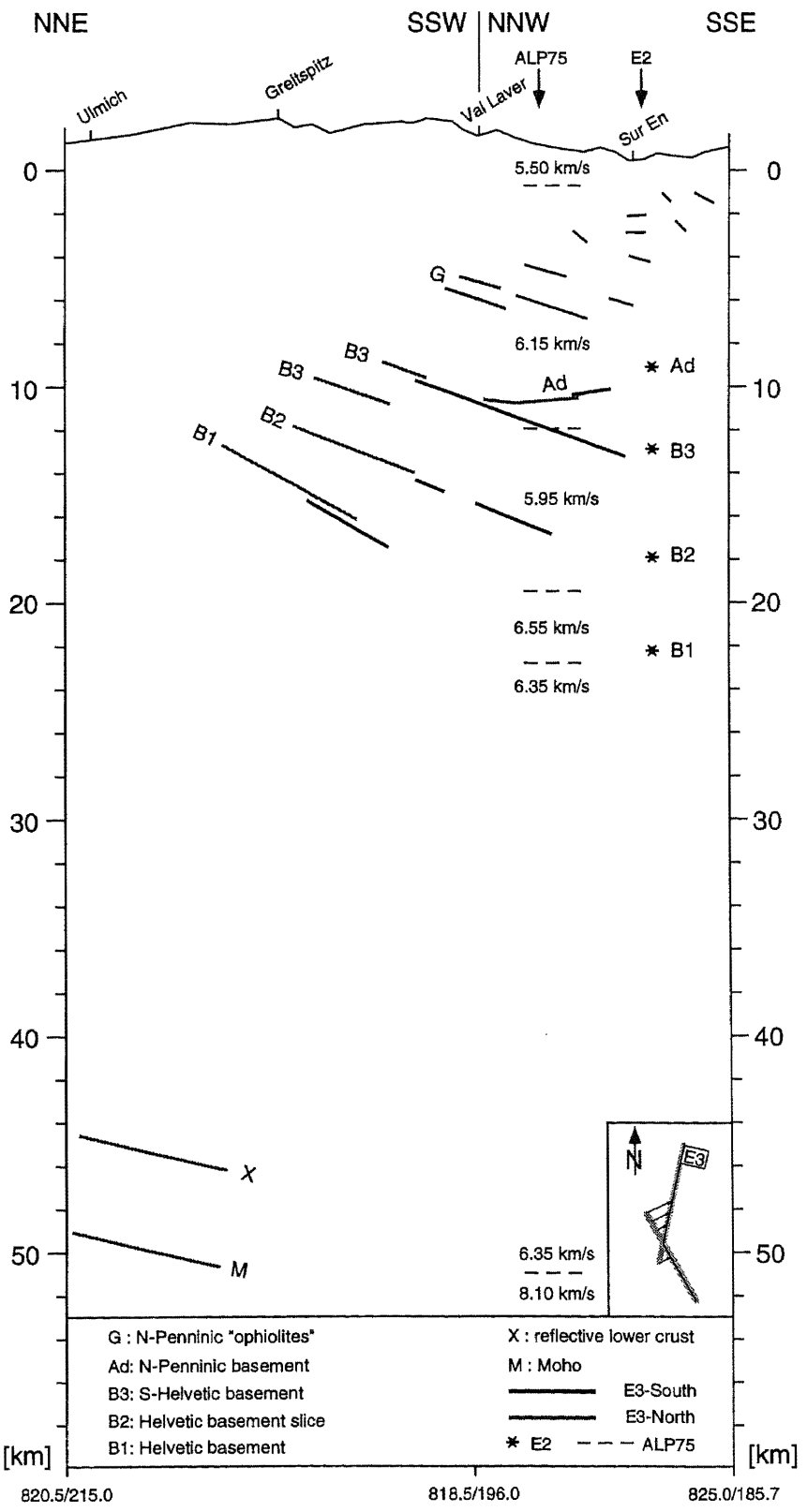

Figure 9-17
Simplified line drawing resulting from the projection (see inset) of coherent reflection groups of lines E3-South and E3-North (Figure 9-16c and f) onto the common E3 trace indicated in Figure 9-15. Note that the migrated reflection groups of the two lines line up smoothly indicating that distortions due to projection are moderate.
Stars = intersecting reflection groups of line E2 (Figure 9-11), dashed lines = intersecting discontinuities from the ALP75 velocity-depth model by Yan & Mechie (1989). Vertical to horizontal scale = 1:1.

Based on the correlation with E2, the next deeper reflection group *Ad* (Figure 9-17) is interpreted as marking the top of a large-size N-Penninic basement unit, which in the W corresponds to the Adula nappe. Reflection group Ad forms an exception in the E3 reflection geometry as it is subhorizontal to slightly NNE-dipping. Together with the underlying reflection group *B3*, *Ad* forms a triangle indicative of the northern end of this Penninic basement nappe. The reflectivity of *Ad* is tentatively attributed to the impedance contrast between crystalline basement rocks (Adula) and high-velocity marbles and basalts of the overlying Aul thrust sheet (cf. Pfiffner et al. 1991, Sellami et al. 1990).

Helvetic basement: Reflection group *B3* (Figure 9-17) can be correlated with the top of the S-Helvetic basement unit imaged in line E2. In line E1, this discontinuity corresponds to the top of the Gotthard unit and is identical with the basal Penninic thrust. Reflectivity is explained by possible remnants of S-Helvetic cover-sediments (Triassic dolomites) and/or a velocity anisotropy produced by mylonitization along the basal Penninic thrust. In the ALP 75 velocity-depth model by Yan & Mechie (1989), the corresponding velocity discontinuity marks the top of a velocity inversion zone (Figure 9-17). Similar to line E2, the next deeper reflection group *B2* can be attributed to the top of a local Hevetic basement slice underlying the Engadine window. Reflectivity could stem from Mesozoic carbonates interlayered with crystalline basement. Reflection group *B1* (Figure 9-17) marks the deepest coherent upper crustal reflections along the E3 transect. These reflections are therefore interpreted as originating from the top of the seismically transparent European upper crust. As such it would correspond to the Helvetic basement, i. e. the Aar massif as encountered further W and NW. As in the case of *B2*, reflectivity of *B1* can be attributed to a sediment layer sandwiched between crystalline basement. This sediment layer, probably consisting of carbonates, might correspond to the high-velocity layer (6.55 km/s, Figure 9-17) observed in the ALP75 velocity-depth model by Yan & Mechie (1989).

Lower crust and Moho: Reflections between *X* and *M* (Figures 9-16c and 9-17) are comparable to the seismic character of the lowermost crust in lines E1 and part of E2. They are explained as the seismic expression of a subhorizontally laminated high-and-low velocity structure (section 9.3). The reflectivity of the lowermost crust as well as the one associated with the Conrad discontinuity is, however, absent in most of line E3. This observation is in agreement with the eastern part of the intersecting line E2, where a reflective lower crust and a reflective Conrad discontinuity are not observable either. This lack of reflectivity is speculatively attributed to Alpine deep-crustal deformation resulting in strong scattering of the seismic energy (see discussion in section 9.3). The Conrad discontinuity shown in the crustal cross-section of Figure 9-19 is thus based on extrapolated data from the N and W only (section 9.5, Egloff 1979, Ye 1992). It was drawn to indicate that a differentiation between upper and lower crust along E3 is nevertheless likely to exist.
The base of the crust, i. e. the reflection Moho, is placed at the bottom of the reflection package between *X* and *M*. It dips about 13° to the SSW. As the reflection package tapers off to the S, the Moho as shown in Figure 9-19 corresponds solely to an extrapolation of *M*. This extrapolated Moho discontinuity, however, fails to match the refraction-derived Moho by Yan & Mechie (1989) by approximately 3 km (Figure 9-17). The misfit is indicative of depth-distortions due to out-of-plane energy in the ALP 75 refraction data.

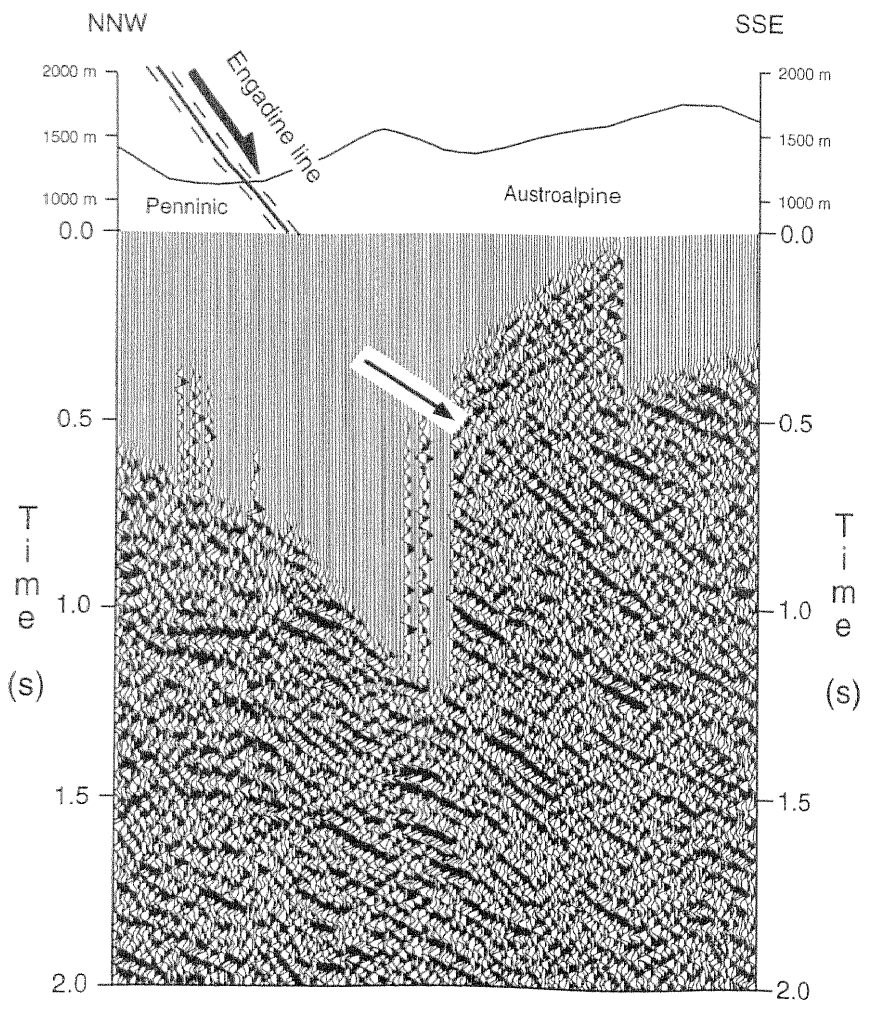

Figure 9-18
Extract of the southernmost part of the E3 reflection data (see also Plate 9-6). SSE-dipping reflections (arrow) can be correlated with the Engadine line at surface which essentially acts as a normal fault in the investigatea area. Note the change from subhorizontal reflections in the NNW to SSE-dipping reflections in the SSE. This change in orientation is attributed to dragfolding associated with faulting along the Engadine line.

9.4.3 Discussion and conclusion

Correlation between E2/ALP 75 and E3: The strongly SSE-dipping reflections in line E3 indicate that reflected out-of-plane energy in the seismic strike-lines E2 and ALP 75 has to be expected. It is thus not surprising that none of the intersecting E2-reflection groups (depth-migrated along strike) and ALP 75-discontinuities exactly match the migrated reflection groups of line E3 (Figure 9-17). Correlation of the E3 seismic data with the results of lines E2 and ALP 75 is nevertheless possible and facilitates the identification of the individual reflections. Moreover, a limited amount of 3D structural information can be gained in the area of intersection. There, the WSW–ENE striking E2 profile shows subhorizontally oriented Penninic and Helvetic basement units, whereas in line E3, the same basement units are dipping SSE (Helvetic units) or NNW (Penninic unit). Consequently, an ENE-strike (~055° N) can be deduced for the basement units underlying the Engadine window, which closely corresponds to the regional strike observed at surface (Kläy 1957, Cadisch et al. 1963). The good agreement in strike between units at the surface and deep basement units suggests that the formation of the Engadine window may be closely linked to deformation within the underlying basement (see below).

Geologic interpretation (Figure 9-19): The geologic interpretation of line E3 shows that the Engadine tectonic window is underlain by an up to 10 km thick pile of N-Penninic Bündnerschiefer. The latter is probably composed of a number of thrust sheets, as indicated by coherent reflectivity within the Bündnerschiefer. These units form the core of the domal antiform constituting the Engadine window. This antiform apparently does not significantly affect the underlying basement units, which is compatible with the E2-interpretation (Figure 9-12) where the basement units underneath the Engadine window are subhorizontally oriented. From this it can be concluded that the N-Penninic Bündnerschiefer units must be detached from the underlying basement nappe-stack during window formation, i. e. they may be regarded as forming a large-scale detachment fold.
Another result of the geologic interpretation of line E3 is that the Engadine window seems to be underlain by a Helvetic basement slice (HBS). The latter is also recognized along strike in line E2, where it laterally ends towards the W in the area between shot points Monstein and Flüela (Figure 9-12). The HBS-basement slice is thus of limited lateral extent, seemingly restricted to the area of the Engadine window and could thus be responsible for the axial plunge of this structural high.

Engadine line: Based on paleostress analysis and large-scale nappe correlation, the Engadine line (Figure 9-15) has recently been recognized as a post-collisional tectonic lineament along which oblique slip and block rotation took place in Late Tertiary times (Schmid & Froitzheim 1993). In the area of line E3, the Engadine line essentially acts as a brittle normal fault with down-faulting of the SE block (Figure 9-19). The vertical throw is estimated to be approximately 4 km (Schmid & Haas 1989). On a large scale, movements along this part of the Engadine line juxtaposes Austroalpine basement and N-Penninic Bünderschiefer. Such a lithologic contrast should give rise to steep reflections and to a lateral P-wave velocity change. SSE-dipping reflections correlating with the surface position of the Engadine line can indeed be observed in the E3 data (Figure 9-18). The reflections dip about 55° to the SSE at depth, which is within the dip range expected from geologic surface data. Moreover, a change in reflection orientation from subhorizontal between 1 and 1.5 s to SSE-dipping further S can be observed in the Bündnerschiefer units below the Engadine fault (Figure 9-18). This change may reflect drag-folding in the fault's footwall (Schmid & Froitzheim 1993).
The expected P-wave velocity change across the Engadine line was in fact

E3

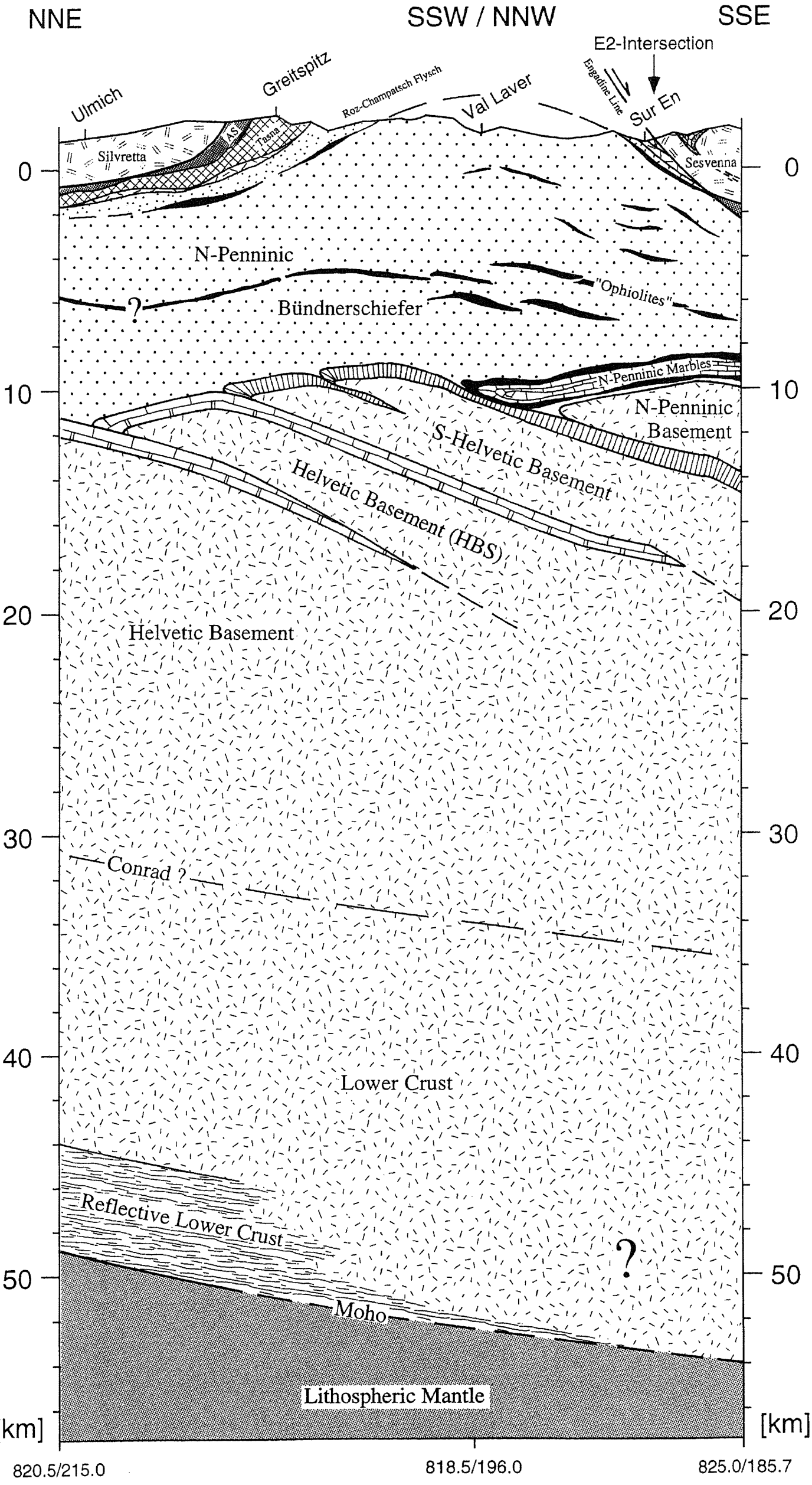

Figure 9-19
Crustal-scale cross-section through the Engadine tectonic window based on the interpretation of the E3 seismic reflection data, the intersecting seismic profiles E2 and ALP75 and surface geology. The trace of the cross-section is indicated in Figure 9-15. Coordinates correspond to the Swiss National grid net. No vertical exageration.

observed in a short seismic refraction profile in the Radurschl valley where travel times could not be explained without assuming a lateral inhomogeneity (Scheliga 1971, Giese & Prodehl 1976). The derived lateral velocity change was attributed to the contact between the juxtaposed Austroalpine basement and N-Penninic Bündnerschiefer.

Model for the formation of the Engadine window: Large-scale open folds of Late Oligocene age (Domleschg-Phase, see Schmid et al., Chapter 14) affecting Austroalpine and Penninic units trend E–W to NE–SW and formed in response to dextral transpression along the Insubric line (Figure 9-8b) and the coeval intrusion of the Bregaglia (30 Ma) and Novate batholiths (27 Ma). Given the similar shape and orientation of the NE-striking antiform constituting the Engadine window a correlation of the Engadine uplift with this phase of post-collisional shortening is at least plausible. Moreover, thrusting in the Helvetic basement further NW is also related to Late Oligocene – Early Miocene post-collisional NNW–SSE shortening (see Pfiffner et al, Chapter 13.1 and Schmid et al., Chapter 14). From this we infer that both thrusting in the Helvetic basement and open folding of N-Penninic and Austroalpine units are roughly coeval and related to post-collisional shortening in Late Oligocene to Early Miocene times.

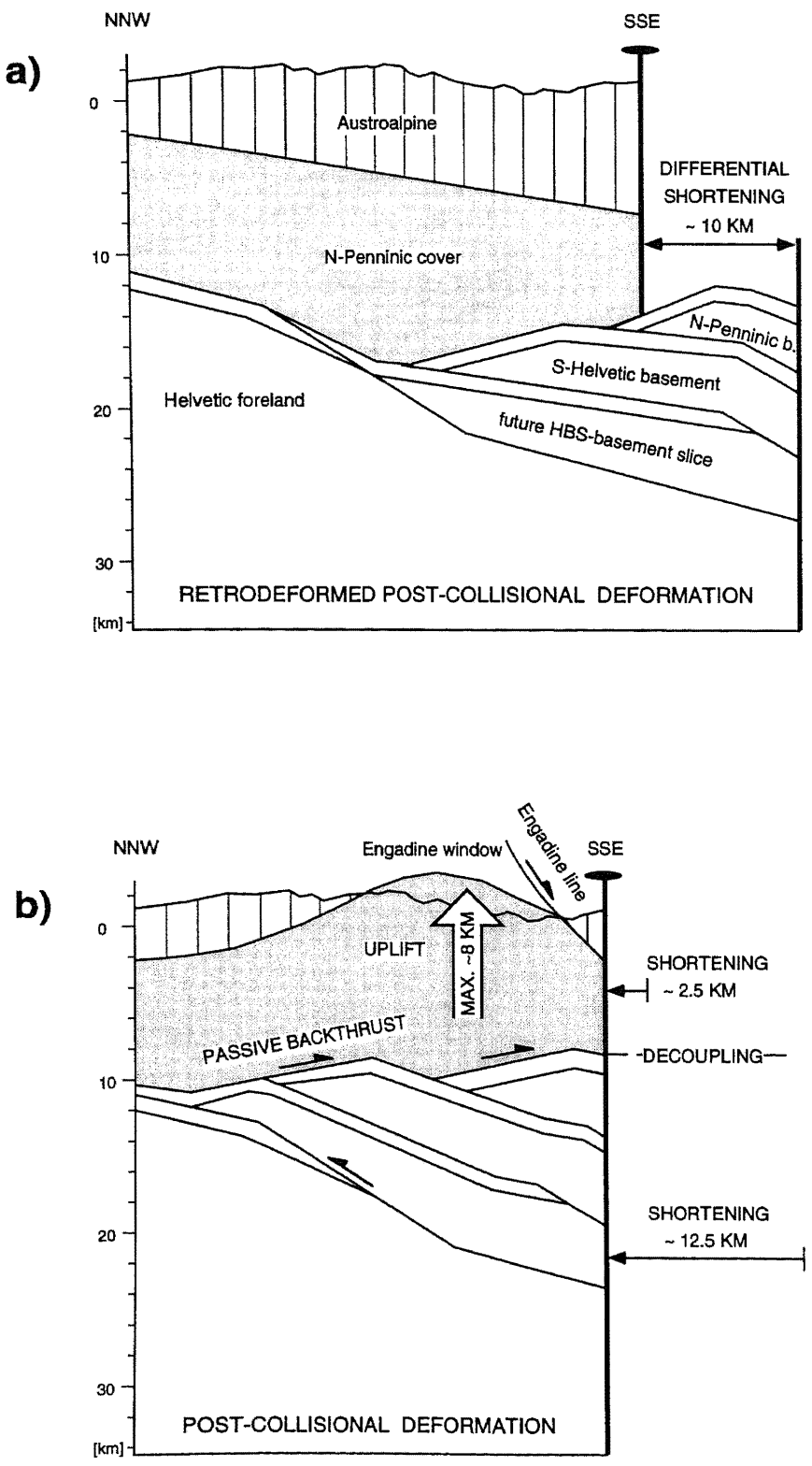

Figure 9-20
Tectonic model for the formation of the Engadine window. (a) Retrodeformation of post-collisional deformation shows a differential shortening of ~10 km between the Austroalpine lid and the European basement suggesting a decoupling between the two units. (b) Post-collisonal shortening leads to the indentation of an upper crustal wedge bounded by a passive back thrust at the top and an active NW-vergent thrust at the bottom. The indentation is associated with detachment folding, local uplift and extension resulting in the present-day domal shape of the Engadine tectonic window.
No vertical exaggeration.

Using area- and line-length balancing methods, retrodeformation of the post-collisional structures in a NNW-SSE cross-section across the Engadine window shows that shortening associated with the formation of the HBS-basement slice is in the order of ~12.5 km, whereas unfolding of the basal Austroalpine thrust in the section considered corresponds to a shortening of ~2.5 km only (Figure 9-20a). The striking difference in shortening suggests a decoupling between the Austroalpine lid and the European basement units during post-collisional deformation. Such a decoupling is likely to be positioned at interfaces with maximum differences in rock strength. In the retrodeformed section (Figure 9-20a), a major detachment could be expected at the interface between the European basement and the N-Penninic Bündnerschiefer units (large-scale detachment and thrusting of the Penninic cover nappes followed this contact throughout the Swiss Alps). Thus, our model includes a protruding European upper crustal wedge bounded by a passive back-thrust at the top and an active NNW-vergent thrust at the bottom (Figure 9-20b). Such passive back-thrust models have been reported from various orogens by Banks & Warburton (1986). Assuming (1), that the HBS-basement slice imaged in lines E2 and E3 is restricted to the area of the Engadine window (see above), (2), plane strain in the area considered and (3), a complete decoupling between Bündnerschiefer and European basement, the indentation of the upper crustal wedge must lead to a local uplift of maximally 8 km in the area of the Engadine window. This local uplift, accomodating ~12.5 km of post-collisional shortening, leads to the domal shape of the Engadine window. Moreover, the resulting tectonic uplift of ~8 km, which is probably an overestimate due to assumption (3), is likely to induce extension in the overlying units. An expression of this extension could be found in the the Late Oligocene – Early Miocene activity along the Engadine line (Schmid & Froitzheim 1993), extensional brittle faults in the Engadine window (Kläy 1957) and the E2 low-angle normal fault (section 9.3). Summarizing we suggest that the Engadine window is essentially the result of post-collisional deformation with the superposition of large-scale detachment-folding above a passive back thrust, local uplift and extension in Late Oligocene to Early Miocene times.
Viewed at a large scale, the Engadine structural high could be coeval with the uplift of the external massifs. Moreover, it seems possible that the HBS-basement slice underlying the Engadine window is arranged in a right-step en-échelon manner in respect to the external basement uplifts. Such a geometry is compatible to dextral transpression with NNW-SSE directed shortening between the European and Adriatic plates in Late Tertiary times, as suggested by plate reconstructions by e. g. Savostin et al. (1986).

In summary, the following conclusions may be drawn:
1) A good correlation exists between reflections as observed in lines E2 and E3, rendering the geologic interpretation relatively reliable.
2) The Engadine window is cored by an up to 10 km thick pile of N-Penninic Bündnerschiefer underlain by an ENE-striking basement nappe-stack consisting of N-Penninic and Helvetic basement units.
3) The antiform constituting the Engadine window does not seem to affect the underlying basement units implying that the N-Penninic Bündnerschiefer must be detached from the basement during window formation.
4) The Engadine window could be the result of the indentation by an upper crustal wedge producing large-scale detachment folding, local uplift and extension in Late Oligocene to Early Miocene times.

9.5 Deep seismic fan-recordings and a 3D crustal model of the eastern Aar massif

L. Hitz & O.A. Pfiffner

In 1986, the receiver spread of the E1 seismic reflection profile was additionally used for various far-offset measurements. They included both in-line and fan-recordings. In the first part of this section the fan data shall be described in detail and their geologic interpretation will be given. In a second part, the elaborated network of 2D profiles will be combined into a 3D crustal model to get new insight into the structure of the eastern Aar massif uplift.
The results of this work are based on two fundamental assumptions, which are necessary to locate the reflecting subsurfaces in the seimic fan data. The assumptions are: (1) CDP equals CMP and (2) the CDP-lines run parallel to the true dip of the imaged subsurface. Assumption (1) allows the positioning of the individual CDP-lines in space (Figure 9-21), whereas assumption (2) allows a correct depth conversion of the reflection data by means of ray-theoretical depth migration. Both assumptions are crude approximations of the true situation. Valasek (1992), however, showed that mispositioning due to these assumptions is minimal for moderately dipping crustal layers (0° to 15°) such as observed in this study.

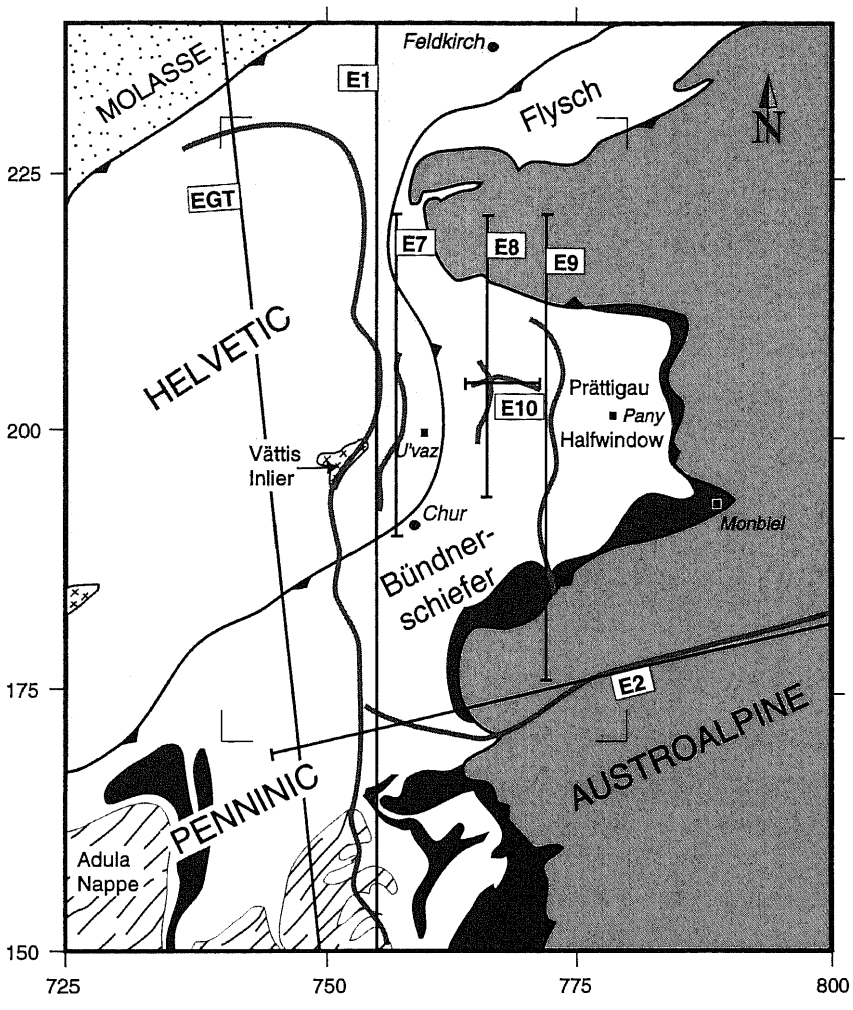

Figure 9-21
Simplified tectonic map of the study area with locations of NRP 20 seismic reflection lines and the EGT seismic refraction line. Grey lines correspond to CDP postions, straight black lines correspond to the traces of geological cross sections. Squares indicate fan-shot locations and rectangles show locations of Figures 9-28 and 9-29. Coordinates are given in the Swiss National Grid system.

9.5.1 The data

The reflection seismic fan data presented here consist of 7 dynamite shots with a 300 kg charge each. Two shots were fired from shot-location "Untervaz" (760.230/198.660, average lateral offset 5.4 km). They were recorded in the rolling 240 channel receiver-spread of line E1. With a CDP spacing of 40 m, the resulting CDP-line from the two shots measures 19.2 km. In the following, the "Untervaz" line will be referred to as line E7. From the second shot-location "Pany" (778.660/202.500, average lateral offset 23 km), only one shot was fired resulting in a 9.6 km long CDP-line. It will be referred to as line E8. Finally, from shot location "Monbiel" (791.850/192.230, average lateral offset 40 km) four shots were fired giving rise to a 33.9 km long CDP-line. It will be referred to as line E9. In addition to the three fan profiles, a 4.3 km long near vertical line situated between lines E8 and E9 was recorded by the Institute of Geophysics of the ETH Zürich (Figure 9-21). The line consists of two dynamite shots of 1.5 kg charge each and will be referred to as line E10. The seismic sections E7 to E9 are presented Plates 9-7 to 9-9. Line E10 is shown in Figure 9-22.

Line E7 (see Plate 9-7) is characterized by an approximately 1.5 s thick reflection package dipping from 12 s in the N to 13 s in the S. In addition, a conspicuous subhorizontal reflection band can be seen at 9.5 s. It is included in the interpretation, as it can be correlated with reflection bands of the same character in neighboring profiles. Line E8 (see Plate 9-8) shows a well developed deep reflection package dipping southward from 12 to 13 s. Its thickness is in the order of 2 s. North-dipping reflections at 11 s and south-dipping less coherent reflections between 9 and 10 s are also present. The strong reflectivity at 7 s in the center of E8 will not be considered for interpretation due to its very limited extension and also due to the apparent lack of equivalent reflections in the nearby profiles. Line E9 (see Plate 9-9) essentially reveals the same deep reflectivity as the previous two profiles: a south-dipping reflection package from 12.5 to 14 s with a thickness in the order of 1.5 to 2 s, and a less coherent south-dipping reflection band from 10 to 12 s. Despite their small lateral extension, north-dipping reflections at 6 s between horizontal km 30 and 34, and south-dipping reflections at 4 to 6 s between km 20 and 27 should be noted. As will be shown below, they can be correlated with reflections in the line E2 (section 9.3) and in the E10 profile. In contrast to the fan data, the near-vertical line E10 (Figure 9-22) provides information of the uppermost crust. It shows two distinct apparently east-dipping reflections at 1.2 to 1.6 s and 1.8 to 2.3 s, respectively. At the western end of the profile, the lower reflection band flattens out, whereas the upper band looses its strong reflectivity almost completely. Sporadic reflections below the lower reflection band are considered as random noise from a nearby timber factory. For the purpose of the geologic interpretation, a computer-based transformation of the reflection seismic data into line drawings (Valasek 1992) followed by ray-theoretical depth migration (Holliger & Kissling 1991) were performed. Velocities for depth migration were derived from a velocity model used by Valasek (1992) for line E1, which represents a simplified version of the findings of the EGT refraction profile by Ye (1992). The above described reflections were then identified on the depth migrated sections. The results of this processing are shown in the simplified line drawing of Figure 9-23. Note that up-dip migration of reflections considerably increased the profile lengths. The length of the geologic profiles of Figures 9-24 to 9-27 is thus determined by the length of the migrated sections (Figure 9-21).

9.5.2 Geologic interpretation

Looking at the seismic sections E7 to E9 (see Plates 9-7 to 9-9) it is clear, that the profiles yield only information of the deep crust. They can, however, be complemented by surface geological data and by the seismic lines E1, E2 and E10, which all contain shallow data. It becomes thus possible to construct geological cross-sections from the surface down to the crust-mantel boundary. The cross sections along lines E7 to E10 are shown in Figures 9-24 to 9-27. In the following, it will be explained how they were constructed, beginning with the base of the crust and ending with the highest sedimentary units.

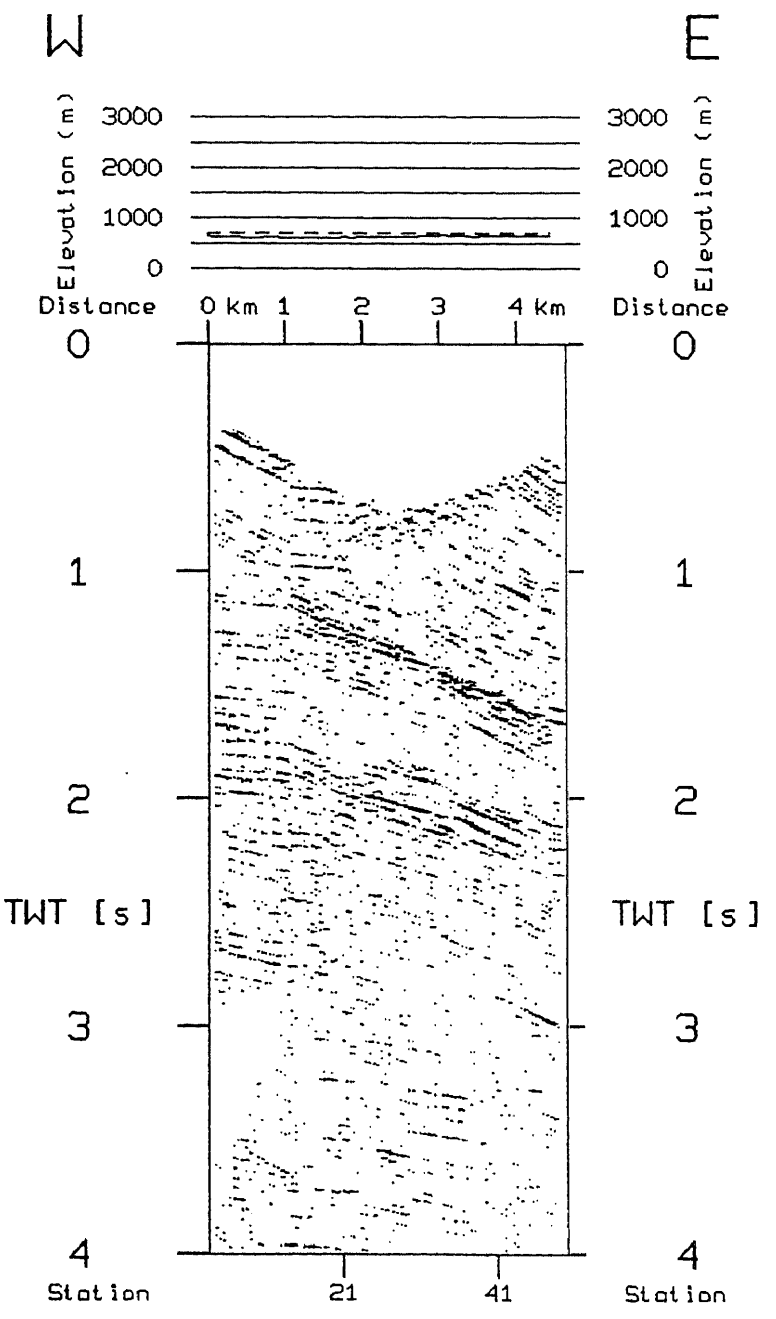

Figure 9-22
Unmigrated near-vertical seismic line E10 showing two destinct apparently east-dipping reflections at 1.2 to 1.6 s and 1.8 to 2.3 s respectively. At the western end of the profile, the lower reflection band flattens out, whereas the upper band looses its strong reflectivity almost completely. For location see Figure 9-21.

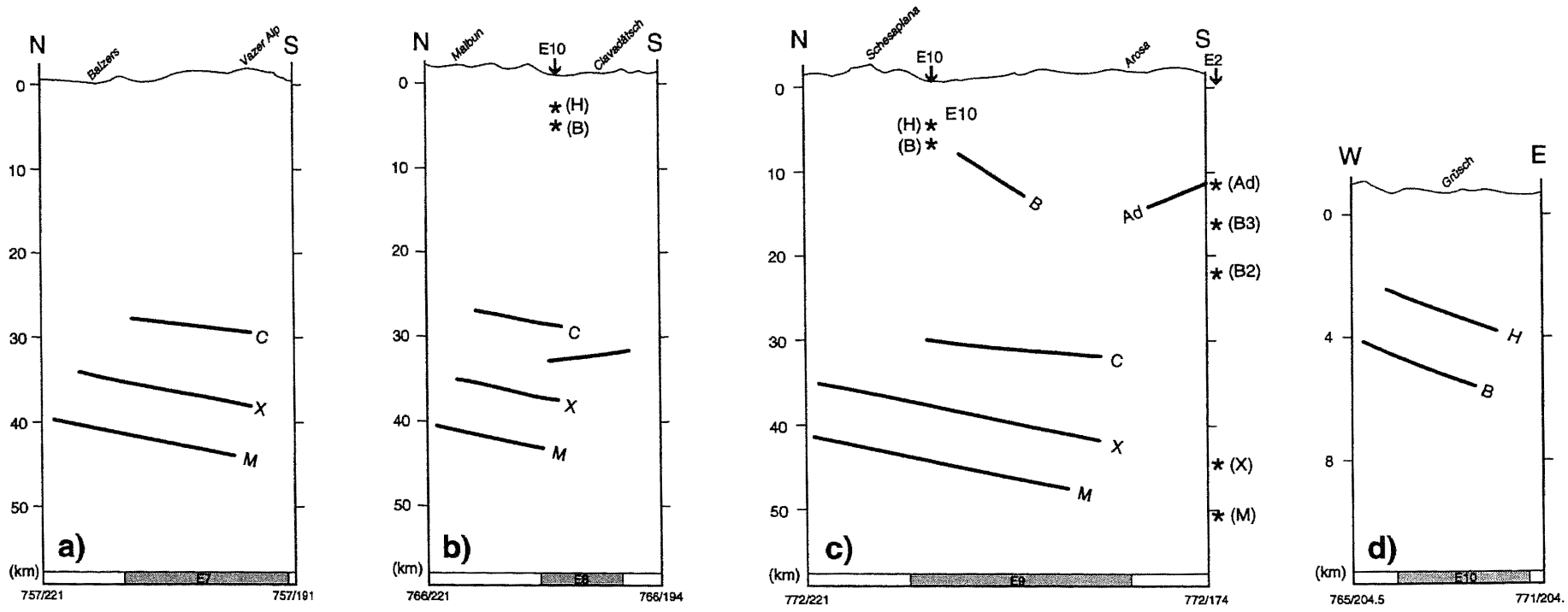

Figure 9-23
Depth-migrated reflections considered for interpretation of (a) line E7, (b) line E8, (c) line E9 and (d) line E10. Stars correspond to migrated reflections of intersecting profiles. White bars at the bottom of each section correspond to the profile length added by the migration process (up-dip migration of dipping reflections). Coordinates are given in the Swiss National Grid system.
M: Moho, X: top of laminated lower crust, C: Conrad, Ad: top of Adula basement nappe, B: top of Aar massif, H: top of Infrahelvetic cover.

Moho discontinuity: In all three fan profiles, the base of the deepest reflection package (*M* in Figure 9-23 a-c) corresponds to the base of the crust, i. e. the Moho discontinuity. This interpretation is based on (a) depth position and dip of reflection group M, which can be correlated with a P-wave velocity jump from 6.5 km/s to 8.3 km/s in the EGT seismic refraction profile (Ye 1992) and (b) the strong reflectivity, which is characteristic for the lower crust immediatly above the Moho in all NRP 20 lines and in many other sampled areas of the world (cf. Klemperer et al. 1986). The southward dip of the Moho ranges from 9° in line E7 to 12° in line E8.

Laminated lower crust: The highly reflective bands immediatly above the Moho (between M and *X* in Figure 9-23a-c) are interpreted as the seismic expression of a laminated lower crust. Such heterogeneous reflection fabrics have been derived from numerical models with alternating high and low velocity layers (cf. Braile & Chiang 1986). Geologically, the layering may have originated from stretching of a thickened heterogeneous lower crust during post-thickening crustal collapse. In the case of the Alpine lower crust, Rey (1993) suggests a late Variscan age (late Carboniferous to Permian) for this event. The thickness of the laminated lower crust in lines E7 to E9 is in the range of 5 to 6 km and compares with the one in line E1, the Western Alps (cf. Valasek 1992) or the Pyrenees (cf. Bois & ECORS 1991).

Conrad discontinuity: The conspicuous reflection bands above the laminated lower crust in a depth range of 9.5 to 12 s (*C* in Figure 9-23a-c) are interpreted as marking the top of the lower crust, i. e. the Conrad discontinuity. This interpretation is based on the correlation with a p-wave velocity jump from 6.2 km/s to 6.5 km/s with similiar depth position and dip in the EGT refraction profile (Ye 1992). In addition, the Conrad discontinuity is defined by the same erratic line-up of short reflections in line E1 (*C* in Figure 9-5a). The southward dip of this discontinuity is slightly smaller than the Moho dip with 7° in lines E7 and E9, and 10° in line E8. This implies a minor thickening of the lower crust towards the south.

Aar massif: In line E10, the lower reflection band (*B* in Figure 9-23d) is interpretated as the top of the crystalline basement, which in the area corresponds to the top of the Aar massif. This interpretation is based on a correlation with line E1, where the top of the Aar massif marks the last coherent reflection band above the Conrad reflections (*B1* and *B2* in Figure 9-5a), i. e. the Aar massif itself is seismically transparent (Pfiffner et al. 1990b). This is also the case in line E10, where no continuous reflections can be found under reflection band B. Reflectivity possibly stems from a high-velocity dolomite layer imediately above the crystalline basement (see also section 9.2). The shallower reflection band in line E10 (*H* in Figure 9-23d) is interpreted as the basal thrust of the allochthonous Helvetic nappes. Reflectivity of *H* is explained by lithological velocity contrasts, which are possibly enhanced by velocity anisotropies along the thrust plane. The observed loss of reflectivity towards the western end of line E10 (Figure 9-22) suggests, that the reflectors might change their orientation from an apparent E-dip to a more horizontal orientation. In this case, coherent seismic energy would reflect out of the E10 receiver spread and thus would explain the loss of coherent reflections towards the W. The implied westward flattening could further indicate, that the crest of the ENE-dipping Aar massif culmination is situated immediatly to the W of the migrated section. Assuming that this interpretation is correct, joining of this Aar crest with the Aar crest exposed in the Vättis inlier (Figure 9-21) results in an orientaion of the Aar massif's crest-line of approximately 060/20. This orientation in turn agrees well with the surface orientation of major fold axes in the crystalline basement, which were formed during the basement uplift (Pfiffner 1977). Additional seismic information of the basement top is available from line E9. There, south-dipping reflections at 4 to 6 s between horizontal km 20 to km 27 (see Plate 9-9) can easily be correlated with the basement top recorded in line E10 (B in Figure 9-23c and d). The considerably less coherent reflectivity of B in line E9 as compared to line E10 is explained by an increased structural complexity of the reflecting surface in the N–S profile and by a more intense scattering of the wavefront in the fan data due to its longer travel distance.
As recording offsets were generally too large to register the top of the crystalline basement in the fan profiles, the top of the Aar massif must be projected from surface and from subsurface positions recorded in lines E1 and E10. For the Aar massif's crest-line, the orientation of 060/20 deduced above was used for projection. As a second key-structure, the deepest basement position north of the culmination, the Aar depression, was used. To find out the latter's orientation, all the seismic lines crossing this depression were examined (W1, C1, E1, see Pfiffner et al., Chapter 13.1). The depth of the Aar depression varies between –8.1 km in line W1, –9.6 km in line C1 and –9.0 km in line E1. On a map, the points lie on a remarkably straight line striking N65°E. As depth varies only minor with distance (variations between C1 and E1 is only 0.6 km corresponding to a dip angle of 0.3°), the dip of the depression for the projection purpose is set to 0°. Consequently, the Aar depression north of the culmination is projected along 065/00 into the fan profiles. For the further construction of the basement top between projected crest and depression, the two points were joined by a straight line, which serves as an envelope for the northern flank of the Aar massif. Its more detailed geometry was then taken from the modeled structure of the E1 profile by Stäuble & Pfiffner (1991) and Stäuble et al. (1993).

Gotthard "massif": The Gotthard "massif", outcropping in the central Alps, is seismically imaged in lines E1, E2 and E3 (see sections 9.2 to 9.4). The latter's eastern continuation is thus quite well established and allows the prediction, that the northern part of the Gotthard "massif" should be encountered in the southern end of line E9. Due to large offset recordings, however, no reflections from the Gotthard top can be observed. The depth and the geometry of the Gotthard "massif" as shown in the cross-section along E9 (Figure 9-26) is thus purely based on projections from line E1 and on the correlation with line E2.

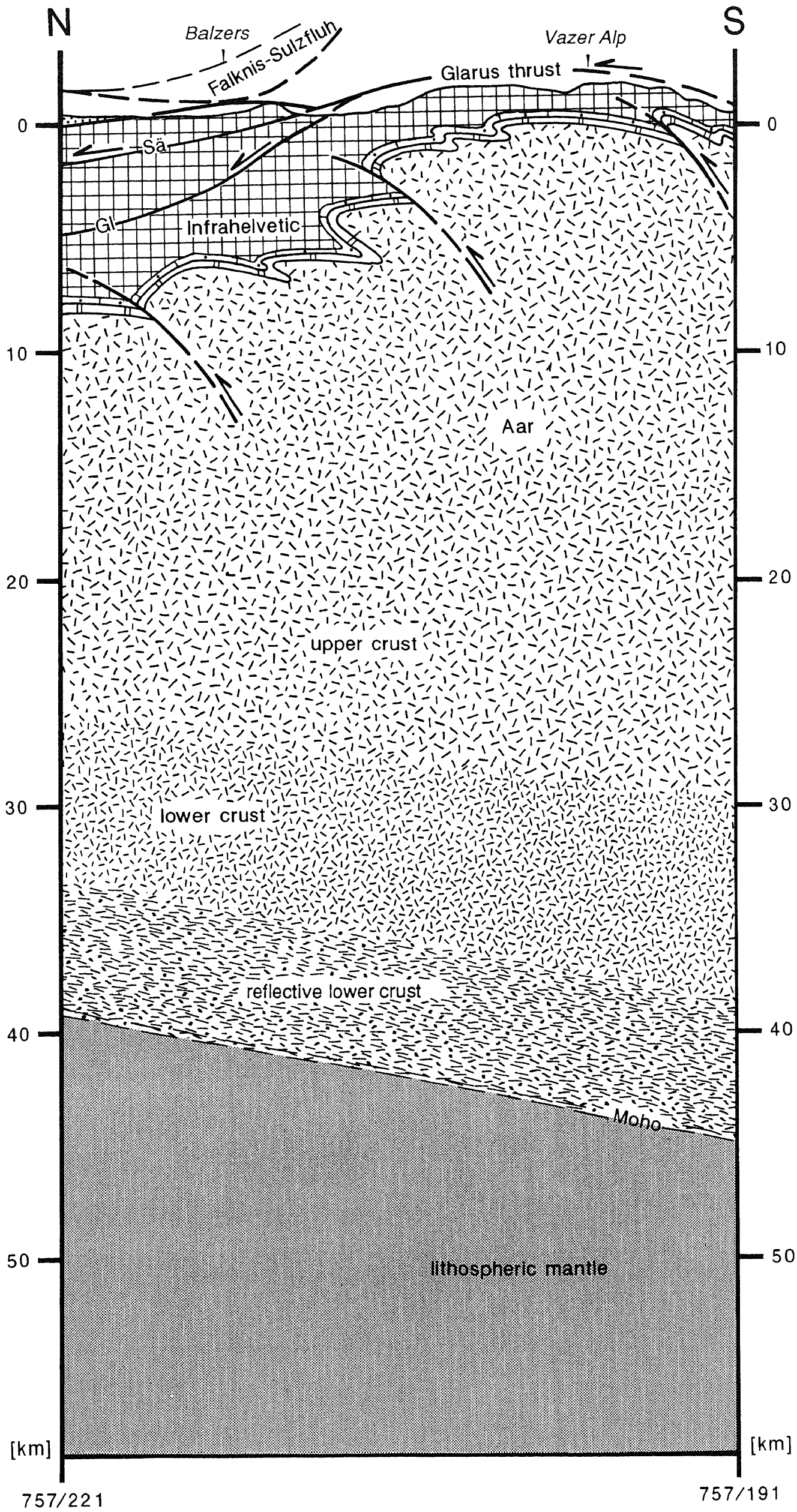

Figure 9-24
Geologic cross section along line E7 based on the interpretation of the seismic data (see Plate 9-7 and Figure 9-23a) and on projections from surface data and line E1 (see Figure 9-8). The trace of the cross section is straight N-S and follows km 757 of the Swiss National Grid system.

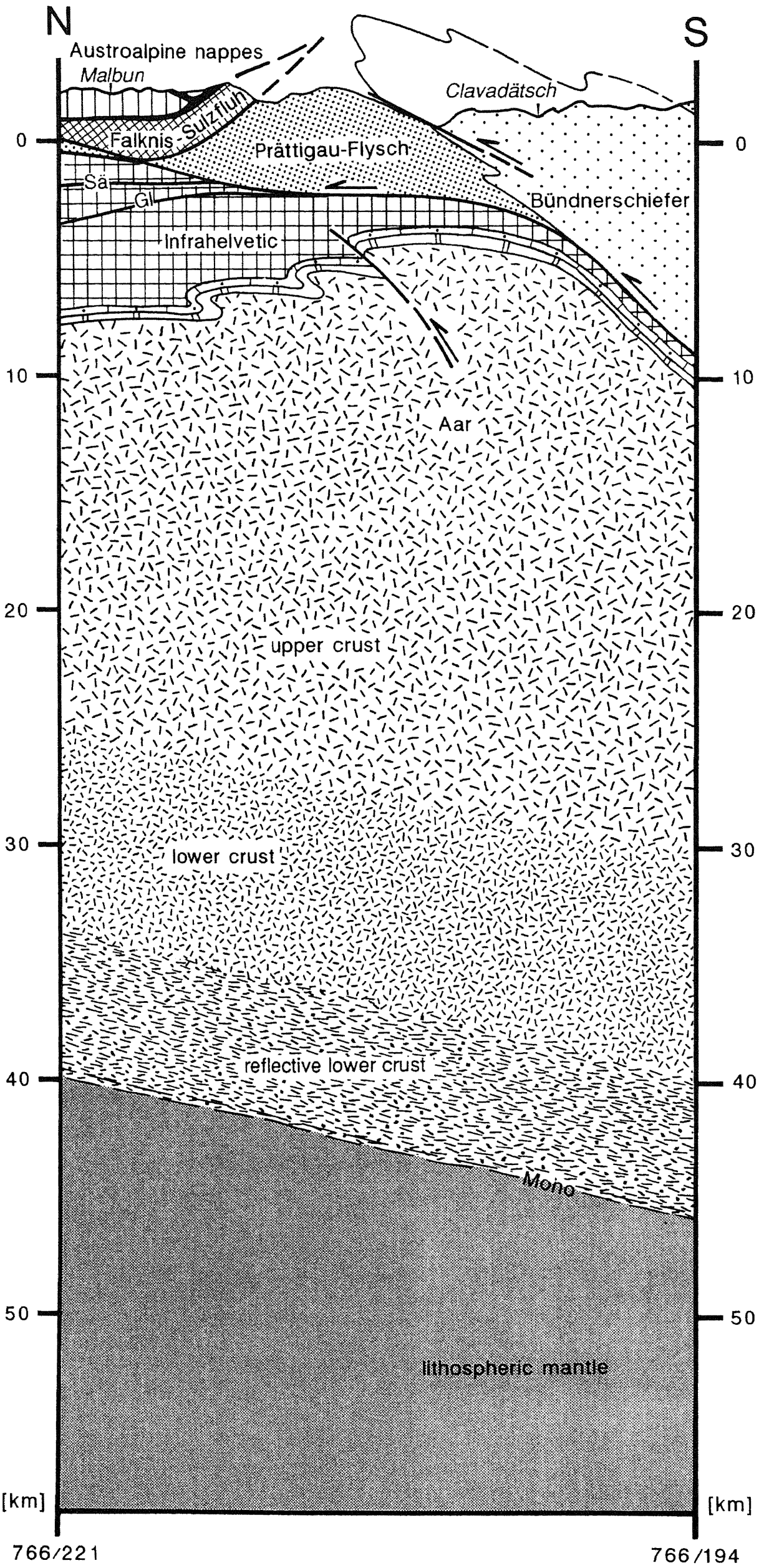

Figure 9-25
Geologic cross section along line E8 based on the interpretation of the seismic data (see Plate 9-8 and Figure 9-23b), projections from surface data and the line E1 cross section (see Figure 9-8) and on the interpretation of the intersecting line E10 (see Figure 9-27). The trace of the cross section is straight N–S and follows km 766 of the Swiss National Grid system.

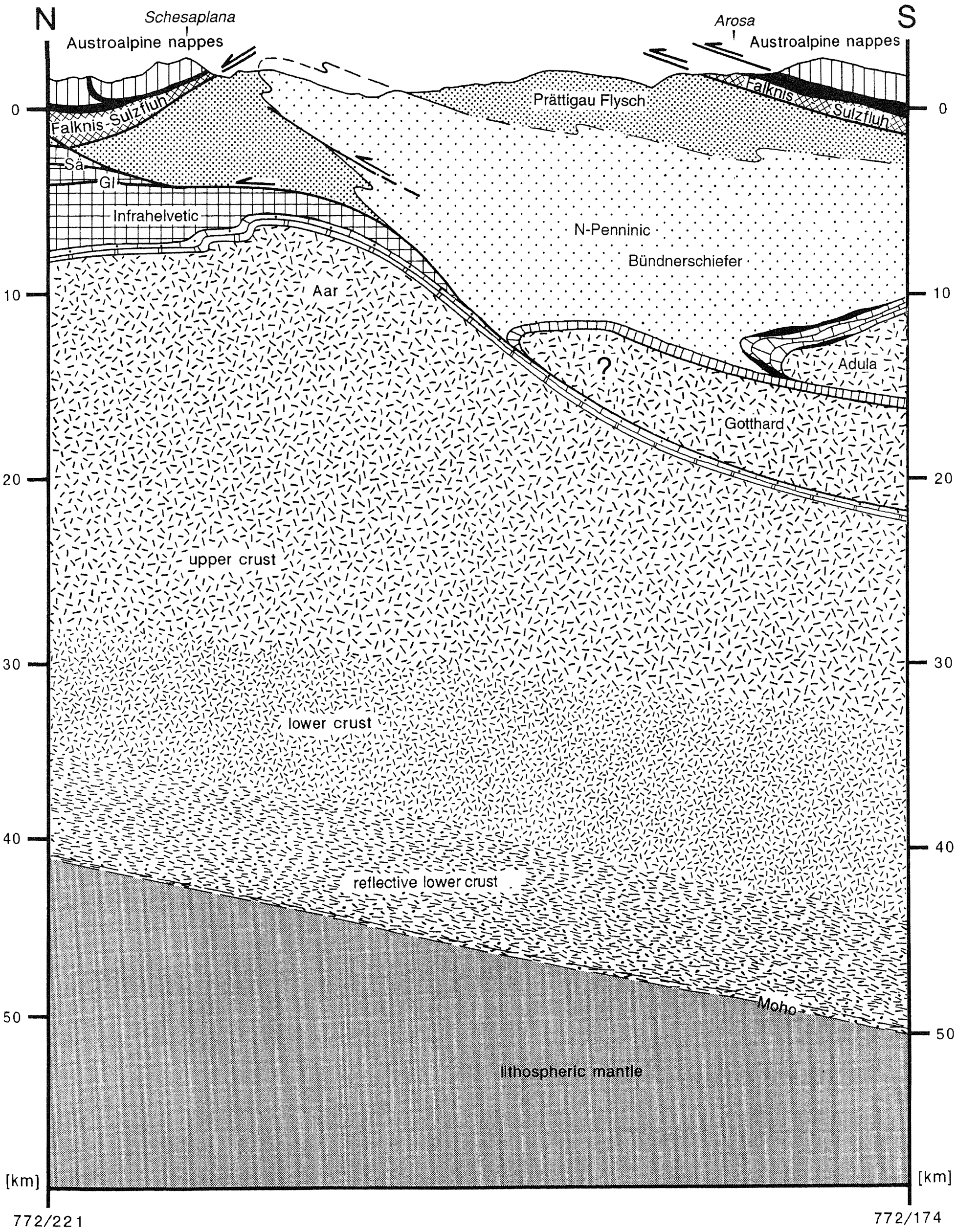

Figure 9-26
Geologic cross section along line E9 based on the interpretation of the seismic data (see Chapter 4 and Figure 9-23c), projections from surface and the E1 cross section (see Figure 9-8) and on the interpretations of the intersecting lines E10 (see Figure 9-27) and E2 (see Figure 9-12). The trace of the cross section is straight N–S and follows km 772 of the Swiss National Grid system.

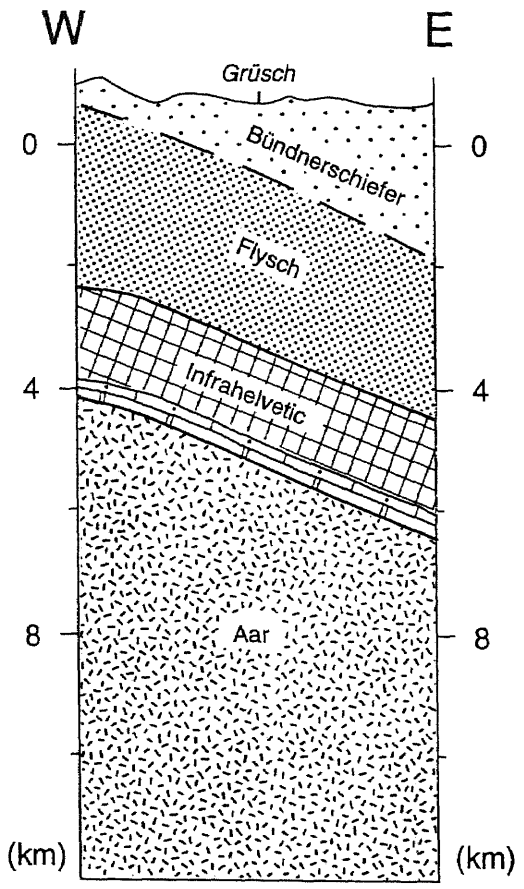

Figure 9-27
Geologic cross section along line E10 based on the interpretation of the seismic data (see Figure 9-22). The trace of the cross section is straight W–E and follows km 204.5 of the Swiss National Grid system.

Adula nappe: In line E9 (see Plate 9-9), the north-dipping reflections at 6 s between horizontal km 30 and km 34 can be correlated with reflections from the top of the Penninic Adula nappe in line E2 (*Ad* in Figure 9-23c). Reflectivity of this discontinuity can be explained with lithological velocity contrasts between cover sediments and the Adula crystalline basement rocks. The top of the Adula nappe is also seismically imaged in line E1 (see section 9.2). Joining the northern Adula front in line E1 with the corresponding structure in line E9 results in a Adula tip line with an orientation of 060/25. This orientation is comparable to the trend of the main structural elements of the Aar massif as described above and to the result of 3D seismic modeling along E1 by Litak et al. (1993).

Overlying sedimentary units: For the overlying sedimentary units, seismic information is available only from lines E1, E2 and E10. However, due to the strong ENE dip of the basement, there is an excellent surface control on the higher units. The azimuth for projection was kept constant at N65°E, corresponding to the average strike of the basement structures described above. The projection dip was chosen according to the positions of the structures involved, i. e. 20° for a position above the Aar crest, 0° for a position above the Aar depression and a linearly interpolated value for a position between crest and depression. These projection trajectories are based on the assumption, that the basement uplift essentially controls the axial plunge of the higher tectonic units, a point that will be discussed in the next section. The following sources of surface data were used to constrain the projections:

Helvetic Zone: Pfiffner 1977 and 1978, Trümpy 1980, Pfiffner et al. 1990a, Pfiffner 1993.
Bündnerschiefer and Prättigau Flysch: Nänny 1948, Nabholz 1951, Christ & Nabholz 1959.
Falknis-Sulzfluh nappes and Arosa imbricates: Lorenz 1901, Brauchli & Leupold 1915, Trümpy 1916, Cadisch 1922, Allemann et al. 1985.
Austroalpine nappes: Oberhauser 1970, Tollmann 1976, Oberhauser 1980, Allemann et al. 1985.

9.5.3 3D model

The interpretations discussed above, together with the results of lines E1, E2 (sections 9.2 and 9.3) and the EGT refraction profile (Ye 1992) form a dense network of 2D crustal information (Figure 9-21). Based on this network, structure contour maps for the following discontinuities were constructed: the Moho (Figure 9-28a), the top of the laminated lower crust (Figure 9-28b), the top of the lower crust, i. e. the Conrad (Figure 9-28c) and the top of the crystalline basement (Figure 9-29). The 3D geometry of the three lower crustal layers were obtained by linear interpolation between data points and sub-

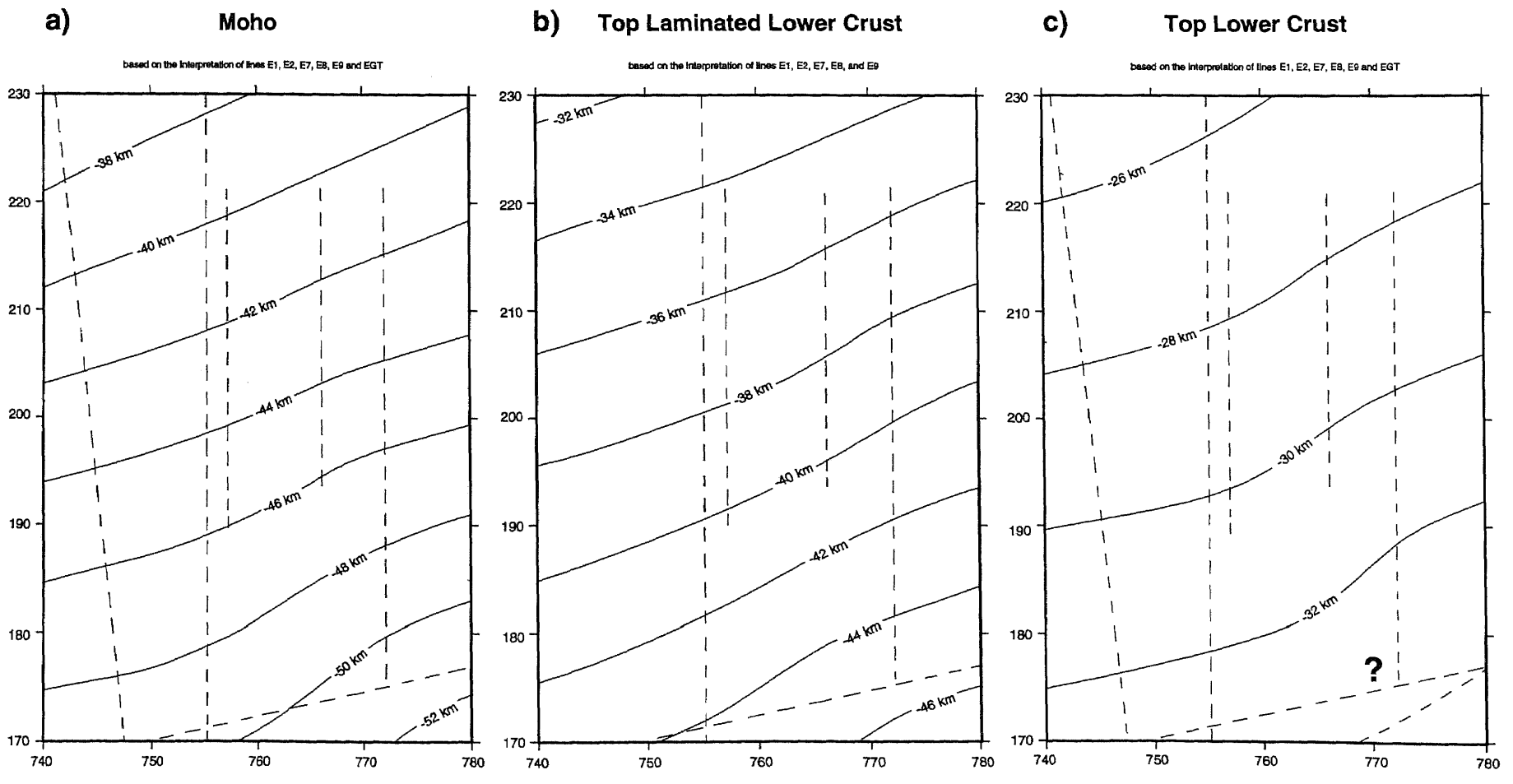

Figure 9-28
Stucture contour maps of the deep crustal discontinuities imaged in the seismic reflection lines E1, E2, E7, E8 and E9 and in the EGT seismic refraction profile (stippled straight lines, see also Figure 9-21). The depth accuracy is estimated to be in the order of ± 2 km. All discontinuities show similar and simple 3D geometries with a constant ENE strike and dip angles between 12° (Moho and top of the laminated lower crust) and 8° (Conrad).

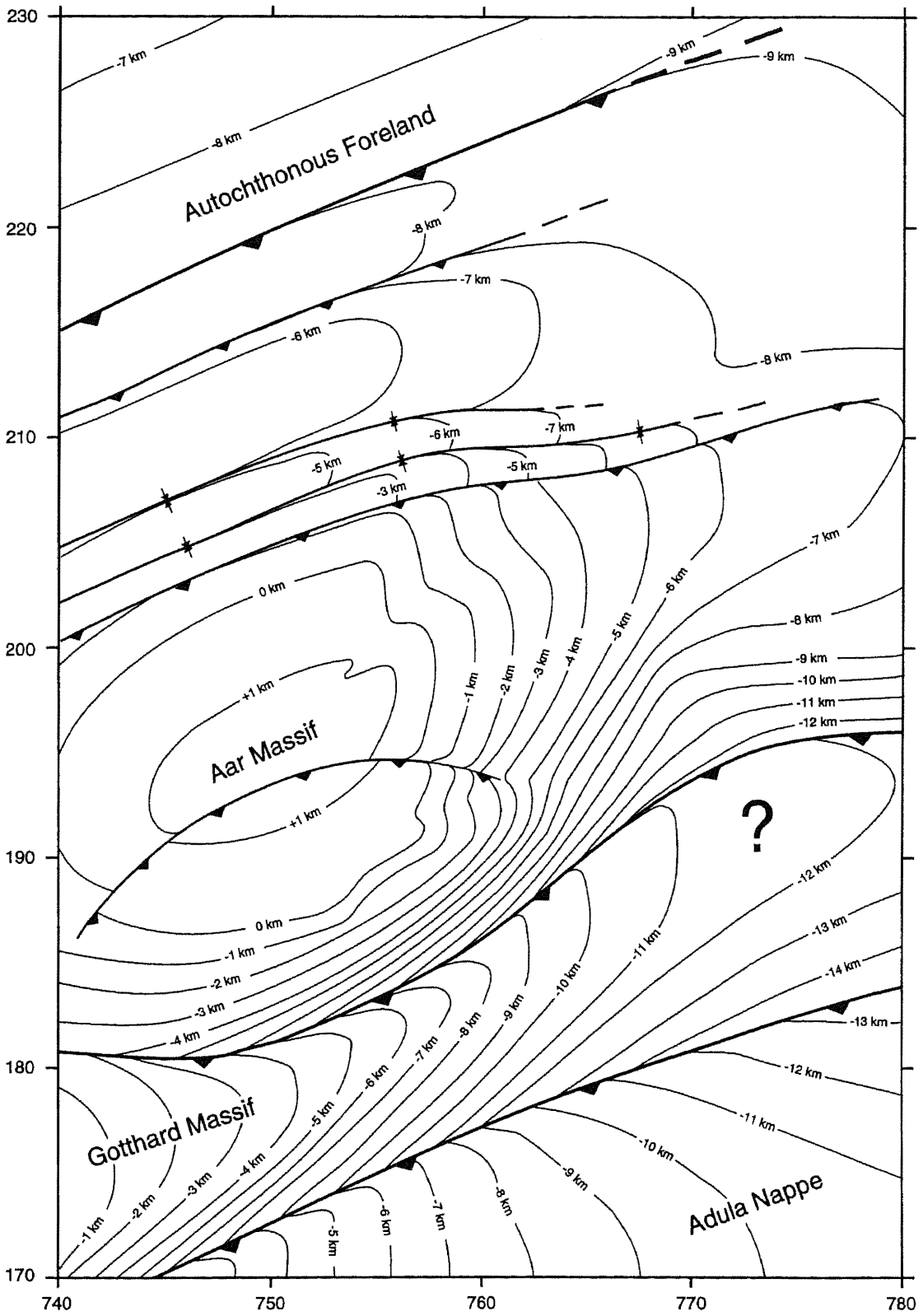

Figure 9-29
Structure contour map of the the top of the crystalline basement imaged in lines E1, E2, E7, E8, E9 and E10 (see also Figures 9-21 and 9-28). The depth accuracy is estimated to be in the order of 0 (surface control) to ± 1.5 km. The 3D geometry reveals complicated domal surfaces formed by a combintion of fold-and-thrust tectonics. The structural disharmony with respect to the lower crust (see Figure 9-28) implies a crustal decoupling mechanism during the formation of the basement uplifts and nappes (Aar, Gotthard, Adula).

sequent smoothing with a 2 km long running average filter (program INTERPS by Valasek 1992). Contouring of the top basement surface was entirely made by hand. The accuracy of the vertical position of the different interfaces is largely controlled by the velocity function used for depth-migration and decreases with dip and time (cf. Holliger 1991 for migration error analysis). The resulting vertical error for a velocity fluctuation of 0.2 km/s relative to 6.0 km/s are approximately 1.8 km for the Moho discontinuity, 1.2 km for the Conrad discontinuity and a maximum of 0.5 km for top basement surface. As Valasek (1992) and Litak et al. (1993) have shown, depth distortions in N–S profiles caused by side-swipes measure approximately 0.5 km for the Moho and Conrad discontinuities, and up to 1 km for the top of the crystalline basement in the area considered. The depth accuracy are thus roughly estimated to be in the order of ± 2 km for the Moho, the top of the laminated lower crust and the Conrad discontinuity, and around ± 1.5 to 0 km (surface control) for the top of the crystalline basement.

Moho discontinuity (Figure 9-28a): The European Moho contours are constrained by both reflection and refraction seismic data. The Moho geometry reveals a smooth surface with an average strike of N70°E and an average dip of 12°. Comparison with the Moho map in this area by Valasek (1992) shows a remarkably good agreement in strike and dip, with depth positions differing by a maximum of 1 km. The good agreement illustrates the relatively simple and continuous geometry of the European Moho, considering that Valasek's map is based on a far less dense network of 2D seismic lines. In addition, the good fit between the refraction and the reflection derived Moho illustrates, that the two methods are imaging the same discontinuity.

Top of laminated lower crust (Figure 9-28b): The top of the laminated lower crust is constrained by seismic reflection data only. As might be expected from the 2D data, the 3D geometry of the top of the laminated lower crust is nearly identical with the Moho geometry. The two discontinuities are seperated by 5 to 6 km. This thickness compares to the ones determined in the central and western portions of the Swiss Alps (cf. Valasek 1992). However, it is only half the thickness of the laminated lower crust found in DEKORP profiles in the European foreland (cf. DEKORP 1990). Assuming a pre-Alpine origin of this structure (Rey 1993), it is possible that the reduced thickness resulted from crustal thinning and stretching during Mesozoic rifting.

Conrad discontinuity (Figure 9-28c): The contoured surface of the top of the lower crust, i. e. the Conrad discontinuity, is constrained by seismic reflection and refraction data. However, it has to be stressed, that the Conrad discontinuity is very poorly defined in the reflection seismic data and that the interpretation is thus somewhat speculative. The actual Conrad geometry might be more complex as appears in Figure 9-28c. With this restriction in mind, the Conrad geometry strongly resembles the geometries of the underlying surfaces. The slightly smaller average dip angle (8°, as compared to 12° for the Moho and the laminated lower crust) implies a minor thickening of

the lower crust towards the SSW. The same observation is made by Ye (1992) in the EGT refraction profile. Comparison with the Conrad structure contour map of Valasek (1992) reveals differences in depth and strike by a maximum of 2 km and 10°, respectively. These differences lie within the estimated error bounds.

Top of crystalline basement (Figure 9-29): The structure contour map of the top of the crystalline basement shows the first basement body encountered going downward from the topographic surface. The map is based on reflection data and geological surface data.
The map's NW corner is characterized by an undisturbed SSE dipping surface. It strikes N66°E with a dip of 10°. This orientation is very similar to the orientation of the deep crustal discontinuities. Consequently, this part of the basement belongs to the relatively undisturbed European foreland. Immediately S of the –9 km structure contour, the top basement surface starts to rise to a maximum elevation of +1 km in the Vättis inlier (Figure 9-21) to form the eastern Aar massif culmination. The uplift shows the overall geometry of a dome, bordered by a depression in the N (marked by the northernmost basement thrust) and by the Gotthard "massif" in the S. The northern flank of the dome is characterized by overturned folds and thrust slices (see also Pfiffner et al., Chapter 13.1), whereas the southern side reveals a less complex geometry with a steep SSE-dip of approximately 50°. To the ENE, the basement uplift strongly diminishes in amplitude. In fact, one might suspect that the Aar massif culmination ceases to exist some kilometers further ENE and that basement shortening might be transferred to an equivalent structure possibly arranged in an en-échelon pattern (see also Figure 13-25).
To the S, the eastern Aar massif is shown to be overthrust by the Gotthard "massif". This second basement unit is considerably less constrained. Its overall geometry is that of a ENE dipping, slightly reclined antiform, lacking positive indications of internal fold-and-thrust structures such as observed in the Aar massif. In addition to this contrast in structural style, the eastern Gotthard "massif" seems to widen towards the WSW and ENE, indicating that it has been deformed by the uplift of the the eastern Aar massif culmination.
To the S of the Gotthard "massif", the crystalline basement top is represented by the front of the Penninic Adula nappe. The latter's geometry is well constrained by surface and reflection seismic data (see also Litak et al. 1993 and section 9.2). The frontal Adula nappe shows a change in geometry from an overturned ENE plunging antiform in the WSW to a more or less horizontal wedge-shaped body in the ENE. An average axial plunge of 20° can be deduced from the contours which is comparable to the axial plunge of the eastern Penninic nappe stack determined from surface data (cf. Milnes & Schmutz 1978, and Schmid et al., Chapter 14).
When comparing the top of the crystalline basement in Figure 9-29 (based on seismic data) with the one in Figure 9-6 by Pfiffner et al. (1990a, based on surface data solely), significant differences emerge. For example, the top of the Aar massif N of the culmination is deeper by up to 3 km in the new map. Similarly, the top of the Gotthard "massif" at coordinates 750/180 is at approximately –1.5 km in Pfiffner et al. (1990a) but at –4 km in Figure 9-29. It is interesting to note, that 3D seismic modeling by Litak et al. (1993) already pointed into exactly this direction. In addition, the top basement contour in the new map is more structured, illustrating that the cover sediments at the surface conceal important basement structures at depth.

9.5.4 Discussion and conclusion

The results of the deep seismic fan recordings show, that the crust-mantle boundary, the top of the laminated lower crust and the Conrad discontinuity (Figure 9-28a-c) have similar 3D geometries with ENE strikes and dips between 12° (Moho, top laminated lower crust) and 8° (Conrad). The thickness of the laminated lower crust remains constant at around 5 to 6 km, whereas the thickness of the lower crust increases from 12 km in the N to 16 km in the S. This thickening is also reported from other NRP 20 transects and the EGT refraction profile (Valasek 1992, Ye 1992). It indicates, that collision tectonics affected the European lower crust as far N as the external massifs.
In sharp contrast to the simple geometry of the lower crustal units, the top of the crystalline basement is structurally much more complex with reliefs of up to 10 km. The relief and the associated disharmony with the underlying units suggests, that not only the nappes (Adula etc.), but also the basement "massifs" (Aar, Gotthard) must be considered allochthonous. This implies that an intracrustal decoupling mechanism must have taken place during the formation of the basement units. The decoupling horizon must be situated somewhere between the top of the lower crust and the top of the crystalline basement. It has been suggested that velocity inversion zones found beneath the Alps are possible candidates for such detachments (cf. Mueller 1990), owing to the presence of elevated fluid pressures.

The structure of the allochthonous basement units is visible from the mapped pattern of the surface geology (Figure 9-21). For example, the embayment of the basal Austroalpine thrust fault E of Vättis (with the sudden change in strike from a N–S to a SW–NE) can be linked to the Aar massif culmination in the subsurface. Similarly, S of Chur, the strike change from NE–SW to N–S of the Austroalpine base can be linked to the topography of the Gotthard and Adula units (note that this strike change at surface mimics the trend of the structure contours at subsurface). The basement topography is thus taken to be responsible for the general shape of the Prättigau halfwindow (as postulated e. g. by Staub 1934), a fact which is also sustained by the orientation of the principal foliation plane in the Bündnerschiefer, dipping SSE in the area of Chur and E in the area of line E10 (Figure 9-21, Dreibündenstein phase of Pfiffner 1977).
To understand the eastern end of the Aar-Gotthard culmination in a larger tectonic framework, it is useful to inspect the geometry of its western counterpart. As discussed by Pfiffner et al. in Chapter 13.1, the western end of the Aar massif and the Aiguilles Rouges-Mt. Blanc massifs are relayed in a right-step en-échelon manner. Burkhard (1988) postulated a N–S oriented wrench fault in the Rawil depression in between. It can be shown, though, that major fold hinge lines in the Helvetic zone (Morcles and Doldenhorn e. g., see Pfiffner 1993) are also relayed en-échelon and the geologic interpretation of line W1 (see Pfiffner et al., Chapter 13.1) does not point towards the existence of a wrench fault. A similar en-échelon pattern can be postulated at the end of the Aar-Gotthard culmination. Here, the eastern end of the Aar-Gotthard culmination could be relayed with the "Engadine uplift" in a right-step en-échelon manner. As discussed in section 9.4., the ENE striking antiform associated with the Engadine window itself and outlined by the basal Austroalpine thrust, is cored by Penninic cover nappes (Bündnerschiefer units). This antiform is locally uplifted in response to the formation of a NW-vergent basement slice underlying the Engadine window. It seems possible, that this latter basement slice is arranged in a right-step en-échelon manner in respect to the eastern external basement uplift. In addition, considering lines W1, C1 and E1, the northernmost thrust fault of the Aar massif seems to have a constant ENE strike along the entire basement uplift. This orientation is comparable to the strike of Variscan structures in the European foreland like e. g. the Permo-Carboniferous basement trough in NE-Switzerland (Sprecher & Müller 1986). Based on the similarity in orientation, it might be postulated, that the northernmost basement thrust represents a reactivated Variscan structure controling the position of the external basement uplift in the Alps.
Returning to the investigated area, it can be said, that fan shooting into an existing near-vertical deep seismic measurement setup, combined with a short near-vertical measurement, has proven to be very useful in obtaining a detailed 3D crustal model. The new insights gained from this 3D model can be summarized as follows:

1) The Moho discontinuity, the top of the laminated lower crust and the Conrad discontinuity have all similar and simple 3D geometries with a constant strike to the ENE and dip angles between 8° and 12°. The laminated lower crust has a constant thickness of 5 to 6 km, whereas the lower crust thickens from 12 km in the NNW to approximately 16 km in the SSE. This change in lower crustal thickness might reflect mild lower crustal thickening during Tertiary compression.
2) The 3D geometries of the top of the crystalline basement contacts reveal complicated domal surfaces formed by a combination of fold-and-thrust tectonics. The structural disharmony with respect to the lower crust implies a crustal decoupling mechanism during the formation of the basement uplifts and nappes. The decoupling horizon must be situated between the Conrad discontinuity and the top of the crystalline basement.
3) Comparison of surface data and the top-basement geometry clearly reveals a kinematic link between the shape of the Prättigau halfwindow and the formation of the Aar massif culmination.

Acknowledgements

J. Ansorge, G. Eisbacher and R. Marchant are thanked for reviewing this chapter. Many thanks go also to E. Lanz and S. Sahli for plotting and drawing assistance. We would like to thank in particular J. Ansorge, N. Froitzheim, M.R. Handy, E. Kissling, St. Mueller, St. Schmid and G. Schreurs for comments on early versions of this chapter and many fruitful discussions. H. Horstmeyer and P. Valasek are thanked for introducing L. H. to seismic data processing.